

https://dspace.org/

Application of interferometery to supersonic channel flow

Hermann, Walter

2015-08-03
http://hdl.handle.net/10539/18180

Downloaded from a DSpace repository. https://dspace.org/

APPLICATION OF INTERFEROMETRY TO
SUPERSONIC CHANNEL FLOW.

Walter Herrmann

APPLICATION OF INTERFEROMETRY
TO
SUPERSONIC CHANNEL FLOW

by

Walter Herrmann

Thesis presented to the University of the Witwatersrand for the degree of Doctor of Philosophy

This work has been carried out with the aid of a grant by the Council for Scientific and Industrial Research..

Application of Interferometery

to

Supersonic Channel Flow

This thesis is entirely my own work, except where references are quoted, and no part of the work forming the basis of this thesis has been incorporated in a thesis submitted for another degree.

Signed. Walter Herrmann
Walter Herrmann

Date 7 January 1954

Abstract

The general theory of interference, taking into account the effect of finite source size and spectrum band width is presented in detail and extended to explain the formation of interferograms and operation of the Mach - Zehnder Interferometer. An analysis of the errors, including those due to boundary layers, refraction and finite aperture, is made and the uncertainty interval of the instrument is found to be only a few percent, depending on the application.

The interferometer is applied to the measurement of densities in two supersonic channels, and the resulting density contours compared to those obtained by Characteristic theory, and found to correspond within the uncertainty interval. Application of the interferometer to boundary layer flow is indicated, and the details of the flow in the channels discussed.

The use of pressure holes to determine a reference density for interferogram evaluation is investigated, and found to be in order providing that the pressure holes are small and smooth.

Total head and static probes for use with a Machmeter are calibrated, and the performance of large angle conesfor the measurement of Mach number is checked.

Contents

Introduction 1

Chapter 1; General Interference Theory

1. Wave Analysis 2
2. Fringe Analysis 3
   2.1 Equation of Fringes in Space.
   2.2 Equation of Fringes on a Screen
3. Practical Considerations and Visibility
   3.1 Angular Aperture and Field
   3.2 Telecentric Systems
   3.3 Effect of Aperture on Visibility
   3.4 Position of least Confusion
   3.5 Optimum Source Size.
4. Fringes in Non-Homogeneous Light. 11
   4.1 Effect of Broadening of the Spectral Band. 4.2. Visibility in Non-Homogeneous Light.
   4.3 Approximate Single Spectrum Line. 4.4 Gaussian Intensity Function Line. 4.5 Error Resulting due to Non-Homogeneous Light.
   4.6 White Light Fringes 4.7 Visibility with a Doublet.

Chapter 2; Mach-Zehnder Interferometer Theory 17

1. Characteristics of the Interferometer 17
   1.1 Description of the Elements.
   1.2 Linear Interferometer Analogy
   1.3 Effect of the Controls.
   1.4 Focussing 1.5 Adjustment of Fringe Shape and Spacing.
2. Formation of Interferograms. 22
   2.1 Displacement of Fringes
   2.2 Evaluation of Finite Fringes
   2.3 Evaluation of Infinite Fringes
   2.4 Axially Symmetric Phenomena.
3. Errors in Evaluation 24
   3.1 Zero Errors. 3.2 Error due to the Boundary Layer 3.3 Error due to Refraction 3.4 Error due to Divergent Light.

Chapter 3; Description of the Apparatus.

1. Interferometer 32
   1.1 Constructional Features
   1.2 Optics.
2. Adjustment Technique 37
3. Supersonic Channels 40
4. Additional Measuring Techniques 40

Chapter 4; Test Procedure and Results.

1. Interferograms 42
1.1 Density Evaluation from Finite Fringes. 1.2 Density Evaluation from Infinite Fringes 1.3 Density Evaluation from Composite Fringes. 1.4 Boundary Layer Evaluation
2.1 Wall Pressure Tests 50
2.2 Probe Tests 2.3 Cone Tests

Chapter 5; Accuracy
1. Finite Interferograms 54
1.1 y, 1.2 y_0 1.3 b 1.4 ℓ
1.5 Pressure and Temperature
1.6 Boundary Layer Correction
1.7 Resultant Uncertainty in the Density 1.8 Resultant Uncertainty in Mach Number.
2 Infinite Interferograms 61
3 Wall Taps and Static Probes 62
4 Total Head Probe 62
5 Cones 62

Chapter 6; Discussion of Results

1. Channel Flow 63
1.1 Characteristic Theory
1.2 One-Dimensional Theory
1.3 Verification of Isentropic Flow. 1.4 Flow in the Throat
1.5 Flow in the Test Section
2. Boundary Layer Flow. 68
2.1 Boundary Layer Profiles
2.2 Boundary Layer - Exit Shock Wave Interaction.
3. Instrumentation 72
3.1 Interferometer. 3.2 Reference Density using Pressure Taps.
3.3 Probes 3.4 Cones
4. Points for Further Research 76

Conclusions 77

Bibliography 79

Appendix 1. Interferograms and Plates (i)

Appendix 2. Tables (ixx)

Appendix 3. Curves (i x)

List of Illustrations

Fig.		Page
1	Image Plane of the Interferometer	8
2	Image Plane of a Telecentric System	9
3	Sources of Finite Size	9
4	Elements of the Interferometer	18
5	Linear Analogy	18
6&7	Fringe Relationship	18
8	Refraction Effects	27
9	One Parallel Light Effects	27
10&11	Geometry of Refraction Effects	27
12	Optical Layout of the Interferometer	33
13	General View of the Interferometer	i
14	Close up of the Interferometer with Mach 3 Channel	ii
15	The Interferometer Showing Arc Lamp	ii
16	Setup for Adjustment	ii
17	Mirror Holders for Mach Zehnder Interferometer	36
18	The Interferometer Plate Holders	iii
19	Fringes Produced by the Interferometer Plate Only	iii
20	M 2 Channel with Fringes distorted by Plate Glass	iv
21	Zero Fringes in #1U2 Channel	iv
22	Zero Fringes in M3 Channel	iv
23	-ve Vertical Fringes	v
24	Infinite Fringes	v
25	-ve Vertical Fringes	v
26	-ve Horizontal Fringes	vi
27	+ve Horizontal Fringes	vi
28	Zero Horizontal Fringes	vi
29	White Light Horizontal Fringes	vi
30	M 2 Channel	vii
31	M 3 Channel	vii
32	Optical Layout of the Schlieren System	42
33	Total Head Probe	42
34	Static Probe	41
35	#2 M2 Exit Rest	viii

Fig.		Page.
36	#2 M2 Throat Test	viii
37	#2 M2 Exit	viii
38	#2 M2 Density Contours	ix
39	#2 M2 Throat Density Contours	ix
40	M3 Density Contours, Throat	ix
41	Zero of Fig. 40	x
42	M3 Density Contours, Working Section	x
43	Zero of Fig. 42	x
44	#2 M2 Composite Density Contours	xi
45	M3 Composite Density Contours	xi
46	#2 M2 Schlieren	xii
47	M3 Schlieren	xii
48	#0 M2 Schlieren	xii
49	#0 M2 Infinite Fringes	xiii
50	#0 M2 Schlieren	xiii
51	#0 M2 Infinite Fringes	xiii
52	#1 M2 Schlieren	xiv
53	#1 M2 Schlieren	xiv
54	#1 M2 Infinite Fringes	xiv
55	#2 M2 Shadowgram	xv
56	#2 M2 Schlieren	xv
57	#2 M2 Infinite Fringes	xv
58-62	Static Probe in #2 M2 Channel	xvi
63-67	Total Head Probe in #2 M2 Channel	xvii
68-72	Cones in #2 M2 Channel	xviii

List of Important Symbols

b	fringe width.
C_p	Specific Heat at constant pressure.
C_v	Specific Heat at constant volume.
I	Intensity
K	Gladstone - Dale constant
ℓ	length of the test section
M	Mach Number
n	fringe number
P,p	Pressure
R	Gas Constant
t	time
T	Temperature
V	Visibility
x y z	Space Co-ordinates
Δ	Phase difference
δ	Increment in Δ
λ	Wavelength of light
Λ	Increment in λ
β	Spectral line half width
μ	Refractive Index
ρ	Density
γ	Ratio of Specific Heats
$()_o$	Refers to stagnation values
$()'$	Refers to uncorrected values
$()_1$	Refers to free stream values

Errata

p. 29 Equation 44 should read

$$\frac{f}{s} = \frac{\rho^4}{8} \cdot \frac{grad^3 \mu}{\mu^3}$$

p LII & LIII Table No. 22 & 23
Tables of pressures along the
Centreline are interchanged.

Acknowledgements and thanks are due to Professor W.J. Walker for his guidance and help in many phases of the work, and to Dr. Harris of the Council for Scientific and Industrial Research for his advice in the optical problems, and also to the staff of the Mechanical Engineering Laboratory for their advice and help in building the Interferometer and necessary apparatus.

Introduction

During the program of study of flow in supersonic channels in the Mechanical Engineering Laboratory of the University of the Witwatersrand it was found necessary to obtain more quantitative data than was yielded by Schlieren and probes which were available. Work done at Princeton (Ref. 9, 10) indicated that a Mach - Zehnder interferometer would be ideal for this type of measurement, and this instrument was designed and built. It appeared however that the available references on the operation and theory of the instrument left much to be desired, dealing mainly with idealised interferometers, so that a thorough analysis of the theory was undertaken, and has here been presented in detail.

The performance of the interferometer has been checked, and the interferometer then used to investigate the channels and calibrate the cones and probes reviously used.

Chapter 1.

General Interference Theory

It has been thought best to present the general interference theory quite fully, in such a way that it would be applied to any type of interferometer, or for that matter to any type of interference. Much of the theory has had to be adapted to the general case.

Wave Analysis.

Assuming that light is propagated in waves, it is possible to deduce the wave equation without making any assumptions as to the nature of the light vector. (Ref.1)

The wave equation may be written as

$$y = a \sin(\omega t - \gamma) \quad . \quad . \quad . \quad . \quad . \quad . \quad (1)$$

where a represents amplitude
t represents time
ω and γ are constants.

When two or more seperate disturbances are impressed upon an element in a medium simultaneously, the motion may become very complex, but in this case the principle of direct superposition may be taken to hold, since experiment agrees with theory based on this assumption. Considering two such wave trains acting approximately along the same line, with equal periodic times,

$$y_1 = a_1 \sin(\omega t - \gamma_1)$$
$$y_2 = a_2 \sin(\omega t - \gamma_2)$$

The resultant displacement at time t is

$$y = y_1 + y_2$$
$$= a_1 \sin(\omega t - \gamma_1) + a_2 \sin(\omega t - \gamma_2)$$

which becomes

$$y = a \sin(\omega t - \gamma)$$

where

$$a \cos\gamma = a_1 \cos\gamma_1 + a_2 \cos\gamma_2$$
$$a \sin\gamma = a_1 \sin\gamma_1 + a_2 \sin\gamma_2$$
$$\tan\gamma = \frac{a_1 \sin\gamma_1 + a_2 \sin\gamma_2}{a_1 \cos\gamma_1 + a_2 \cos\gamma_2} \quad . \quad . \quad . \quad . \quad (2)$$

Now maxima and minima depend on the amplitude, which depends upon the Cosine term

But $\gamma = \frac{2\pi}{\lambda} x$

where λ is the wavelength.

$$\text{Cos}\,(y_1 - y_2) - \text{Cos}\,\frac{2\pi}{\lambda}(x_1 - x_2)$$

which is the phase difference Δ between the two disturbances.

Then the maxima and minima occur when $\Delta = 0, 2\pi, 4\pi, \ldots$ etc. and $= \pi, 3\pi, 5\pi, \ldots$ etc. respectively.

Hence for a field illuminated by two similar wave trains the phase difference varying over the field, bright and dark bands will appear, being loci of equal Δ. These are known as interference fringes.

The amplitude of the disturbance determines the intensity of illumination at a given point, since the amplitude is inversely proportional to the distance from the source and intensity of illumination is inversely proportional to the square of the distance from the source.

$$I \propto a^2$$

where I denotes the intensity of illumination.

Hence from equation (2) for $a_1 = a_2$

$$I \propto 2a^2(1 + \text{Cos}\,\Delta) \quad . \quad . \quad . \quad . \quad . \quad . \quad (3)$$

2. Fringe Analysis.

2.1 Equation of Fringes in Space.

Consider two exactly similar sources close together radiating wave trains of equal wavelength in all directions. Then at a point P in space the wave trains are in a condition to interfere, fringes appearing as loci of equal phase difference.

Suppose the sources A & B are a distance 2c apart, and the phase difference at P is 2m.

The locus of P is a hyperbola, of equation

$$\frac{x'^2}{m^2} + \frac{y'^2}{m^2 - c^2} = 1 \quad . \quad . \quad . \quad . \quad . \quad (4)$$

In three dimentions the loci will be hyperboloids of two sheets, the equation being

$$(c^2 - m^2)\,x'^2 - m^2 y'^2 - m^2 z'^2 = m^2(c^2 - m^2)$$

For a completely general case the system need only be rotated through an angle θ about the Z axis, since rotation about the Z axis will not alter conditions.

The general equation of fringes in space then is

$$Ax^2 + By^2 - 2Hxy - Gx^2 - D = 0 \quad . \quad . \quad . \quad (5)$$

Where

$$A = c^2 \cos^2\theta - m^2 \qquad D = m^2 (c^2 - m^2)$$
$$B = c^2 \sin^2\theta - m^2 \qquad H = c^2 \sin\theta.\cos\theta$$
$$C = m^2$$

3.2 Equation of Fringes on a Screen

If a screen is now placed on the X axis at a distance d from the origin, parallel to the Y Z plane, the equation of fringes observed on the screen will be given by the interpenetration of the screen with the hyperboloids.

Hence setting x = d in equation (5), the equation of fringes on a screen becomes

$$B.y^2 - 2Hy - C.m^2 - F = 0 \quad . \quad . \quad . \quad . \quad . \quad . (6)$$

Where

$$B = c^2 \sin^2\theta - m^2 \qquad C = m^2$$
$$E = dc^2 \sin\theta.\cos\theta \qquad F = m^2(c^2 - m^2) - (c^2\cos^2\theta - m^2)d^2$$

This is a system of conics, displaced from the origin. Particular cases will now be examined.

(a) $\theta = 0$

Here $B = - m^2$ $\qquad E = 0$
$C = m^2$ $\qquad F = (c^2 - m^2)(m^2 - d^2)$

and equatio (6) becomes

$$y^2 + z^2 = \frac{(c^2 - m^2)(d^2 - m^2)}{m^2} \quad . \quad . \quad . \quad . (7)$$

This is a family of co-axial circles, of radius

$$r = \frac{\sqrt{(c^2 - m^2)(d^2 - m^2)}}{m} \quad . \quad . \quad . \quad . \quad . (8)$$

or approximately, if $d \gg m$, $c \gg m$

$$r_o = \frac{cd}{m} \quad . \quad . \quad . \quad . \quad . \quad . \quad . \quad . \quad . (9a)$$

putting $\delta m = \Delta$, and for a particular fringe $\Delta = n\lambda$ where n is an arbitrary number, the radius of a fringe is

$$r_f = \frac{2cd}{n\lambda} \quad . \quad . \quad . \quad . \quad . \quad . \quad . \quad . \quad . (9b)$$

which is the same result obtained by approximate methods usually employed. (Ref.2)

(b) $\theta = \pi$

Here $B = (c^2 - m^2)$ $\qquad E = 0$
$C = m^2$ $\qquad F = m^2(c^2 - m^2 + d^2)$

Equation (6) becomes

$$\frac{Y^2}{m^2} - \frac{z^2}{(c^2 - m^2)} = \frac{(d^2 - m^2 + c^2)}{(c^2 - m^2)} \quad . \quad . \quad . \quad (10)$$

This represents a family of central hyperbolas, their distance apart on the Y axis being given by

$$y_o = m \left(\frac{d^2 - m^2 + c^2}{c^2 - m^2} \right)^{\frac{1}{2}} \quad . \quad . \quad . \quad . \quad . \quad (11)$$

Again, approximately if $d \gg m$, $c \gg m$

$$y_o \doteq \frac{2md}{2c} \quad . \quad . \quad . \quad . \quad . \quad . \quad . \quad . \quad (12)$$

or as before, in terms of wavelength

$$y_f = \frac{n\lambda d}{2c} \quad . \quad . \quad . \quad . \quad . \quad . \quad . \quad . \quad (12a)$$

which again is the result obtained by approximate analysis.

(c) $\theta > 0 > \phi$

In this case the type of curve the fringes assume may be predicted by examining the discriminant of equation (6).

$$m^2 (m^2 - c^2 \sin^2\theta)$$

Case i. Discriminant positive

or $\sin\theta < \pm \frac{m}{c}$

The curves are ellipses, with their centres displaced to one side along their major axis.

Case ii. Discriminant zero

or $\sin\theta = \pm \frac{m}{c}$

The curves are parabolas also displaced from their centre

Case iii. Discriminant negative

or $\sin\theta > \pm \frac{m}{c}$

The curves are hyperbolas, similarly displaced from the origin.

In each case, the centre of the system is displaced a distance ξ along the Y axis, where

$$\xi = \frac{dc^2 \sin\theta\cos\theta}{m^2 - c^2 \sin^2\theta} \quad . \quad . \quad . \quad . \quad . \quad (13)$$

In each case the y intercept will be

$$y = \frac{2dc^2 \sin\theta.\cos\theta \pm \left[4m^2(c^2 - m^2)+(d^2 + c^2 \sin^2\theta - m^2)\right]^{\frac{1}{2}}}{2(c^2 \sin^2\theta - m^2)} \quad . \quad . \quad . \quad . \quad (14)$$

Or approximately, if $d \gg c$. $c \gg m$

$$y \doteq dc\left(\frac{c \sin\theta.\cos\theta \pm m}{c^2 \sin^2\theta - m^2}\right) \quad . \quad . \quad . \quad . \quad . \quad (15)$$

Hence at $\sin\theta = \frac{m}{c}$. or in the case of a parabola

$$y_0 \doteq \frac{d}{m}\left(\sqrt{c^2 - m^2} + c\right)\frac{c^2}{2} \quad . \quad . \quad . \quad . \quad (16)$$

From the foregoing it can be seen that the shape of fringes depends upon the relative positions of the sources A & B with respect to the screen, varying from a straight line when $\theta = 90°$, through hyperbolas, parabolas, and ellipses to circles at $\theta = 0°$. The spacing of the fringes depends upon the relative spacing of the sources, and their distance from the screen.

5. Practical Considerations and Visibility

In practice it is possible to produce interference only by arranging reflecting surfaces or lenses to produce two images of the same source, the wave trains proceeding from these images then being in a condition to interfere. The use of such components will naturally impose a limit upon the field of view, since they are limited in size, and it will be necessary before proceeding further to develope the ideas of field and aperture for an interferometer. The concept is not as simple as in the case of a lens system, since the interferometer has ,strictly speaking, neither object or image plane, but the usual definitions of aperture and field have been used and adapted. (See Ref. 4 for usual definitions.)

5.1 Angular Aperture and Field

The images of all the stops and diaphrams of the system are plotted in the fringe space, which may be termed the image space of the interferometer. (See Fig.4). There will in general be one stop which subtends the smallest angle α at the centre of the image plane. This will be the image of the aperture stop A', and α may be called the angular aperture of the system. The aperture limits the area of the source illuminating any one point in the image plane.

In addition there will be a further stop which will subtend the smallest angle β at the centre of the aperture stop. This will be the image of the field stop F', and the angle β may be termed the angular field of the interferometer. The field obviously determines the portion of the fringe system which will be visible.

3.2. Telecentric Systems

An interesting and useful case occurs when the system is telecentric. This is the system usually employed for the Mach-Zehnder Interferometer.

If a lens is introduced in the image space, at a distance equal to its focal length from the aperture stop, the image of the aperture stop will be located at infinity. (See Fig. 2) The aperture stop A subtends a small finite angle θ at the first nodal point of the lens system L. By the property of nodal points (Ref.2) the image of A, i.e. A' must subtend this same angle at the other nodal point N'. Since A' is at infinity however, it will subtend the same angle θ at any other point of the system, and hence at the centre of the image plane P. Thus by definition, the angular aperture α of the system will be equal to angle θ, the angle subtended by the aperture stop at the nodal point of the lens system L.

Since A' now lies at infinity, the angle subtended by the field stop at the centre of A' will be zero, and thus the angular field ζ=0, although of course the actual size of the field will by no means be zero. This implies that the portion of the field of fringes in view will be infinitely small, but since fringes can be made as close together as desired by altering the spacing of the sources, the fringes over this portion of the field may be taken to be straight lines. This is very useful wherever straight fringes are desired.

3.3 Effect of Aperture on Visibility.

In practice, sources are always of finite aperture, and can be considered as many point sources side by side. Each point source pair will in general produce its own system of fringes which will not generally coincide with the systems produced by any other source pairs. This may cause the fringes to overlap and become blurred or even obliterated, and possibly distorted, and it is necessary to establish conditions under which fringes may be observed.

Visibility will be defined in the same manner as by Michelson (Ref.3)

$$V = \frac{I_{max.} - I_{min.}}{I_{max.} + I_{min.}} \quad . \quad . \quad . \quad . \quad . \quad (17)$$

With finite aperture illumination will no longer be either a maximum or a minimum, but some intermediate value. Each pair of rays will in general have its own phase retardation δ.

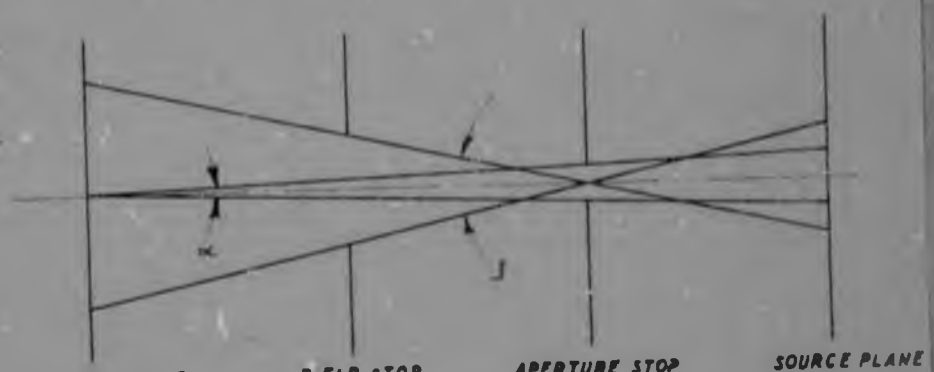

IMAGE PLANE OF THE INTERFEROMETER FIG.1

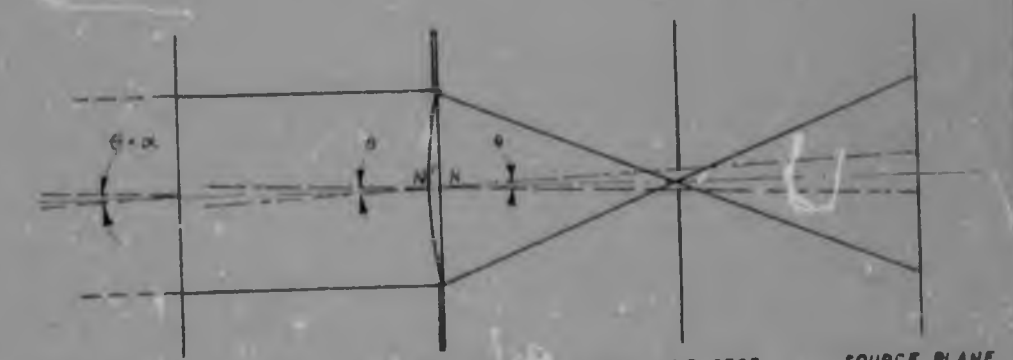

IMAGE PLANE OF A TELECENTRIC SYSTEM. FIG.2

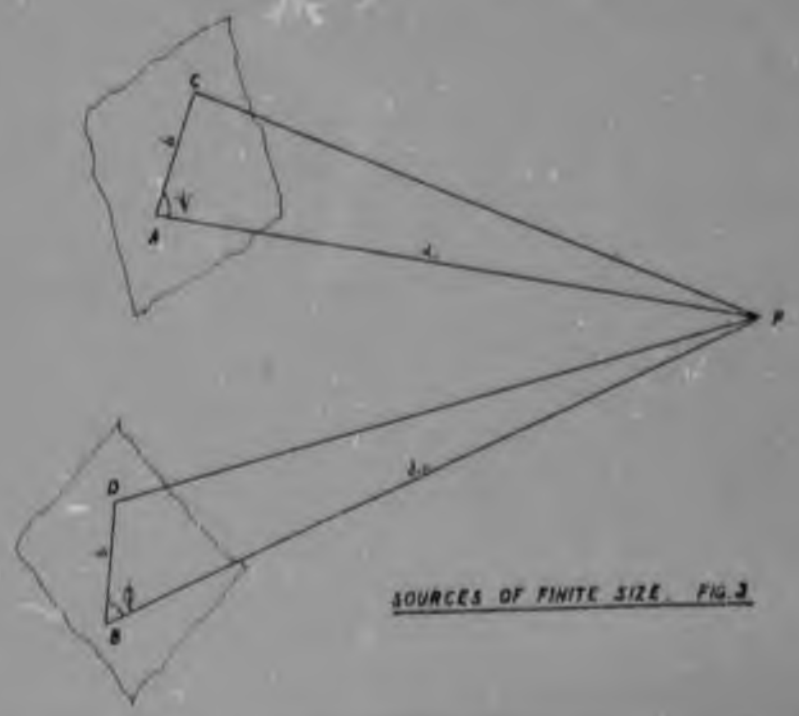

SOURCES OF FINITE SIZE. FIG.3

From equation (3), for each point source

$$I = 2a^2 (1 + \cos \Delta)$$

Integrating over the whole source, the intensity at point P is given by

$$I = 2a^2 \int_{\Delta-\gamma}^{\Delta+\gamma} (1 + \cos \Delta).d\Delta$$

where γ is the maximum increment of Δ over the source.

$$I = 2a^2 (2\gamma + 2 \sin\gamma \cos \Delta)$$

For I a maximum $\Delta = 0, 2\pi$ ...etc.

$$I_{max} = 4a^2 (\gamma + \sin\gamma)$$

For I a minimum, $\Delta = \pi, 3\pi$ ...etc.

$$I_{min} = 4a^2 (\gamma - \sin\gamma)$$

Substituting these values in equation (17)

$$V = \frac{\sin\gamma}{\gamma} \quad . \quad . \quad . \quad . \quad . \quad . \quad . \quad . \quad (18)$$

Which is the same result obtained by Michelson for his interferometer by other means. (Ref.3) It may be noted that equation (18) is quite general, no assumptions having been made as to the means employed to produce interference. In order to obtain the visibility for a given set of conditions it is only necessary to find the maximum path length difference and substitute this in equation (18).

3.4 Position of least Confusion.

Examining equation (18) above, the limit of V as γ approaches zero is unity, so that Visibility is greatest when γ is least. It is useful to see what this implies.

Consider two extended sources (Fig. 3) illuminating a point P on the screen. Since the sources are images of the same object, choosing a reference point in A will fix a corresponding point in B. Similarly a point C in one will have a corresponding point D in the other. If A and C are a distance b apart, and the distances of A and B from P are d_1 and d_2 respectively.

$$\gamma = (PC - PD) - (d_1 - d_2)$$

or rearranging.

$$\gamma = (PC - d_1) - (PD - d_2) \quad . \quad . \quad . \quad . \quad . \quad (19)$$

Assuming now that source A is fixed, but that source B can be tilted, the first term of equation (19) remains constant, while the second depends only on the inclination of B, and can always be made equal to it by suitably rotating B about some axis in its plane, for one particular position of C and D.

Under such conditions, γ will not in general be zero for any other position of C and D, but it can be shown that there will be some inclination of B with respect to A such that γ will be a minimum for all points in the source. This position will give the best visibility of fringes at P, and the system may then be regarded as being in focus. It is interesting to note that each point P will have a condition of focus which is not necessarily the same as that for any other point P' say, and the focus will gradually deteriorate with distance from the centre of the screen.

The exact mathematical treatment of the conditions of focus is very complex, and of little value, since focussing is usually most conveniently carried out by observing the fringes as the instrument is adjusted.

3.5 Optimum source size.

Since it is desirable in practice to use as large a source as possible, it is useful to examinethe effect of source size upon visibility.

Referring again to Fig. 3, we have by the geometry of the figure

$$PC^2 = d_1^2 + b^2 + 2d_1 b \cos\psi$$

$$PD^2 = d_2^2 + b^2 + 2d_2 b \cos\phi$$

From equation (19) we get

$$\gamma = (d_1^2 + b^2 + 2bd_1\cos\psi)^{\frac{1}{2}} - (d_2^2 + b^2 + 2bd_2\cos\phi)^{\frac{1}{2}} - (d_1 - d_2) \quad (20)$$

The terms d_1, d_2, ψ, and ϕ can generally be found from the geometry of the particular interferometer under examination. Since the sources may be considered [illegible] will be the greatest diameter of the source for a [illegible]. Thus γ may be evaluated for typical conditions and substituted in equation (18) to obtain the visibility.

Checking our case, the source image distance is 45cm. For an order of interference of 200

$$d_1 = 45 \qquad d_2 = 45{\cdot}01152 \qquad \lambda = 5760\ \text{Å}$$

Let $\psi = \phi = 88^\circ$

Then for a source size of 5 cm., γ is found to be

$$\gamma = 0{\cdot}000.100$$

Substituting this in equation (18)

$$V = \frac{0{\cdot}000.0998}{0{\cdot}000.1000} = 99{\cdot}8\ \%$$

If $\psi = \phi$, but $\psi = 88{\cdot}5^\circ$ $\phi = 88^\circ$, with the same foregoing conditions,

$$\gamma = 0{\cdot}28?.130$$

$$V = \frac{0{\cdot}279.3614}{0{\cdot}28?.1300}$$

V = 98·6 %

This is similar to the result obtained by Bennet (Ref. 12), who examined an idealised rectangular Mach-Zehnder interferometer, under special conditions.

From these results it is evident that for a correctly focussed interferometer a source of 5cm. or larger could be employed. The limit is usually set by the accuracy with which focussing can be carried out.

4. Fringes in Non-Homogeneous Light

4.1 Effect of Broadening of the Spectral Band

In practice no source emits radiations of a single wavelength, and in order to allow as much light as possible to enter the interferometer, it is desirable to use as broad a spectral band as permissable. It will therefore be necessary to investigate the effect of broadening of the spectral band upon the visibility and fringe spacing.

The width of fringes depends upon wavelength (equation 12a). Thus if a whole series of radiations of different wavelengths are present, each will produce its own system of fringes, differing in fringe width from the other systems. Fringes will overlap and become blurred, and unless the range is small, the fringes may become obliterated.

4.2 Visibility in Non-Homogeneous Light.

Consider two homogeneous beams superimposed on one another, with the same wavelength, but with a constant phase retardation between them.

By equation (3), the resultant intensity is

$$I = 2I_0 (1 + \cos\Delta)$$

If now the beams are composed of a series of wavelengths, the energy distribution of the spectrum being determined by $f(\lambda)$, then the resultant intensity will be the summation of intensities due to each wavelength.

$$I = \int_{\lambda_0}^{\lambda_1} f(\lambda) (1 + \cos\Delta)\, d\lambda \quad . \quad . \quad . \quad . \quad . \quad (21)$$

Following roughly a method used by Michelson in describing his interferometer (Ref. 1 & 3) we proceed as follows.

The phase retardation varies with wavelength according to

$$\Delta = \frac{2\pi}{\lambda} 2m$$

If we write $\lambda = \lambda_0 + \Lambda$

where Λ is an increment in λ

or $\lambda = \lambda_0(1 + \frac{\Delta}{\lambda_0})$

Then we may write

$$I = \int_{\Lambda_1}^{\Lambda_2} f(\Lambda)\left\{1 + \cos\frac{2\pi 2m}{\lambda_0}(1 + \frac{\Delta}{\lambda_0})^{-1}\right\}d\Lambda$$

This integral cannot be solved as it stands, but may be approximated to by Taylors expansion.

writing

$$(1 + \frac{\Delta}{\lambda_0})^{-1} = (1 - \frac{\Delta}{\lambda_0}) + ...$$

and neglecting higher powers of $\frac{\Delta}{\lambda_0}$, we have

$$I = \int_{\Lambda_1}^{\Lambda_2} f(\Lambda)\left\{1 + \cos\frac{2\pi 2m}{\lambda_0}(1 - \frac{\Delta}{\lambda_0})\right\}d\Lambda \quad . \quad . \quad .(22)$$

Expanding

$$I = \int_{\Lambda_1}^{\Lambda_2} f(\Lambda)d\Lambda + \cos\frac{2\pi 2m}{\lambda_0}\int_{\Lambda_1}^{\Lambda_2} f(\Lambda)\cos(\frac{2\pi 2m}{\lambda_0^2}\Lambda)d\Lambda + \sin\frac{2\pi 2m}{\lambda_0}\int_{\Lambda_1}^{\Lambda_2} f(\Lambda)\sin(\frac{2\pi 2m}{\lambda_0^2}\Lambda)d\Lambda$$

Now for I a minimum $2m = 1\ \lambda_0,\ 3/2\ \lambda_0 \ldots (\frac{2n-1}{2})\lambda_0$

$$I_{min} = \int_{\Lambda_1}^{\Lambda_2} f(\Lambda)\left\{1 - \cos(2n-1)\pi\frac{\Delta}{\lambda_0}\right\}d\Lambda \quad . \quad . \quad . \quad (23)$$

And for I a maximum $2m = 0,\ \lambda_0, \ldots n\lambda_0$

$$I_{max} = \int_{\Lambda_1}^{\Lambda_2} f(\Lambda)\left\{1 + \cos 2n\pi\frac{\Delta}{\lambda_0}\right\}d\Lambda \quad . \quad . \quad . \quad . \quad (24)$$

If $f(\Lambda)$ is known, the integrals above may be evaluated and substituted into equation (17) to obtain the visibility.

A.) Approximate single spectrum line.

Although the spectrum lines of most gas discharges more readily resemble the Gaussian intensity function, it is often useful to roughly check visibility by assuming the line to be of a square shape with an abrupt drop of intensity on either side.

In this case $f(\Lambda) = 2a^2$

and $\Delta\Lambda = \lambda - \lambda_0$

λ_o being the wavelength of the line

If the spectral half line width is $\mathcal{J}$ equations (23) and (24) become

$$I_{max} = 2a^2 \int_{-\mathcal{J}}^{+\mathcal{J}} \left\{ 1 + \cos 2n\pi \frac{\Delta}{\lambda_o} \right\} d\Delta$$

$$= 4a^2 \left\{ \mathcal{J} + \frac{\lambda_o}{2n\pi} \sin 2n\pi \frac{\mathcal{J}}{\lambda_o} \right\}$$

$$I_{min} = 2a^2 \int_{-\mathcal{J}}^{+\mathcal{J}} \left\{ 1 - \cos(2n-1)\pi \frac{\Delta}{\lambda_o} \right\} d\Delta$$

$$= 4a^2 \left\{ \mathcal{J} - \frac{\lambda_o}{(2n-1)\pi} \sin(2n-1)\pi \frac{\mathcal{J}}{\lambda_o} \right\}$$

Visibility then is given by

$$V = \frac{\frac{1}{2n\pi} \sin 2n\pi \frac{\mathcal{J}}{\lambda_o} + \frac{1}{(2n-1)\pi} \sin(2n-1)\pi \frac{\mathcal{J}}{\lambda_o}}{\frac{1}{2n\pi} \sin 2n\pi \frac{\mathcal{J}}{\lambda_o} - \frac{1}{(2n-1)\pi} \sin(2n-1)\pi \frac{\mathcal{J}}{\lambda_o} + 2\frac{\mathcal{J}}{\lambda_o}} \quad . \quad (25)$$

If n is very large $(2n-1) \doteq 2n$ and the expression simplifies to

$$V = \frac{\frac{1}{2n\pi} \sin(2n\pi \frac{\mathcal{J}}{\lambda_o})}{\frac{\mathcal{J}}{\lambda_o}} \quad . \quad . \quad . \quad . \quad . \quad . \quad . \quad (26)$$

n represents the number of phase retardations and corresponds to the number of fringes counted from the fringe produced by zero phase difference i.e. the central fringe. (This is also called the zero fringe by some authors)

Visibility varies inversely with the fringe number, decreasing as n increases, and thus the visibility of the fringes diminishes for fringes further from the central fringe. Only a limited number of fringes will be distinguishable. ~~(The visibility is also dependent on the line width which contains n, and hence the visibility is periodic, groups of fringes being more distinct than their neighbours)~~

Supposing that the required number of fringes is 400, i.e. n=200, λ_o = 5760 Å and the line half width $\mathcal{J}$ = 4 Å

then from equation (25) the Visibility is found to be V = 0·487, which is just about the minimum to give a sufficient contrast for photography.

4.4 Gaussian Intensity Function Line

While spectrum lines of gas discharges under conditions of high temperature and pressure are known to have envelopes differing somewhat from the Gaussian intensity function, this function will none the less give a sufficiently accurate picture of lines generally met with in Gas discharge tubes employed for interferometric work.

In this case $f(\Lambda) = e^{-k^2\Lambda^2}$

It will be considerably simpler to integrate equation (22) directly.

We have

$$I = \int_{-\infty}^{+\infty} e^{-k^2\Lambda^2} \left\{ 1 + \cos \frac{4m\pi}{\lambda_0} \left(1 - \frac{\Lambda}{\lambda_0} \right) \right\} d\Lambda$$

The constant k is usually very large and therefore the error introduced by writing the lower limit of Λ as $-\infty$ instead of $-\lambda_0$ will be extremely small when it is considered that λ_0 is of the order of 5000.

By Fierce Integral No. 492

$$I = \frac{\pi^{\frac{1}{2}}}{k} + \int_{-\infty}^{+\infty} e^{-k^2\Lambda^2} \cos \frac{2m2\pi}{\lambda_0} \left(1 - \frac{\Lambda}{\lambda_0} \right) d\Lambda$$

$$= \frac{\pi^{\frac{1}{2}}}{k} \left\{ 1 + e^{-\frac{\pi^2(2m)^2}{\lambda_0^4 k^2}} \cdot \cos \frac{2m2\pi}{\lambda_0} \right\} \quad . \quad . \quad . \quad . \quad (27)$$

Then for I a minimum $2m = \frac{1}{2}\lambda_0, 3/2\,\lambda_0, \ldots (\frac{2n-1}{2})\lambda_0$

$$I_{min} = \frac{\pi^{\frac{1}{2}}}{k} \left\{ 1 - e^{-\frac{\pi^2(2n-1)^2}{4\lambda_0^2 k^2}} \right\}$$

And for I a maximum $2m = 0, \lambda_0, \ldots n\lambda_0$

$$I_{max} = \frac{\pi^{\frac{1}{2}}}{k} \left\{ 1 + e^{-\frac{\pi^2 n^2}{\lambda_0^2 k^2}} \right\}$$

Substituting these values into the Visibility equation (18) we get

$$V = \frac{e^{-\frac{\pi^2 n^2}{\lambda_c^2 k^2}} + e^{-\frac{\pi^2 (2n-1)^2}{4\lambda_c^2 k^2}}}{2 + e^{-\frac{\pi^2 n^2}{\lambda_c^2 k^2}} - e^{-\frac{\pi^2 (2n-1)^2}{4\lambda_c^2 k^2}}} \quad . \quad . \quad (28)$$

If n is very large this approximately reduces to

$$V \doteq e^{-\frac{\pi^2 n^2}{\lambda_c^2 k^2}} \quad . \quad . \quad . \quad . \quad . \quad . \quad . \quad (29)$$

Using the same values as for the previous example. V = 0·765 which is considerably better than the value obtained before.

Bennet (Ref. 11) using a different definition of visibility obtained a similar result for the particular case of an idealised Mach-Zehnder Interferometer. It may be noted that the above treatment requires no specific conditions for producing interference, and equations (28) and (29) can be applied directly to any interferometer.

4.5 Error in Fringe Spacing due to Inhomogeneous Light

To obtain an expression for Visibility in the previous section it was assumed that maxima and minima of intensity appeared where $2m = 2n\lambda_c$ and $(2n-1)\lambda_c$ respectively. This is not strictly accurate since the fringes due to the various wavelengths are not evenly ranged on either side of those due to the mean wavelength, those due to the maximum wavelength being further from the mean than those due to the minimum wavelength. Thus the position of the fringe is displaced slightly towards the end due to the higher wavelength. Such a displacement would disturb the even spacing of the fringes and may lead to error in evaluation where displacements of straight fringes must be measured. The error can be evaluated by integrating equation (27) with respect to y.

For a maximum or minimum $\frac{dI}{dy} = 0$

This implies that $\text{Tan}\,\frac{2\pi.2m}{\lambda_c} = -\frac{2\pi.2m}{4\beta k^2}$ from equation (27)

Writing

$$\alpha = \frac{2\pi.2m}{\lambda_c} \quad \text{and} \quad \beta = 4\lambda_c^2 k^2$$

Then

$$\text{Tan}\,\alpha = -\frac{\alpha}{\beta}$$

This can be evaluated providing that $\frac{\alpha}{\beta}$ is small by assuming $\alpha = n\pi - \varepsilon$ where ε is small

Hence

$$\text{Tan}\,\varepsilon = \varepsilon = \left(\frac{n\pi}{\beta} - \frac{1}{\beta}\right)$$

$$\text{or} \quad \epsilon = \frac{n\pi}{1-\beta} \qquad . \quad (30)$$

$$\text{and} \quad \alpha = n\pi\left(\frac{\beta}{1+\beta}\right) \qquad . \quad (31)$$

Substituting for α and β we obtain

$$\frac{2\pi \cdot 2m}{\lambda_0} = n\pi\left\{\frac{4\lambda_0^2 k^2}{1+4\lambda_0^2 k^2}\right\}$$

$$2m = \frac{n\lambda_0}{2}\left\{\frac{4\lambda_0^2 k^2}{1+4\lambda_0^2 k^2}\right\}$$

Substituting for n from equation (12) we obtain

$$y_0 = \frac{nd\lambda_0}{2e}\left\{\frac{4\lambda_0^2 k^2}{1+4\lambda_0^2 k^2}\right\} \qquad . \quad (32)$$

where only maxima and minima are considered.

This value of y_0 is greater than equation (12) by a factor ξ where

$$\xi = \frac{4\lambda_0^2 k^2}{1+4\lambda_0^2 k^2} \qquad . \quad (33)$$

Considering the line $\lambda_0 = 5760$ Å and of half width at half intensity $\Lambda_\beta = 4$ Å

$$k^2 = \frac{\log_e 2}{\Lambda_\beta^2}$$

$$\text{and} \quad \xi = \frac{4\lambda_0^2 \log_e 2}{\Lambda_\beta^2 + 4\lambda_0^2 \log_e 2}$$

which on evaluation becomes

$$\xi = \frac{71,796,800}{71,796,812}$$

The error is entirely negligible, and it may be concluded that no error will be introduced into evaluation of interferograms due to a non-homogeneous source.

This again tallies with the conclusions of Bennet (Ref 11)

4.6 White Light Fringes

If ξ becomes large the approximations used in the foregoing are no longer valid. However it is obvious that visibility will drop off very rapidly after only a few orders of n, only about 10 fringes being observed in practice. This is very useful in setting up and will be referred to again later.

4.7 Visibility with a Doublet

Consider a doublet, with predominant wavelengths λ_1, λ_2, and widths $\delta\lambda_1$ and $\delta\lambda_2$, energy $2a_1^2$ and $2a_2^2$, or the relative energy of the one to the other $a_1^2/a_2^2 = \gamma$

Then

$$I_{min.} = 2a_1^2 \left[\xi_1 - \frac{1}{(4n-2)\pi} \sin(4n-2)\pi\xi_1 \right] + 2a_2^2 \left[\xi_2 - \frac{1}{(4n-2)\pi} \sin(4n-2)\pi\xi_2 \right]$$

And

$$I_{max.} = 2a_1^2 \left[\xi_1 - \frac{1}{4n\pi} \sin 4n\pi\xi_1 \right] + 2a_2^2 \left[\xi_2 - \frac{1}{4n\pi} \sin 4n\pi\xi_2 \right]$$

The visibility then is given by

$$V = \frac{\sin 4n\pi\xi_1 + \gamma \sin 4n\pi\xi_2}{4n\pi\left[\xi_1 + \gamma\xi_2\right]}$$

In general, for r lines

$$V = \sum_{i=0}^{r} \frac{\gamma_i \sin 4n\pi\xi_i n}{4n\left[\sum_{i=0}^{r} \gamma_i \xi_i\right]}$$

The solution applies only in the plane of least confusion or for two perfect point sources. For an extended source, the above value must be multiplied by that found in Section 3.3.

The general solution is a Fourier series, and with certain spectra may give rise to groups of fringes with higher visibility than their neighbours. This phenomenon is observed with unfiltered mercury vapour light.

Chapter 2

Mach-Zehndar Interferometer Theory

1. Characteristics of the Interferometer

Although a number of interferometers have been utilised for density evaluation, the one due to Zehnder and L.Mach is by far the most suitable for wind tunnel applications as it allows simultaneous density measurement over the whole field, without traversing the test section twice, which would introduce large refraction errors. All the theory of the foregoing chapter applies directly to the Mach-Zehnder interferometer, and will here be extende to describe the practical operation of the instrument.

1.1 Description of the Elements.

The layout of the optical system is shown in Fig.4. S is the light source, filtered to obtain monochromatic light. L_1 is the collimator lens usually introduced to produce a telecentric system. O is the object plane, or the position of the wind tunnel, and L_2 serves to focus the object plane and the fringes, which are localised in the object plane onto the screen or photographic plate P. The interferometer itself consists of 4 mirrors, arranged at the corners of a rectangle, as shown. Mirrors 1 and 2 are only lightly silvered to partly reflect and partly transmit light, and act as"beam splitters". Mirrors 3 and 4 are first surface mirrors. The light entering the interferometer is split into two beams at mirror 1, recombining at mirror 2, these two beams are in a condition to interfere producing fringes at P. The interferometer is in effect an extended form of the Jamin refractometer with the two beams separated further, thus giving a much larger field of view. The four mirrors can be tilted about horizontal and vertical axes and mirrors 3 and 4 may be traversed along the path of the light beams.

1.2 Linear Interferometer Theory

In the theoretical approach of the last chapter the interaction of wave trains from two coherent sources was described. In order to apply this to the Mach-Zehnder

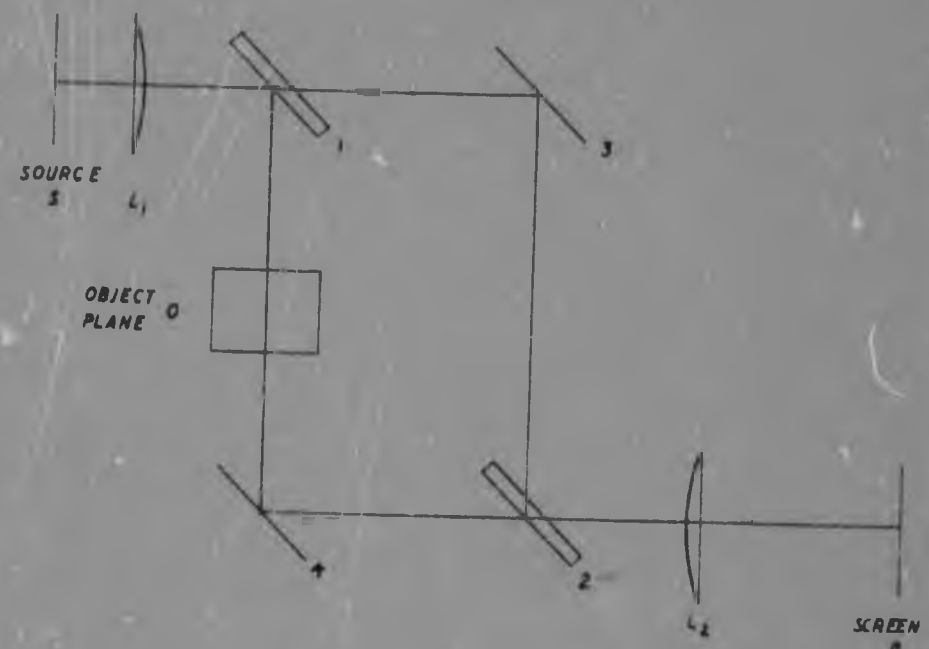

ELEMENTS OF THE INTERFEROMETER FIG. 4

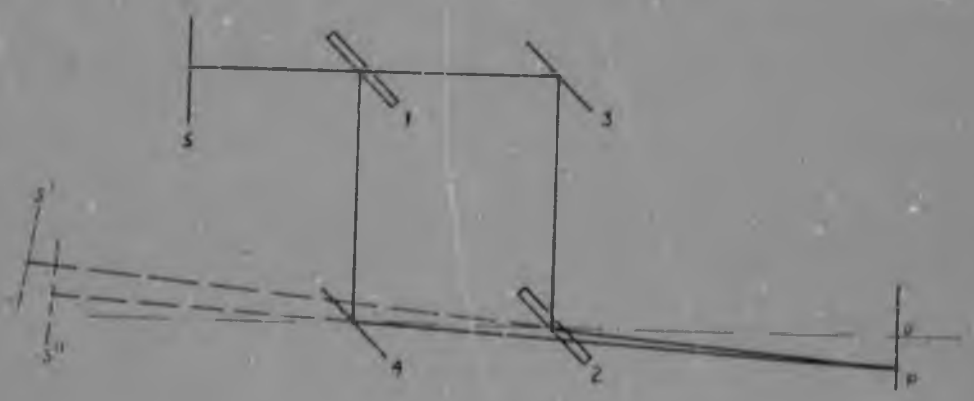

LINEAR ANALOGY FIG 5

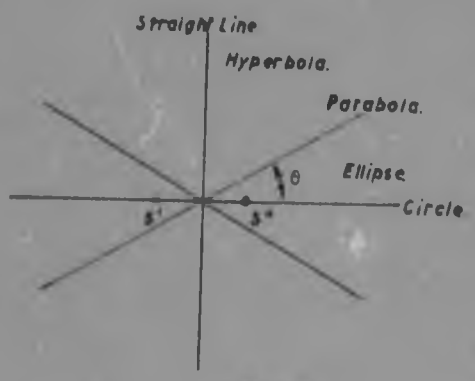

FIG. 6.

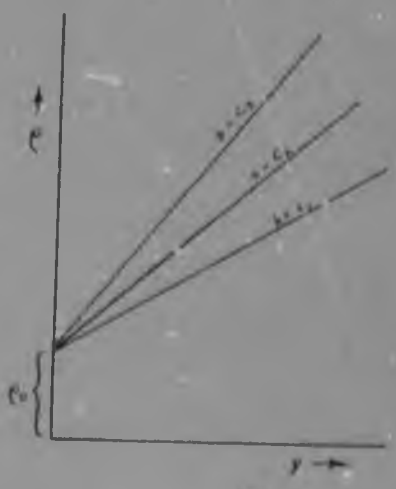

FIG. 7

instrument it is only necessary to trace back the rays through the interferometer and locate the two virtual images of the source. The whole instrument may then be replaced by the analogy of these source images. If we consider the mirrors 1 and 2 slightly tilted, i.e. no longer parrallel to mirrors 3 and 4 , and then trace back the rays as shown in Fig.5 the positions of the source images S' and S" due to the two beams can easily be established by simple geometric considerations. In most applications it is not necessary to determine the exact locations of S' and S", but only to visualise their relative positions. If the effect of the controls of the various mirrors on the positions of the source images is known, then it is possible to replace the interferometer by its analogy in order to understand the adjusting technique.

1.3 Effect of the Controls.

It can be seen (Fig. 5) that mirrors 1 and 3 effect the position of the source image S', and that mirrors 2 and 4 effect the position of the source image S". There are three possible adjustments to the mirrors, each of which will now be considered.

(i) Rotation about a Vertical Axis.

If a mirror is rotated about its vertical axis, the respective source image will also be rotated about the same axis in a horizontal plane, but through twice the angle. In the case of mirrors 1 and 4 the source image will rotate about the image of the mirror axes in mirrors 3 and 2 respectively. The nett effect is a horizontal displacement, combined with a slight tilting of the image plane about a vertical axis.

(ii) Rotation about a Horizontal Axis.

If a mirror is tilted about its horizontal axis, the respective source image will also rotate about this axis (or its image, as above). In this case, since the mirrors are aligned at 45° to the optical axis, the nett effect on the source image will be a vertical movement, combined with a slight tilting of the image plane about the mirror axis. A small horizontal movement and a very small tilt about a vertical axis will also be present.

(iii) Mirror Traverse

If mirrors 3 or 4 are traversed without rotation the respective source images will move in a line normal to

the mirrors i.e. at 45° to the optical axis, remaining parallel to itself. The nett result is a movement towards or away from the screen combined with an equal horizontal displacement. The image plane is not tilted.

Unfortunately these movements are not as simple as may be desired for quick and easy adjustment of the relative positions of the source images, but the source images can at least be adjusted independently, which is a considerable advantage.

1.4 Focussing.

It has been indicated in Chapter 1 (Sect. 7.4) that the fringes are in focus on the screen only when the source images are inclined at the proper relative angle to each-other. Hence, if we consider S' as fixed for the moment, then for a particular source spacing i.e. for a particular position of S", S" must be inclined at the proper angle relative to S' to bring the fringes into focus on the screen. Tilting S" to the proper angle without changing its position can be accomplished by rotation of mirrors 3 and 4. If mirror 3 is rotated, S" will move laterally, and will also be tilted. Mirror 4 can then be rotated in such a way that S" is returned to its original position. Since S" has now been rotated about a shorter radius however, the tilt due to rotation of mirror 3 will not be equal to the tilt due to rotation of mirror 4 and the nett result will be a residual tilt of the source image S". If the process is carried out in the right direction the source image S" may be tilted in any way and to any degree to obtain focus. It may be noted that for adjustment about horizontal mirror axes there will in addition be a small residual horizontal displacement, which of course alters the source image positions relative to one another slightly, and must be compensated for.

Focussing could have been carried out on source image S' by tilting mirrors 1 and 2, or by moving both sources keeping their spacing constant, but altering their relative inclinations. Thus focussing can be carried out using any two mirrors, the most rapid effect being produced by adjusting mirrors 1 and 2, since the difference of their distances from the source images, and therefore the radii of rotation, is greatest.

1.5 Adjustement of fringe shape and spacing

The fringe shape and spacing has been shown to be dependant on the relative positions of the sources (Chap. 1 Sect. 3.2). Spacing of the fringes is dependent on the source image spacing 2e, and the fringes are circles, ellipses, parabolas, hyperbolas, or straight lines as the angle θ (see Chap.1 Sect.2.1) varies from 0° through 90°. (Fig.6) Adjustement of the source image spacing and relative position can be carried out in a manner similar to focussing. Referring to Section 1.4 on focussing, if mirror A were rotated in such a way that A' is returned ot its original inclination instead of its original position, then the nett result of the adjustements will be a lateral displacement of the source image, without altering the conditions of focus. By traversing one of the mirrors the source images can be moved nearer or further from the screen, and thus any desired relative position of the source images can be achieved with any desired focus conditions. The movement of the source images is not simple so that a considerable amount of skill is involved in adjustement. Only experience will indicate which adjustment is indicated for a desired result.

It may be noted that when θ is adjusted to 90° by suitable traversing of the mirrors, then the source images are equidistant from the screen and the path length difference is zero. Thus the white light fringes will appear. When using non-monochromatic light it is necessary to adjust for the white light fringe since the visibility here is greatest, only a limited number of fringes being observable on either side as explained in Chapter 1 (Sect.4.3)

If the system is telecentric (Sect. 3.2 Chap.1) all the fringes except those for extremely small angles of θ will appear to be straight. For small θ only two or three fringes will be in view at the same time due to the small field angle of the system. Thus curved fringes can only be observed if the system is not telecentric, and if the field angle is quite large.

If in addition to adjusting the source images to be equidistant from the source (i.e. $\theta = 90^{\circ}$) the source images are made parallel, then the phase retardation over the field will be constant and the whole field will be light or dark. This is termed infinite interference, since it may be regarded as the limiting case of infinitely wide fringes. This case is very useful and will be reffered to again later.

2. Formation of interferograms

2.1 Displacements of fringes

Hitherto it has been assumed that the medium in which the interferometer is placed is homogeneous, and of uniform refractive index. If a density disturbance is now introduced into the one beam of the interferometer, the optical path length of that beam will alter and the phase retardation between the two beams will be changed. Now the fringe width has been shown to depend upon the phase retardation (Chap. 1 sect. 3.2) and hence the fringes will be displaced. If the density disturbance is not uniform, but can be described in terms of co-ordinates y and z perpendicular to the light path, then the degree of fringe displacement will also be a function of y and z, and by evaluating the fringe displacement over the whole field, it is possible to calculate the density distribution over the field. The fringe displacements will be due to a summation of all the density fields encountered, so that only strictly two-dimensional or axially symmetric phenomena can be evaluated.

The displaced fringe pattern can be photographed and is termed an interferogram.

2.2 Evaluation of finite fringes.

Considering a two dimensional density disturbance, the relation between fringe shift and density disturbance may be established as follows:

If a ray passes through a length ℓ in the medium, first with refractive index μ and then again with refractive index μ_0 the optical path difference will be

$$\Delta = (\mu - \mu_0)\ell$$

If the surrounding medium has a refractive index μ_0, Δ becomes

$$\Delta = \frac{\mu - \mu_0}{\mu_0}\ell$$

$$= \frac{\mu - \mu_0}{\lambda_v}\ell\lambda_0 \quad . \quad . \quad . \quad . \quad . \quad . \quad (34)$$

where λ_v is the wavelength of the light in a vacuum and λ_0 the wavelength in the medium of refractive index μ_0

Now the co-ordinate of a fringe is

$$y_0 = \frac{\lambda d}{2a}$$

The breadth of a fringe b then is

$$b = \frac{\lambda_0 d}{2a}$$

Thus $$\frac{y}{b} = \frac{\Delta}{\lambda_0} \quad . \quad . \quad . \quad . \quad . \quad . \quad . \quad (35)$$

Now the Gladstone-Dale law states that

$$\frac{\mu - 1}{\rho} = \text{Constant} = k$$

where ρ is the density and k the Gladstone-Dale constant Rewriting we get

$$\frac{y}{b} = \frac{\mu - \mu_0}{\lambda_0} l$$

and $$\rho = \rho_0 \left(1 + \frac{\lambda_0}{k l (\mu_0 - 1)} \frac{y}{b} \right)$$

or $$\rho = \frac{\rho_0 \lambda_0}{k l (\mu_0 - 1)} \frac{y}{b} + \rho_0 \quad . \quad . \quad . \quad (36)$$

Equation (36) is of the form

$$\rho = A \frac{y}{b} + \rho_0$$

where A and ρ_0 are constants for a given set of test conditions, depending only on the conditions of the ambient air. Hence a series of calibration curves can be drawn, each for a given value of b, from which the density can readily be read off for corresponding values of y. (Fig. 7)

The graphical method has been found considerably faster than the calculations of Hershader and Pinkler (Ref. 8 & 6)

2.3 Evaluation of Infinite Fringes

In this case a density disturbance will produce fringes which are loci of equal density i.e. isopycnals, and the whole interferogram may be evaluated by calculating the density change per fringe, and numbering the fringes from an area of known density.

Now we have by equation (34)

$$\frac{\Delta}{\lambda_0} = \frac{\mu - \mu_0}{\lambda_0} l$$

or for a phase retardation of n wavelengths $\Delta = n\lambda_0$

$$n = \frac{\mu - \mu_0}{\lambda_0} l$$

The Gladstone-Dale expression may be written

$$\mu - \mu_0 = k(\rho - \rho_0)$$

and hence

$$(\rho - \rho_0) = \frac{\lambda}{Kl} \frac{n}{} \quad . \quad . \quad . \quad . \quad . \quad (37)$$

The density change per fringe or isopycnal will be

$$\delta\rho = \frac{\lambda}{Kl} \quad . \quad . \quad . \quad . \quad . \quad . \quad (38)$$

By counting fringes from an area of known density the density may be evaluated from equations (37) or (38)

3.4 Axially Symmetric Phenomena

If the flow is not strictly two dimensional, then the evaluation becomes possible only in cases with simple symmetry, such as axially symmetric phenomena, e.g. a cone in a circular jet. The method of solution entails splitting the circular field into a large number of rings, and solving each ring in turn, beginning with the outer one. This staircase radial density function method was first used by Schardin, and is very laborious, involving the use of a table of 5000 coefficients. (see Ref. 6 & 9) More complicated flows have not yet yeilded to solution.

5 Errors in Evaluation

5.1 Zero Errors

Due to the fact that the optical components of the interferometer are not perfectly finished, the undisturbed fringes will not be perfectly straight, which will introduce errors into evaluation. In addition, any vibration or drifting of the fringes when the nozzle is running will add further errors. The order of these errors can be estimated by calculating the density change per fringe shift.

From equation (36) we have

$$\frac{(\rho - \rho_0)}{\rho_0} = \frac{\lambda_0}{l(\mu_0 - 1)} \frac{Y}{} \quad . \quad . \quad . \quad (39)$$

or

$$\frac{(\rho - \rho_0)}{\rho_0} = \frac{\lambda_0}{l K \rho_0} \frac{Y}{b} \quad . \quad . \quad . \quad (40)$$

where $\frac{\rho - \rho_0}{\rho_0}$ and $\frac{y}{b}$ may be expressed as percentages. Since λ_0 or K_0 depend upon the density, it is evident that a high density wind tunnel will minimise the error, for this reason, a tunnel operating at a high Mach number will generally involve a greater zero error than one operating at a moderate Mach number. Errors may also be reduced by using a shorter wavelength of light or a larger wind tunnel.

3.2 Error due to boundary layer

It is impossible to produce a truly two dimensional disturbance, since the moving air confined by a solid boundary implies the existence of a boundary layer. Since the light ray integrates the various densities traversed, it is necessary to allow for the boundary layer effect. Hershader has given the calculation, which is reproduced here. (Ref.8)

The usual method of calculation of density follows from equation (36) which may be written

$$\rho' - \rho_0 = \frac{\lambda}{lK_0} \frac{y}{b}$$

where ρ' is the observed density

If now a boundary layer of thickness ϵ is considered, in which the density distribution is given by $\rho(z)$, and writing $l - 2\epsilon = l_1$

Then

$$\frac{y}{b} \lambda_0 = K_0(\rho' - \rho_0)l \quad . \quad . \quad . \quad . \quad (41)$$

and

$$\frac{y}{b} \lambda_0 = K_0(\rho' - \rho_0 l_1 + 2K_0 \int_0^{\epsilon} \{\rho(z) - \rho_0\}.dz$$

where ρ is the true density

Since the boundary layer density $\rho(z)$ is less than ρ we may write

$$\rho(z) = \rho - \overline{\gamma}\rho(z)$$

where $\overline{\gamma}$ denotes an increment

Then

$$\frac{y}{b} \lambda_0 = K_0(\rho - \rho_0)l - 2K_0 \int_0^{\epsilon} \overline{\gamma}\rho(z).dz \quad . \quad (42)$$

Equating equations (41) and (42) we have

$$\rho - \rho' = \frac{2}{l} \int_0^{\epsilon} \overline{\gamma}\rho(z).dz \quad . \quad . \quad . \quad . \quad (43)$$

The correction integral of equation (43) may be evaluated from theoretical considerations. Alternatively if the density profile in the boundary layer can be found by use of the interferometer, the function $\tilde{\varrho}(z)$ can be plotted and the integral found by measuring the area under the curve.

Errors due to Refraction

The existence of large density gradients in the flow normal to the light direction will cause a certain amount of refraction. The light beam will be deflected, and will traverse a different density configuration than it would have if the beam had not been refracted. This is shown in an exaggerated manner in Fig. 10. However by Fermats principle it is known that the unrefracted ray and the refracted ray will both traverse the same optical path length and arrive at the same point on the screen A', providing that they originated at the same point. Thus the only important considerations are (i) image distortion, and (ii) the difference of the optical path length within the channel.

Hershader (Ref. 8) has given the relevant theory which is briefly reproduced here.

(i) In order to evaluate image distortion it is necessary to calculate the distance EB (Fig. 10), E being the point from which the rays appear to emanate.

Assuming that the density gradient is sufficiently uniform to consider the radius of curvature through the test section uniform, and that this radius is much larger than ℓ, then we have by the geometry of Fig. 10

$$\sin \xi = \frac{\ell}{R}$$

$$\tan \frac{\xi}{2} = \frac{AD}{R} = \frac{(\frac{\ell}{2} + \eta)}{R}$$

$$\tan \xi = \frac{\zeta}{\eta} = \frac{\ell}{(R^2 + \ell^2)^{\frac{1}{2}}}$$

where $EB = \zeta$ $BD = \eta$

Hence

$$\zeta = \frac{R\ell}{(R^2 - \ell^2)^{\frac{1}{2}}} \left(\tan \frac{\xi}{2} - \sin \xi \right)$$

Now $\ell << R$, and it is possible to neglect ℓ^2 compared to R^2. Expanding the term in brackets up to ξ^3 we get

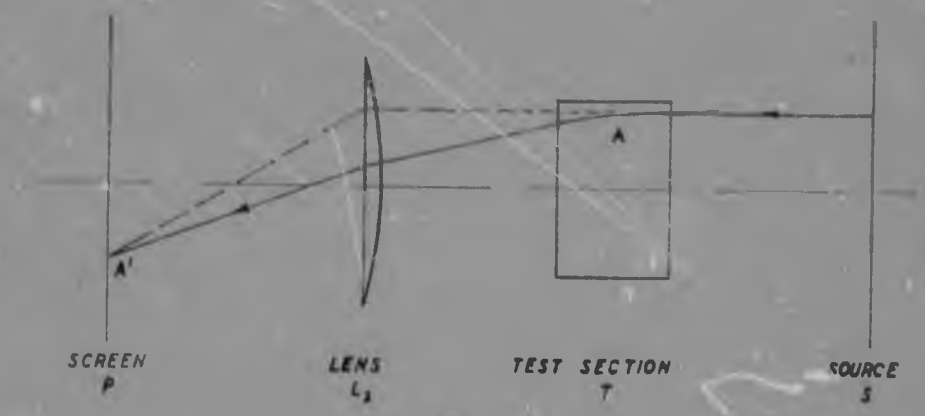

REFRACTION EFFECTS FIG. 8

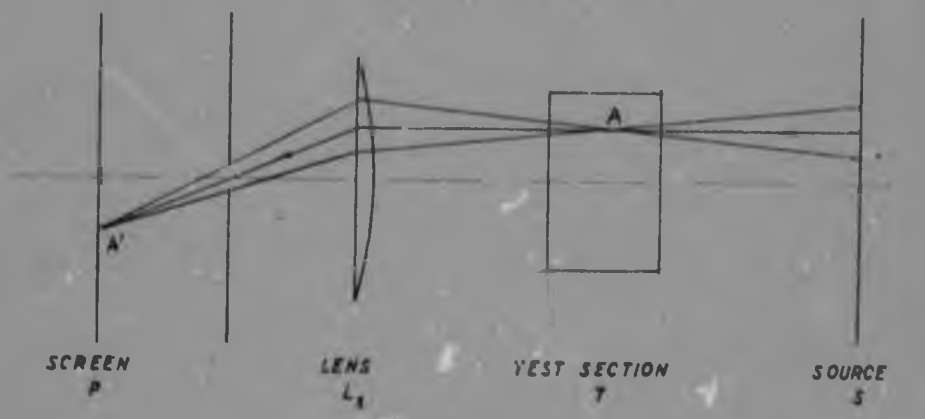

NON-PARALLEL LIGHT EFFECTS FIG 9



FIG. 10

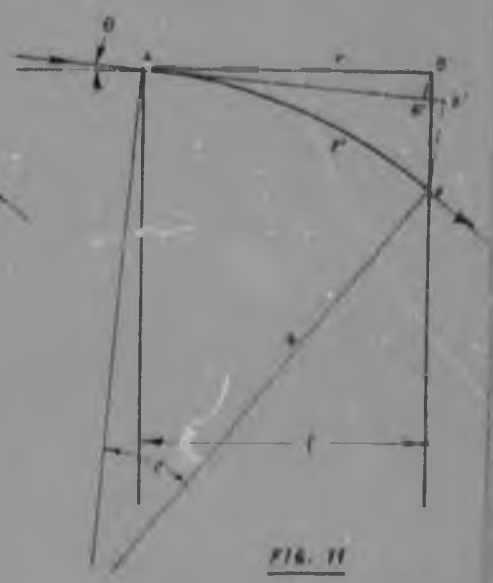

FIG. 11

We get

$$\xi = \frac{\varepsilon^3 l}{8} = \frac{l^4}{8R^3}$$

Now Heath (Ref. 15) has given the relation for a non-homogeneous medium

$$\frac{1}{R} = \frac{d}{dy} \log \mu$$

where y is in the direction of greatest gradient.

$$\frac{1}{R} = \frac{1}{\mu} \text{ grad } \mu$$

and

$$\xi = \frac{l^4}{8} \cdot \frac{\mu^3}{\text{grad}^3 \mu} \quad . \quad . \quad . \quad . \quad . \quad . \quad (44)$$

This equation will be discussed further.

(ii) To calculate the optical path difference we may proceed as follows

Length $AF = R.\varepsilon$

$$= l + {}^1/_6 \, R.\varepsilon^3$$

Now the distance PP' will be given by

$$PP' = R - (R^2 - z^2)^{\frac{1}{2}}$$

where z is the distance of P from A

Since $R \gg z$

$$PP' = \frac{z^2}{2R}$$

The average deviation $\bar{\delta}$ of the ray from the path AC will then be

$$\bar{\delta} = \frac{\int_0^l \frac{z^2}{2R} \, dz}{\int_0^l dz}$$

$$\bar{\delta} = \frac{l^2}{6R}$$

The average refractive index along the path therefore is

$$\mu_1 + \frac{l^2}{6R} \text{ grad } \mu$$

and the difference in optical path due to refraction will be

$$\Delta = (\mu_1 + \frac{l^2}{6R} \text{ grad } \mu)(l + \frac{R\varepsilon^3}{6}) - \mu_1 l$$

where μ_1 is the refractive index along AB

Writing $\varepsilon = \frac{l}{R}$ and $\frac{1}{R} = \frac{1}{\mu_1} \text{ grad } \mu$ we obtain

$$\Delta = \frac{l^2}{6\mu_1} \text{ grad}^2 \mu \left(2 + \frac{l^2}{6\mu_1} \text{ grad}^2 \mu \right)$$

the grad μ is in general very small so that the last term may be neglected.

$$\Delta = \frac{l^3}{3\mu_1} \text{ grad}^2 \mu \quad . \quad . \quad . \quad . \quad . \quad (45)$$

$$\Delta = \frac{K^2 l^3}{3(K\rho_1 + 1)} \text{ grad}^2 \rho$$

This produces an extra fringe shift $\frac{\Delta}{\lambda_0}$, and the observed density will be increased by an amount

$$\partial\rho = \frac{\Delta}{Kl}$$

Expressing this as a percentage

$$\frac{\partial\rho}{\rho_1} = \frac{Kl^2}{3(K\rho + 1)\rho_1} \text{ grad}^2 \rho \quad . \quad . \quad . \quad (46)$$

grad ρ can be evaluated by measuring observed increments on an interferogram

The method is not exact, the greatest objection being that the density gradient is assumed to be constant. However the density profiles do not change rapidly enough over the small range through which refraction occurs to warrant the extra mathematical complication of an exact method. the calculation will in any case indicate the order of error involved.

3.4 Error Due to Divergent Light

If the source has a finite size, all the rays passing through a point in the focal plane of the channel will not traverse the same path, and hence in the region of high density gradients, will not traverse the same density field. This is illustrated in Fig. 9

The rays outside the channel will again have the same optical path length by Fermat's Principle. Since the greatest angle of deviation is small, it is logical to assume that that the various rays will appear to proceed from very nearly the same point. It is thus only necessary to examine the additional phase retardation due to a ray being inclined at a small angle to the optical axis. A method of calculating the optical path length of such a ray has been devised, and proceeds as follows.

If AB represents the direction parallel to the optical axis and normal to the greatest density gradient (see Fig. 11)

Now grad μ is in general very small so that the last term may be neglected.

$$\Delta = \frac{l^3}{3\mu_1} \text{grad}^2 \mu \quad . \quad . \quad . \quad . \quad . \quad . \quad (45)$$

$$\Delta = \frac{K^2 l^3}{3(K\rho_1 + 1)} \text{grad}^2 \rho$$

This produces an extra fringe shift $\frac{\Delta}{\lambda}$, and the observed density will be increased by an amount

$$\partial\rho = \frac{\Delta}{Kl}$$

Expressing this as a percentage

$$\frac{\partial\rho}{\rho_1} = \frac{Kl^2}{3(K\rho + 1)\rho_1} \text{grad}^2 \rho \quad . \quad . \quad . \quad (46)$$

grad ρ can be evaluated by measuring observed increments on an interferogram

The method is not exact, the greatest objection being that the density gradient is assumed to be constant. However the density profiles do not change rapidly enough over the small range through which refraction occurs to warrant the extra mathematical complication of an exact method. The calculation will in any case indicate the order of error involved.

3.4 Error due to Divergent Light

If the source has a finite size, all the rays passing through a point in the focal plane of the channel will not traverse the same path, and hence in the region of high density gradients, will not traverse the same density field. This is illustrated in Fig. 9

The rays outside the channel will again have the same optical path length by Fermat's Principle. Since the greatest angle of deviation is small, it is logical to assume that that the various rays will appear to proceed from very nearly the same point. It is thus only necessary to examine the additional phase retardation due to a ray being inclined at a small angle to the optical axis. A method of calculating the optical path length of such a ray has been devised, and proceeds as follows.

If AB represents the direction parallel to the optical axis and normal to the greatest density gradient (See Fig. 11)

We have from geometrical considerations

$$AB' = l\cos\phi + BD.\sin\phi \quad . \quad . \quad . \quad (47)$$

$$B'D = R - (R^2 - AB'^2)^{\frac{1}{2}} \simeq \frac{AB'^2}{2R} \quad . \quad . \quad (48)$$

$$BD = BC + CD$$

$$= l.\tan\phi + \frac{B'D}{\cos\phi}$$

$$= l.\tan\phi + \frac{AB'^2}{2R\cos\phi}$$

$$= l.\tan\phi + (l\cos\phi + BD.\sin\phi)^2 \frac{1}{2R\cos\phi}$$

Now $BD \ll R$ and $\sin\phi \simeq \phi \ll R$

Therefore neglecting second order terms we get

$$BD \simeq l.\tan\phi + \frac{l^2\cos\phi}{2R} + \frac{l.BD.\sin\phi}{R}$$

or

$$BD \simeq \frac{l.\tan\phi + \frac{l^2}{2R}\cos\phi}{1 - \frac{l}{R}\sin\phi}$$

Since $\sin\phi \ll R$, we may neglect $\frac{l}{R}\sin\phi$ with respect to 1 and write

$$BD = l.\tan\phi \simeq \frac{l^2}{2R}\cos\phi \quad . \quad . \quad . \quad . \quad (49)$$

At a section PP', distant z from A

$$z = PP' = z.\tan\phi + \frac{z^2}{2R}\cos\phi$$

Then the average deviation $\bar{z}$ of the ray from AB will be

$$\bar{z} = \frac{\int_0^l (z.\tan\phi + \frac{z^2}{2R}\cos\phi).dz}{\int_0^l dz}$$

$$= \frac{1}{2} l.\tan\phi + \frac{1}{6}\frac{l^2}{R}\cos\phi \quad . \quad . \quad . \quad (50)$$

Again from equation (47) and (49)

$$AB' = l\cos\phi + l\tan\phi.\sin\phi + \frac{l^2}{2R}\cos\phi.\sin\phi$$

$$. \quad . \quad (51)$$

Now $AD = R\xi$ where ξ is the angle subtended by AD

We may write, neglecting higher powers

$$AD \simeq AB' + \frac{1}{6}R\xi^3$$

or for $\xi \simeq \frac{AB'}{R}$

$$AD \simeq AB' + \frac{AB'^2}{6R^2} \quad . \quad . \quad . \quad . \quad . \quad (52)$$

Then the optical path length difference between CD and AB will be

$$\Delta = (\mu_1 + \bar{\delta} \text{ grad } \mu) CD - l \mu_1$$

Substituting from equations (50), (51), (52) and simplifying we may write

$$\Delta = l^2 \phi \text{ grad } \mu + \frac{1}{2} \frac{l^3}{\mu_1} \text{grad}^2 \mu + \mu_1 l \cdot \phi^2$$

where R = $\frac{\text{grad } \mu}{\mu}$ Cosϕ and setting Sinϕ = Tanϕ = ϕ Cosϕ = 1 , and neglecting third and higher powers of grad μ and ϕ

From equation (45) for a ray at normal incidence we had

$$\Delta_n = \frac{l^3}{3\mu_1} \text{grad}^2 \mu$$

Therefore the additional optical path traversed due to the angle of incidence ϕ is

$$\partial\Delta = l^2 \phi \text{ grad } \mu + \mu_1 l \cdot \phi^2 \quad . \quad . \quad . \quad . \quad (53)$$

or in terms of densities

$$\partial\Delta = Kl^2 \phi \text{ grad } \rho + (K\rho_1 + 1) l \phi^2 \quad . \quad . \quad . \quad (54)$$

Now the maximum variation of optical path length may be assumed to be twice that of the variation of the mean from the extreme rays. Thus taking ϕ as the maximum angle the Visibility will be impaired by a factor

$$V = \frac{\sin 2\partial\Delta}{2\partial\Delta} \qquad \text{from equation (48)}$$

The fringes will be widened by a factor $\frac{2\partial\Delta}{\lambda_0}$, the fringes due to the inclined rays being distributed on either side of that due to the ray at normal incidence. It is possible that the mean position of the fringe will be altered, since the fringes are not distributed perfectly evenly about the central fringe, and this point will be discussed later, when an estimate of the errors involved will be made.

Chapter 3

Description of Apparatus.

1. Interferometer

An Interferometer suitable for use with the existing channels constructed by Rose and Lolclough was designed and built after careful study of the theoretical requirements and references on existing instruments (Ref. 6,7)

The leading specifications of the instrument are:

Size of Optics	3" dia.
Size of Interferometer	6" - 18"
Size of Field	1½" - 2½" approx.
Magnification	1 : 1
Light Source	Hg vapour, 5461 Å

A diagram of the optical layout, including auxiliary light sources is shown in Fig.12. Fig.13 shows the Interferometer with all auxilliary optics removed for clarity, and Figs.14-16 are detailed views of the apparatus. The interferometer plate holders are shown in Figs.17&18.

2. Constructional Features

Kinematic design has been applied wherever possible to attain stability of the instrument. The interferometer plates are mounted in gimbals - ranging on case hardened conical points. They are held against these hardened balls by spring pressure to ensure positive positioning. The gimbals are controlled by adjusting screws working against stiff coil springs in such a way that horizontal and vertical adjustments are completely independent. It was found necessary to provide a fine adjustment to allow critical focussing. This is of the cantilever spring type,

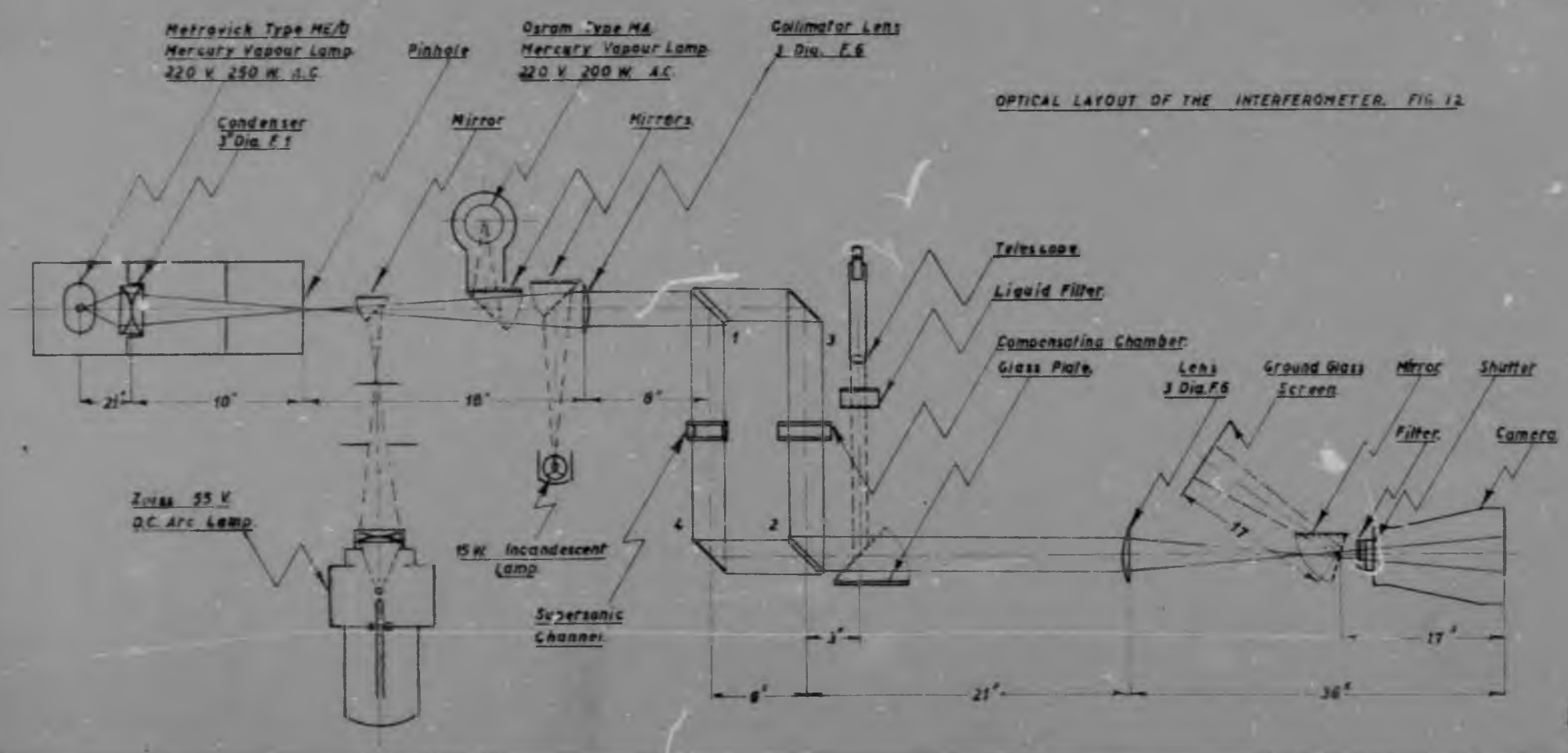

OPTICAL LAYOUT OF THE INTERFEROMETER. FIG. 12.

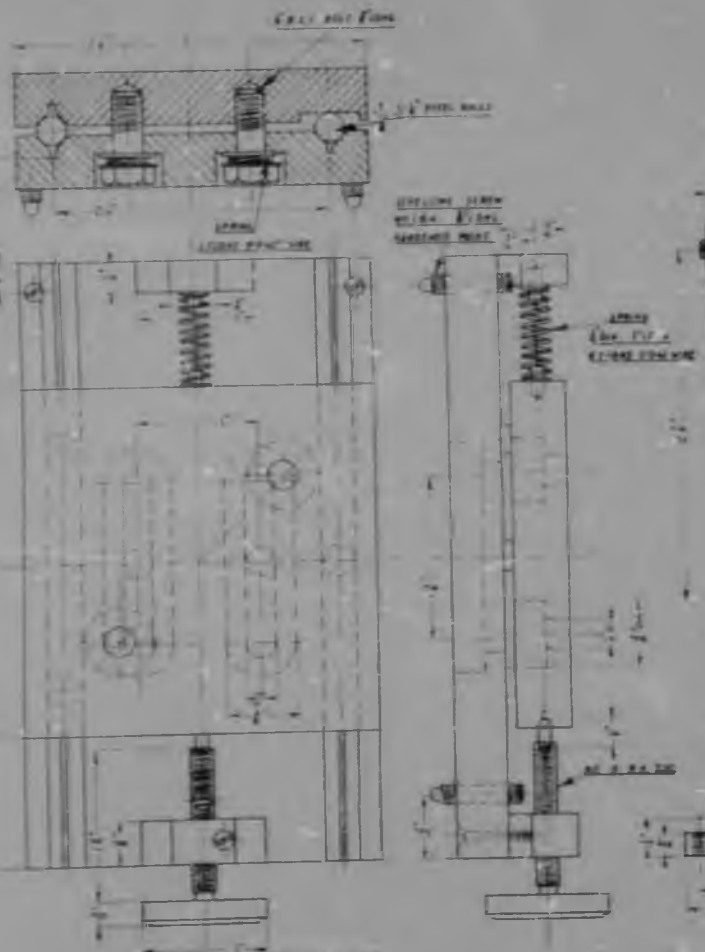

TRAVERSE

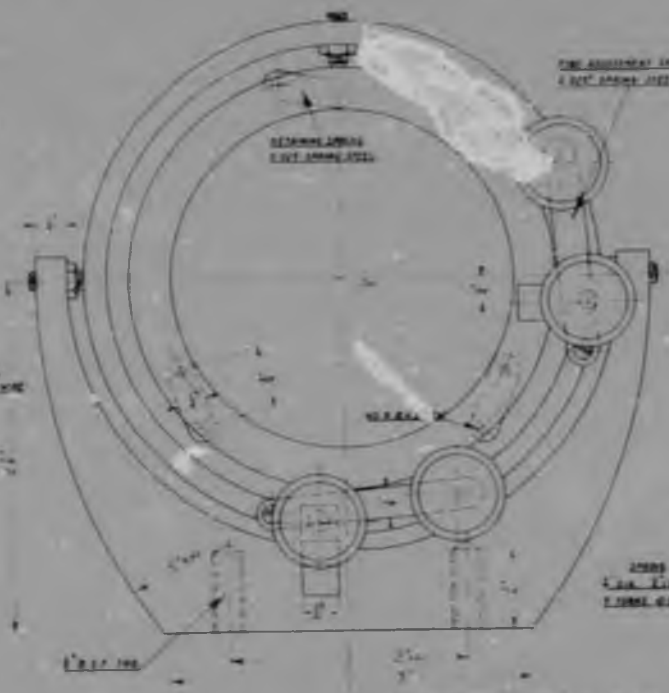

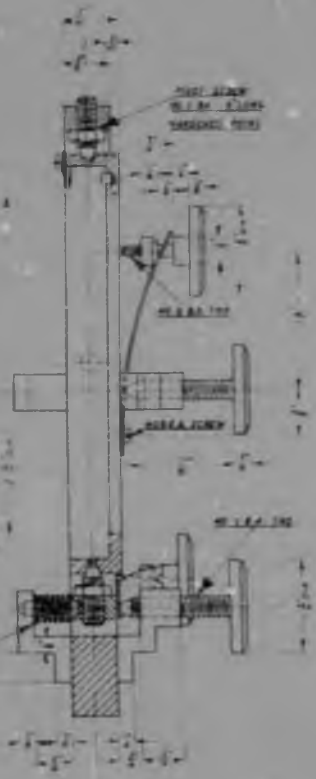

INTERFEROMETER PLATE HOLDER

UNIVERSITY OF THE WITWATERSRAND

MIRROR HOLDER FOR

MACH-ZEHNDER INTERFEROMETER

SCALE: 1½ FULL SIZE

Designed by: W. [illegible] | Drawn by: W. [illegible]

FIG 17

shown in Fig.17. A full turn of the fine adjustment screw gives approximately 1' of arc adjustment, allowing a very fine control.

The two fully silvered plates may be traversed being mounted on a carriage supported on three balls running in grooves and a flat as shown. The grooves have been carefully machined and stoned to give a smooth travel, the carriage is held down by spring pressure. The traversing screw, which is machine cut runs in an adjustable brass nut, and is fitted with a small distance piece to prevent any irregularity in the screw movement being transmitted to the carriage.

Careful design and machining has resulted in an instrument which is reasonably stable, the fringe pattern not drifting appreciably from day to day.

The individual plate holders are supported on a heavy welded steel base on three hardened screws resting in a hole, V-groove and flat, and are held in place by a spring loaded bolt. This permits them to be removed and replaced without greatly altering the adjustment of the instrument. The setup is very flexible, and the plates may be interchanged or re-arranged as desired. The base rests on a heavy welded frame bolted to four columns constructed of 4" piping. Vibration has been completely overcome by floating the frame, which is of very heavy construction, on four ¼" tee-bolt rubber anti-vibration mountings used in compression. The mountings are somewhat over-loaded, and the system has a natural frequency of about 4 c.p.s. and is heavily damped. The pipe columns are further isolated from the concrete floor by means of rubber shims.

1.2 Plates

The interferometer plates were made and loaned by the Council for Scientific and Industrial Research in Pretoria. They are/ 3" dia. and specified to be ¼ fringe plane and ¼ fringe parallel at 5461 Å. This would seem to leave much to be desired, but the results have been excellent, and fringes produced with these plates (Fig.19) have been found to be straight over the field to within the experimental error involved in measurement. The aluminising on the plates was not quite perfect, and some blemishes show up as dark areas on the interferograms. This does nothowever interfere with evaluation.

Several workers have successfully used plate glass channel windows (Ref 7) and a search was made for suitable glass. Fig.20 is a typical result. One batch was found which gave reasonable results, and were interferograms using this glass are shown in Fig.21 & 22. Both show small irregularities due to striations, as well as a little curvature. Optical glass, specified as ¼ fringe plane and parallel was obtained for the 4inch 2 channel. The results are satisfactory. No glass could be obtained for the 4inch 3 channel, and results with this channel are therefor not reliable.

The light source is a mercury vapour type AH/1 lamp used with an Ilford 607 gelatin filter to isolate the 5461 Å green line, capable of producing about 500 clear fringes. This used with a 1/100th second shutter was found to be sufficient, since the flow is steady and the same lamp could be used for setting up and adjustment. 1/100th sec. exposure was sufficiently fast to stop any slow drift in the fringes due to convection or temperature effects, but any small rapid

oscillation of the fringes will merely broaden them slightly, giving a mean position. This is an advantage.

The lens together with condenser lenses and pinhole is contained in a light tight housing. The film is held in a view camera, to the front of which is clipped the filter. During tests the room is darkened to eliminate stray light.

Ilford H.P. roll film was used throughout, developed in caustic hydroquinone solution, and subsequently treated with Farmers reducer to produce maximum contrast.

2. Adjustment Technique.

Initial adjustment was carried out by the method described in Ref.6. The Cauer telescope was used to align the plates 1,2 and 3, plate 4 being brought into alignment by bringing into coincidence the two images produced on the screen by the two light beams of the interferometer. Path lengths were made roughly equal using a steel rule. The counting arrangement (Ref.5) was not found necessary.

It was found that further adjustment was greatly facilitated by introducing monochromatic and white light into the field at this point in addition to the light from the main source. Two small auxiliary mirrors were placed near the collimator lens so that they obstructed the light from the main source, which was white spectrum, but reflected light from a filtered low pressure mercury arc lamp, and from an incandescent bulb into the interferometer. In this way three separate areas, illuminated by the main source, monochromatic source and white source are seen in the field.

The far and near crosswire method (Ref.6) was then used, using the pinhole as far crosswire, and

one of the auxilliary mirrors at the collimator lens as the near crosshair. After only two or three adjustments, fringes should appear in the telescope in the monochromatic area. Time can now be saved by merely broadening these fringes and then beginning to traverse to obtain equal path lengths. If traversing is carried on in the right direction, fringes in the monochromatic area will grow more distinct, and presently appear in the area illuminated by the main source. It is necessary to frequently readjust fringe spacing and focus due to the compound motion of the virtual sources in traversing. If the fringes are observed by telescope, rather than on the screen, readjustment of the fringes need not be carried out so frequently, since fringes can be seen much more readily. If at this point the filter is partially removed to leave only a portion of the light from the main source is filtered, fringes will appear in groups, and on traversing in the right direction these will become more distinct, the white light or central fringes finally appearing running continuously into the white light portion of the field. By this method, traversing can be carried out very rapidly.

At this point the fringes must be focussed onto the screen and adjusted to the desired orientation and width. Since the monochromatic source was a large diffuse lamp, critical focussing was done observing the fringes in this area, since the focus conditions for a diffuse source are more critical than for a point source. The final adjustment is to align the channel and compensating chamber parrallelle the light beam, and focussing the channel onto the screen.

By broadening the fringes while keeping them in focus until one fringe covers the whole field, infinite or contour fringes are produced. It may be noted that the proportions of the interferometer are

such that plate 2 has a maximum effect on fringe width without altering focus conditions appreciably, while plate1 alters fringe width very little, but affects the focus. This is very useful in setting up.

Starting with well focussed infinite fringes, horizontal or vertical fringes are produced by tilting plate 2 about its horizontal or vertical axis respectively and refocussing with plate 1. If plate 2 had been tilted in the opposite direction, the same fringe pattern would have been produced, but these fringes would distort in the opposite direction when a density disturbance is introduced. Thus five maintypes of fringes are available and specimens are shown in Figs. 23-28. The type showing the most detail in a desired area is the one to use in a test.

There are two techniques to trace fringes through a shock front to permit fringes to be properly numbered. By using white light only a few fringes are produced and the central fringe can generally be identified. (Fig.29) This method is not always certain. Alternatively if the channel is slightly misaligned so that the shock wave is not aligned perfectly along the light path, fringes through the shock are spread apart and can be traced. This effect is present in Fig.23. The interferogram cannot be evaluated due to errors introduced by the blurring, but the fringe shift across the shock can be measured.

Fig.26 & 27 illustrate the need for careful focussing. If the channel is not in focus on the screen a shadowgraph effect is introduced, which may obscure much of the detail in the vicinity of the shock waves and boundary layers.(Ref.4)

40

3. Supersonic Channels

The channels were constructed by Pope and Colclough (Ref.14) and are designed by the graphical method of characteristics. They are shown in Fig.30 & 31 Holes 0.01½" dia. were drilled into the glass sides to serve as pressure taps, and hypodermic needles were cemented into the holes to connect them to a manometer bank. Co-ordinates of the channel walls are given in Tables 1 & 2.

The Mach 3 channel was found to be unstable in operation, and a number of diffusers were tried. Fig.31 shows a variable second throat type in place. These were however unsuccessful and a cone diffuser placed up well into the channel was used.

The air supply is drawn from two reciprocating compressors operating at 80 psig. Oil and impurities are removed by washing the air with chilled brine, and subsequent drying with a chemical drier and cleaning with activated charcoal. (see Ref.14). The channels are mounted vertically on a settling chamber, the pressure of which is controlled by a hand valve on the air supply.

4. Additional Measuring Techniques.

Schlieren and shadowgraph techniques are used to gain further information. The apparatus used is essentially the same as that used by Pope and Colclough, and is shown diagramatically in Fig.32. For shadowgraphs the knife edge is removed and the screen moved a short distance from the focus.

Total head and static probes were used in the Mach 3 channel and dimensions are given in Fig.33 & 34. These were also used by Pope and Colclough. The probes are held in a cross slide mounted above the channel, which permits them to be traversed while the channel is in operation.

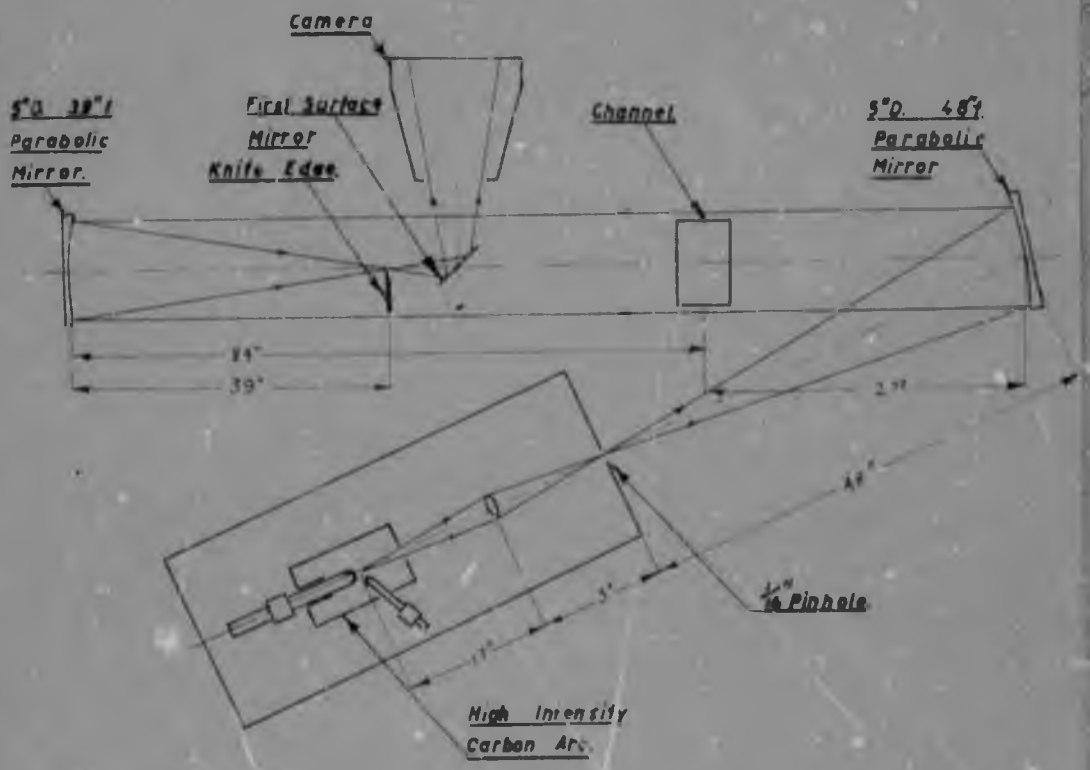

FIG 32 OPTICAL LAYOUT OF THE SCHLIEREN SYSTEM

No Scale

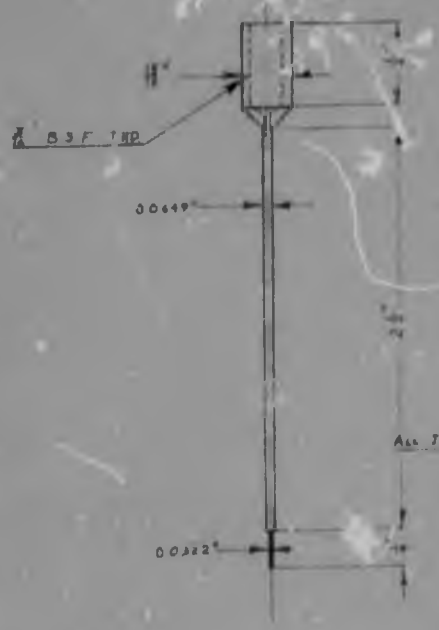

FIG 33 TOTAL HEAD PROBE

Full Size

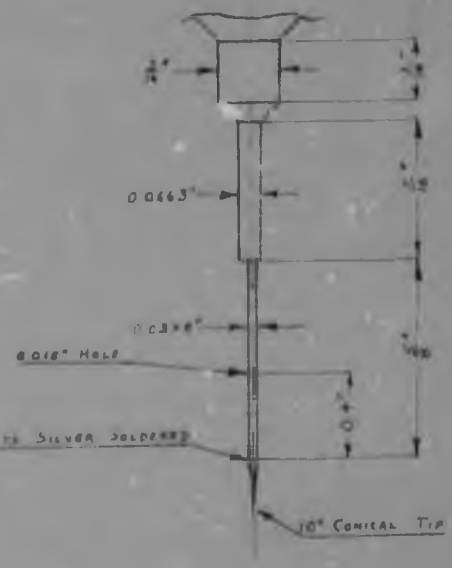

FIG. 34 STATIC PROBE

Scale : 2 Full Size

Chapter 4

Test Procedure and Results.

1. Interferograms.

The following procedure was adopted to obtain all interferograms and schlieren pictures.

The desired fringe configuration or schlieren adjustment was set up, the room was darkened and a plate inserted into the camera. The air supply valve was opened untill the correct air pressure was reached as indicated on a pressure gauge connected to the reservoir, and the shutter released. The valve was opened as quickly as possible and the time between opening the valve and releasing the shutter was as short as possible to prevent large air currents from forming in the space across the interferometer, since this caused the fringes to drift. Before each test a zero or undisturbed interferogram was taken, and the atmospheric pressure, temperature and wet bulb temperature read. Sufficient time was allowed between tests to allow the air currents to settle, so that the zero fringes were again stationary. Usually a series of interferograms was taken, and the one showing best contrast used for reduction. Two interferograms had to be taken to cover the channels, since the field was smaller than the width of the channels. Reference marks on the channel walls allowed the interferograms to be subsequently lined up.

1.1 Density Evaluation from Finite Fringes.

To plot the density contours or iso-pycnals in the channel, a set of finite interferograms was made. These are shown in Figs.35 & 36. Horizontal fringes about 1 cm. wide were used, and the interferograms evaluated as follows:-

Fringe co-ordinates were read off by means of a travelling microscope provided with travel in two mutually perpendicular directions. The interferograms were clamped to a rotating table placed under the microscope. The channel axis was aligned to the direction of travel as follows. With the channel axis approximately horizontal the microscope was set to a definite value on the horizontal scale near one end of the interferogram, and vertical ordinates at the wall were read off. The mean of these ordinates then gave the ordinate on the channel centreline. This was repeated near the other end of the interferogram, and the interferogram rotated until the ordinates on the centreline were equal at both ends.

The zero interferogram was first aligned, and a large number of pseudo units of fringe widths were made. The average of these values was taken as be the value of the undisturbed fringe width.

Fringes on the interferogram were then numbered beginning at zero well outside the channel on the wall interferogram, and in the region of overlap on the throat interferogram. Fringes were traced through the shock front with the aid of a skewed interferogram. The interferogram was then lined up on the table, and the microscope moved to a given vertical setting, and the horizontal ordinates of each fringe were read off down the channel. This was repeated at different vertical settings to cover the channel. Since the flow is symmetrical about the centreline, only half the channel was evaluated in detail, the half containing the pressure taps only being evaluated at a few vertical settings to provide a check. Readings on opposite sides of the centreline were compared and where necessary averaged.

Co-ordinates were converted to scale inch units as follows,

$$y = f\,y' - \bar{y}$$

$$x = f\,x' - \bar{x} \qquad \ldots\ldots (56)$$

where x,y are the required co-ordinates

x',y' are the co-ordinates read from the micrometer

$\bar{x}$,$\bar{y}$ are the co-ordinates of the throat centre on the microscope scales calculated from the microscope readings at the reference marks on the channel walls.

f is the scale factor, found from measurements of the exit dimension on the channel itself and on the interferogram.

The fringe shift in units of fringe width is then given by

$$\frac{y}{b} = N - (y_c - y)\,\frac{1}{b}$$

$$y.\frac{1}{b} = N - \frac{y_c}{b} \qquad \ldots\ldots (57)$$

where N is the fringe number (Ref.5)

y_c is the undisturbed zero fringe ordinate

y is the fringe ordinate

b is the original fringe width

In the case of the exit interferogram, the average ordinates of the fringe No. 0 in the area beyond the channel walls in the stationary air outside the jet was used as y_c, i.e. the density in the channel was compared to the density immediately outside the air jet. On the throat interferogram several co-ordinates on the zero fringe were read off. Since this area was also covered by the exit interferogram, the corresponding fringe shift could be found from the exit interferogram results, and y_c could be calculated. The average of many such calculations was used.

In using equation 57 on a calculating machine care must be taken when either the fringe

number or the direction of shift because negative.

Densities are found from the fringe shift by equation 36 which may be written as

$$\rho = \frac{Y}{b} \cdot \frac{\lambda}{\ell K} + \frac{\rho}{RT}$$

where P and T refer to ambient air.

The following values of the gas constants were used

R = 53.342 ft. lbs./lb. °F

K = 0.003668 ft.²/lb.

λ = 5461 Å = 5.461×10^{-5} cm.

Results are given in Tables 3 & 4.

Curves were drawn plotting density against y ordinates for each x ordinate(Curves No. 1 - 30). The y ordinates corresponding to integral values of density were then read off from these curves, and isopycnals plotted. These are shown in Curve No.31. The density along the centreline has been read from this plot and a graph of density against distance down the channel drawn(Table No. 6 and Curve No 34). The correction due to boundary layer effect found in the next section has been added, and the corrected curve is also shown.

If the flow may be assumed to be isentropic and one dimensional, the density is related to the Mach Number by

$$\frac{\rho_0}{\rho} = \left[1 + \frac{\gamma - 1}{2} M_1^2 \right]^{\frac{1}{\gamma - 1}} \quad . \quad (58)$$

where

ρ_0 is the stagnation density

ρ is the stream density

M is the free stream Mach Number.

See ref. 17)

and $$\beta_e = \frac{\rho_e}{\rho T_0}$$

The Mach number has been found from the converted density using computation curves(Ref 16) and plotted in curve No. 34.

Unfortunately the errors due to the glass walls in the Mach 3 channel, were too large to permit the Mach 3 channel to be accurately evaluated.

In order to check the two-dimensionality of the channel, the channel was turned through 90° and a negative horizontal interferogram made of the area above the brass channel walls, with the light beam parallel to the glass walls. This is shown in Fig. 37 and was evaluated using one fringe just above the channel exit.

In this case, zero fringes were not quite perpendicular to the channel axis. Several readings of the zero fringe co-ordinates outside the glass walls were made and plotted, and a straight line drawn approximating these points.(Curve No. 21.) Values of Y_0 were then read from this curve at the required section. Results are shown in Table No. 5 and plotted in Curve No. 32.

4.2 Density Evaluation from Infinite Fringes

Infinite interferograms were made of the Mach2 & 3 channels. There are density contours with the density increment per fringe given by equation 38. The Mach 2 interferograms are shown in Fig 38 & 39. Fringes were numbered and their co-ordinates along the channel axis measured. The density on the zero fringe was found for the exit interferogram from the pressure tests and for the throat interferogram from the results of the finite interferogram evaluation using the incorrect-

values. Results are given in Table No. 7 and H and have been plotted in Curve No. 35. The values are so corrected for boundary layer effect as before.

The Mach-Zehnder interferograms are shown in Fig. 40 to 43 together with the zero undisturbed interferograms. In the exit section, the density gradient is not sufficient to produce enough fringes for evaluation, and the errors due to the glass walls are very large, so that only the fringes in the throat section have been measured. The density on the zero fringe has been estimated from the wall pressure at Hole No. 6 as described later. Since it is assumed that the pressure hole measures the correct free stream density, the boundary layer correction factor at this station has been subtracted from this density, and the result used to evaluate the density on the other fringes. Correction factors were added to the calculated density to give the corrected density. The Mach number has been found as before. Results are given in Table No. 10 and plotted in Curve No. 36.

1.3 Density Evaluation from Composite Fringes.

Density contours are shown up when a finite interferogram and its zero interferogram are superimposed, and printed together. This has been done, Fig. 44 & 45, using positive horizontal fringes. An advantage of this method over using infinite fringes is that errors due to

glass channel walls and faulty interferometer plates are automatically compensated for; and by moving the interferograms relative to each other in a direction normal to the undisturbed fringes, the density contours can be made to move up and down the channel, thus permitting a contour to be moved to any desired position, or any desired number of contours to be found. These contours have been evaluated in exactly the same way as the infinite fringe contours. Results are shown in Table No. 9 & 11 and plotted in Curve No. 35 for the Mach 8 channel, and Curve No. 36 for the Mach 7 channel. The Mach 8 evaluation has been based on the finite fringe evaluation, and the Mach 7 evaluation on pressure hole.

1.4 Boundary Layer Evaluation

The density boundary layer could also be evaluated from the horizontal finite interferograms. Many co-ordinates were read off along each fringe to be evaluated in the vicinity of the glass channel walls, and the corresponding densities calculated as before. Density profiles in the Mach 7 channel were also evaluated from horizontal negative interferograms(not shown) covering the throat and exit sections. It was assumed that the errors introduced by the slated glass walls were negligibly small over the short distance covered by the fringes in the boundary layer. The position of the zero undisturbed fringe was found from the density indicated at pressure hole No. 6 in the channel walls

It was assumed that the density of the air did not alter appreciably over the area covered by the fringe in the boundary layer, so that the variation in y co-ordinate could be neglected and the boundary layer density profile plotted against distance from the channel wall directly. In the case of the Mach 1 channel, the walls diverge very rapidly, and the x co-ordinates which correspond to the wall were corrected as follows. A large scale curve of the wall contour was drawn, and the point where the fringe met the wall marked. The correction added was then the distance between the x co-ordinate of this point and the x ordinate of the wall at the corresponding y ordinate.

Results are shown in Table No. 11 & 12 and plotted in Curves No. 37 & 38. The profiles .1" below the Mach 2 channel exit on the brass walls, and .1" above on the glass walls(Table No. 5)are plotted together. These curves coincide almost exactly, and it has therefore been assumed that the boundary layer on the glass walls traversed by the light beam is exactly similar to that on the brass walls which has been evaluated. The boundary layer correction factor can therefore be found. From Equation 43(Chapter 2)

$$\rho = \rho' \tau - \frac{2}{l} \int_0^{\frac{l}{2}} \rho\,(z).dz$$

where

ρ is the true density

ρ' is the observed density

and the integral is represented by the area under the boundary layer curve on a base of the free stream density. The areas have been measured and the correction factors found. Results are given in Table No. 14. Curves of correction factor versus distance along the channel have been drawn, and the required correction factors can be read from these.(Curve No. 10)

An estimate of the boundary layer thickness was made from the boundary layer density profiles. the thickness appearing in Schlieren pictures was also measured from Fig. 36. These are shown in Table No. 15 and plotted as a function of the distance down the channel in Curve No. 10.

2.1 Wall Pressure Tests.

Wall pressures at the pressure holes were read at the same time as interferograms Fig. 35 & 42 were made. These pressures are given in Table No. 16 & 17.

If it may be assumed that the wall pressures are equal to the free stream static pressure, i.e. there is no pressure boundary layer, and if dissipation is absent, the corresponding density may be found from the isentropic relations.

$$\rho = \frac{\rho_0}{RT_0} \left(\frac{p}{p_0}\right)^{1/\gamma} \quad . \quad . \quad . \quad . \quad . \quad (59)$$

where subscript o refer to stagnation conditions in the reservoir.

The results are given in Tables 18 & 19 and plotted in Curve No. 15 & 16 together with values found interferometrically, and from one dimensional

theory.

To check the possible error due to reservoir pressure variation, a series of tests were run with different reservoir pressures(Table 18). These values are plotted in Curve No. 41.

Originally holes were drilled into plate glass walls. These were rather large and several were chipped and had ragged edges on the inside. These walls have been designated #1. The results of the tests using these holes were rather erratic, and have been included to show the effect of the size and shape of hole on the pressure. The holes drilled in the optical glass walls were small and smooth and these walls are designated #2. Certain tests were also run with plain optical glass walls without pressure holes, and these are designated #0.

To check the effect of the holes upon the flow, a number of interferograms, schlieren and shadowgraphs were taken using the #0,#1,#2 glass walls, with the channel in its normal position and also with the channel turned through 90°. These are shown in Fig. 48 to 57.

2.7 Probe Tests

Pope and Goldsough(Ref. 14)have used static and total head probes to measure the flow parameter ultimately with the intention of using a Machmeter. To check the validity of using a static probe in this case, a number of tests were run with these probes in the Mach 2 channel under conditions similar to those prevailing for the interferometer tests. The probes were supported by the graduated cross slide. Pressures were read on a mercury manometer for the static probe,

and a test gauge for the total head probe. The probes were carefully aligned parallel to the channel axis midway between the glass walls, and moved to a position near one brass wall at the exit. A photograph was taken using the Schlieren setup with the knife edge removed. Subsequent measurement of this picture gave the initial probe position. The air was turned on and probe measurements made with the probe at various positions across and down the channel. At the end of the run another picture was taken to fix the final position of the probe. Intermediate positions could be found from readings on the cross slides.

Tests were run in the #1 and #2 channels with each probe to check reproducibility of results. Results are shown in Tables 19 & 20. Pressures have been plotted on their corresponding cross section as base in Curves No. 32 & 33.

Average pressures across each section have been taken as pressure along the centreline. Static probe pressures have been converted to densities using the isentropic relations as before, and plotted in Curve No. 35. (Table No. 21)

The pressure read by the impact probe corresponds to the stagnation pressures P_0' behind a normal shock wave, and have been plotted against distance down the channel in Curve No. 34. (Table No. 22 & 23)

To give an idea of the influence of the probe on the flow, a series of Schlieren pictures was taken with each probe in various positions across the channel. These are shown in Fig. 58-67.

If the stagnation pressure and the free stream pressure are known, the free stream mach number is given by the Rayleigh Pitot Tube Relation:-

$$\frac{P_1}{P_0'} = \frac{\left\{ \frac{\gamma+1}{\gamma+1} M_1^2 - \frac{\gamma-1}{\gamma+1} \right\}^{\frac{1}{\gamma-1}}}{\left\{ \frac{\gamma+1}{2} M_1^2 \right\}^{\frac{1}{\gamma-1}}} \quad \ldots \quad (60)$$

where

P_1 is the free stream static pressure

P_0' is the stagnation pressure after a plane wave.

It had been assumed that the pressures read at the wall tape and static probe corresponds to P_1. The stagnation pressures at the corresponding positions have been read from Curve 42, and the Mach No read from Computation Curves plotting the Rayleigh relation(Ref. 16). Results are shown in Table 24 and plotted in Curve 44.

7.1 Cone Tests

The Mach No. of the flow may be estimated from the shock wave angle on a cone in the flow. A series of cones with different apex angles were inserted into the working section of the channels and Schlieren pictures taken. The shock wave angles were then measured using the travelling microscope and the graduated rotating table. Three series of tests were run with the Mach 2 channel using 20, 21, 22 degree cones, and one using the Mach 3 channel. Results are given in Table 25 & 26.

Tests were also made using slightly high and low reservoir pressures, and using the shadowgraph instead of Schlieren in the Mach 2 channel. These results are shown in Table No. 27. A typical set of cone tests is shown in Fig. 62-71. (1967) The Mach No. was read from computation curves plotting the Taylor-Maccoll solution for shock waves on cones(Ref. 16).

Chapter 2

Accuracy

1. Finite Interferograms.

The density is given by equations 36,43, and 54. The accuracy of each of the measured variables will now be discussed.

1.1 & 2

(a) Measurement uncertainty.

A significant error is involved in evaluation, due to the difficulty of estimating the exact centre of a fringe. By repeated readings on one fringe, the uncertainty interval has been estimated to be ± 0.05 fringe widths. This is constant for various fringe widths.

(b) Zero errors.

A large number of readings were taken along several fringes in zero interferograms and the deviation from the mean estimated. Neglecting obviously personal errors, fringe curvature was found to be less than ± 0.05 fringe widths over the entire field.

It has already been mentioned that exposure time was sufficiently long to average out any rapid fringe vibration, and as precautions were taken against air currents, fringe drift may be neglected.

(c) Two dimensionality.

The variation in density along the light path, excluding boundary layer was found to be less than ± 0.4% from Curve No. 34. It is reasonable to extrapolate this result to the channel itself, although this extrapolation may not be valid in

the curved area. Curve No. 14 is itself subject to the error in density, which is greater than ± 0.5 % so that this will be a safe value to use.

(d) Refraction.

Over the larger portion of the channel, the density gradient is very small.

The average distortion due to density gradient is given by equation 44. Using the maximum value of density gradient found from boundary layer surveys, i.e. 9 lbs./cu. ft./inch, at a density of 0.12 lbs./cu.ft. the distortion is of the order of 4.7×10^{-10} inches.

The half width Δ of the central maximum of the diffraction pattern of the lens in this case is of the order of 1.5×10^{-4} inches, and image distortion is therefore negligible. This result holds true for Schlieren as well, so that boundary layer thicknesses can be measured from Schlieren pictures with confidence.

The error in density due to refraction is given by equation 46. The errors for various gradients found in the flow and boundary layer have been computed, and are tabulated below.

Error due to Refraction.

Distance above Target y	grad $\frac{\rho}{\rho_0}$ cu.ft./lb./inch.	Density Error %
Flow	0.05	0.001
0.5	0.5	0.75
0.8	1.0	1.0
1.1	2.0	1.0
1.3	0.9	0.32
1.7	0.75	0.32
1.9	0.6	0.14

(e) Divergent Light

The error in path length due to divergent light is given by equation 54.

If the extreme rays of a ray originating at

the maximum aperture be considered, then for this case the errors have been calculated for various density gradients and tabulated below.

Errors due to Divergent Light

$\frac{grad\ \rho}{gm.ft./lb./inch}$	$\Delta\delta$ x10^{-6} inches	δ Y/b
0.05	2.0	.095
0.5	3.2	.15
1.0	4.4	.20
1.5	5.6	.26
2.0	6.8	.32

Rays originating on either side of the centre of the aperture will produce fringes distributed on either side of the central one, and the total effect will be a blurring of the fringes by a factor roughly twice that of the value in the last column. This is negligible for gradients encountered outside of the boundary layers and shock waves, but may cause fringes to overlap and be obscured in areas of large density gradient. It is for this reason that fringes often have poor visibility in boundary layers and near shock waves, even when the rest of the field is clear. The effect can be reduced by reducing the aperture.

Fringes produced by rays on either side of the central ray are not necessarily distributed evenly about the central fringe, and the resultant fringe can appear to be slightly displaced. The resultant shift will probably be less than 1/4 of the maximum shift computed above, or in the highest density gradient, less than 0.08 fringe width. Under these conditions, fringes would be very indistinct, and there would be a higher uncertainty in measurement.

Combining the uncertainties in y according to the square law, the resultant uncertainty interval is ± 0.11 fringe width.

1.7) y_0.

(a) Estimated from fringes in still air.

In evaluating M2 exit interferograms, the value of y_0 was taken to be the average ordinate of the zero fringe outside the air jet issuing from the channel. The question arises as to whether the air in this region is truly stationary and at the no flow density. The zero fringe was originally straight to within the accuracy previously discussed. Examination showed this fringe to be slightly curved towards the channel exit outside the jet boundaries. Extrapolating the curvature away from the jet, it would appear that the y_0 value was in error to the order of ± 0.11 fringe width.

(b) Estimated from independent density measurement.

The y_0 value for the throat interferogram was calculated from the fringe shift found in the exit interferogram. This involves the uncertainty interval of the exit interferogram result, in addition to the uncertainty involved in matching the two interferograms. The latter may be taken to be ± 0.05 fringe width.

1.) n.

The fringe width was taken as the mean of a large number of measurements. A considerable error is involved due to the difficulty of estimating the centre of the fringes. The uncertainty interval was taken to be equal to the standard deviation of the readings from the mean.

which yeilded an uncertainty interval of 2.5%.

1.4 [illegible]

By repeated measurement, the dimensions of the channel were established to within ± 0.0005" or 0.08% on the glass to glass dimension.

1.5 Pressure and Temperature.

Atmospheric pressure and temperature were read during each test, and it was estimated that the readings corresponded to within ± 0.3% of the ambient air conditions.

Reservoir pressure was read to 0.25 psi., and it was assumed that the readings are within ± 0.4% of the true reservoir pressure. Reservoir temperature was assumed to be equal to atmospheric temperature. Subsequent measurements indicate that this would be slightly high, and an uncertainty interval of ± 1.5% was assigned on this basis.

1.6 Boundary Layer Correction.

The correction applied to the observed density is itself not exact, being computed from an uncorrected density boundary layer curve. Due to the corner effect, the correction to the boundary layer curve is difficult to find, varying from zero at the wall to the full correction in the stream. The full correction does not exceed 10%, so that the area under the curve may be regarded to be accurate to within ± 5%. Refraction may cause a further error of 1.6%. Thus the uncertainty interval for the correction integral may be taken to be 6% at the worst condition, or for the Mach 9 channel, 8%. This will correspond to ± 0.6% for [illegible] and ± 0.[illegible]% for [illegible] of the

density.

1.7 Resultant Uncertainty in Density.

Errors are propagated according to

$$\lambda R^2 = \sum_{i=1}^{n} \left[\frac{\partial R}{\partial v_i} \lambda v_i \right]^2 \quad . \quad . \quad . \quad (61)$$

where v_i are the measured variables

λv_i the corresponding uncertainty intervals

λ the uncertainty interval in the result R.

(See Ref. 18.)

From equation 57

$$\lambda \frac{x}{b} = \left(\frac{\lambda y_0}{b}\right)^2 + \left(\frac{\lambda y}{b}\right)^2 + \left(\frac{y_0 - y}{b} \frac{\lambda b}{b}\right)^2$$

Now y varies from y_0 to about 0.7" where y_0 = 2.3" in the exit interferogram. The largest error occurs at y = 0.7" and is 0.75 fringe widths.

This will also be the added uncertainty for the throat interferogram. Here y varies from y_0 to zero, where y_0 = 0.6", and the maximum error will be 0.82 fringe widths.

The uncertainty interval in X/b thus varies from about 0.02 fringe width at exit, to 0.85 fringe widths in the throat, the variable uncertainty being entirely due to the uncertainty in b.

By equation 40, this implies an uncertainty in the density of ± 0.5%.

The uncertainty due to T and P is

$$\lambda_P = \left\{ \frac{P}{RT} \cdot \frac{\lambda P}{P} \right\}^2 + \left\{ \frac{P}{RT} \cdot \frac{\lambda T}{T} \right\}^2$$

$$= 0.28 \cdot 10^{-4}$$

This is negligible.

The uncertainty intervals in density various factors are tabulated below.

Uncertainty Intervals in Density

	Error in Flow	Error in Boundary Layer
	δ	δ
2 Dimensionality	0.5	0.5
Refraction	—	1.6
Divergent Light	—	0.8
Boundary Layer	0.6	—
Δ/L	0.5	0.5

From the test results, the calculated density is everywhere within 3% of the theoretical value found by the method of characteristics, and at least part of this discrepancy is due to the fact that the real flow does not exactly follow the predicted theoretical flow. It is therefore logical to assume that the uncertainty interval of 6.6% is much too high, the fringe width measurement being more reliable, and assigning an uncertainty interval of 3% to the flow, with a correspondingly higher value in the boundary layer.

1.% Resultant Uncertainty in Mach Number.

Using variables $\delta\beta$ and $\delta\rho$, the uncertainty interval in the Mach number will be given by

$$\delta M^2 = \left\{\frac{1}{\rho M} A\,\delta\rho\right\}^2 - \left\{\frac{2}{M\beta^2} A\,\delta\beta\right\}^2$$

where

$$A = \left(1 - \frac{\gamma-1}{2} M^2\right)^{\frac{\gamma+1}{\gamma-1}}$$

At $M = 2$, $A = 0.6$

and

$$\delta\rho_0^2 = \left\{\frac{\rho_0}{\rho T_0}\frac{\delta p_0}{p_0}\right\}^2 + \left\{\frac{\rho_0}{\rho T_0}\frac{\delta T_0}{T_0}\right\}^2$$

In this case, $\delta T_0 = 2.95 \cdot 10^{-4}$ psi. or 0.25 %

Substituting to find $\frac{\partial \rho}{\rho}$ at N=2.5% uncertainty interval in Mach number is ± 11% for the 0.6% error in the density, and 4% for the 2% density error.

2. Infinite Interferograms.

We have already found that there is an uncertainty of ± 0.04 fringe widths due to original fringe curvature, and ± 0.04 fringe widths uncertainty in measurement. This gives a resultant uncertainty interval of ± 0.056 fringe widths, or if the density be considered at a point, there will be an uncertainty interval in density of 0.56%, by equation 40. For the Mach 3 channel, fringe curvature caused an uncertainty of as much as 0.25 fringe width.

Now the density is found from equation 38

$$\rho = \frac{2\lambda}{L^2} \quad \text{for N fringes}$$

The total uncertainty interval in density therefore is

$$\delta\rho^2 = \left\{ \frac{2\lambda}{L^2} \frac{\delta L}{L} \right\}^2 + \left\{ \frac{2\lambda}{L^2} \frac{\delta\lambda}{\lambda} \right\}^2 + (0.0056, 0.12)^2$$

$\frac{\delta L}{L}$ has been found to be 0.0008

For a change in humidity from 0% to 60% at typical conditons has been calculated from tables to give a change in $\frac{\partial \lambda}{\lambda}$ of 0.0011.

for an extreme case of N=50 fringes

$$\partial\rho = 0.00005$$

or ± 0.8%.

In the case of the Mach 3 channel, this will be ± 2.6%.

The uncertainty interval will be the uncertainty calculated above, combined with the uncertainty in the reference density, found by other means.

3 Wall Pipe and Static Probes

The manometer accuracy may be taken to be the maximum capilliary error for mercury, which in this case is ± 0.05" or 0.7%.

In addition there is a fixed error for a given tap, determined by its shape and size, and by the connecting tubing. No quantitative work appears to have been done for supersonic flow, although the error for subsonic flow can under certain conditions become significant. (Ref.13). An additional fixed error may be involved by assuming the wall pressure to be equal to the free stream pressure. The fixed error will be referred to again later.

4. Total Head Probe

The estimated accuracy of the pressure gauge used in measurement was 0.25 psi. or 2.5%.

In this case, a fixed error may be introduced as before, and this will also be discussed later.

5. Cones

Cones were ground to within 0.1° of the nominal angle. The uncertainty in measurement was of the order of 0.2° from repeated measurements, and from consecutive runs, which gives an uncertainty interval in the Mach No. of about 1%.

Photographic distortion should be absent, as discussed under refraction, and the main uncertainty lies in estimating the position of the shock front. Several shadowgrams were taken for comparison, but the results were erratic, although the shock front is more sharply defined. This is no doubt due to the fact that for shadowgrams the plate is moved from the focal plane, and refraction therefor will cause an error in the position of the shock front.

Chapter 4

Discussion of Results

1. Channel Flow.

The results obtained in tests have been compared to the flow predicted by theory. The theoretical analysis has been carried out as follows.

1.1 Characteristic Theory.

The simplest accurate solution for a two dimensional flow problem such as the flow in a channel is the Characteristic Method(Ref. 17). The Mach net for the Mach 2 channel was drawn using $1/2^{0}$ expansion angle increments(Curve No.45) and for the Mach 3 channel using 1^{0} expansion angle increments(Curve No. 46). A semi-graphical method using some of the elements of the analytical method of Shapiro and Edelman(Ref. 18) was used to speed up the work. A large scale rough Mach Net was drawn out, using no scale, and numbered as outlined in Ref. 18(Curves No. 47&48). The corresponding density ratio, Mach number and Mach angle can then be computed and have been given in Ref. 18 and reproduced in Table No. 28. Instead of calculating co-ordinates of the Mach Net, a somewhat less accurate but much more rapid result was obtained by drawing the Mach Net to scale using these values of the Mach angle. Due to the fact that the channel is designed to reach the final Mach Number after several reflections, many of the elements of the Mach Net have the same number, and the graphical method can be carried out rapidly. Density contours were drawn connecting elements of equal number. For the Mach 2 channel co-ordinates of these contours were read off, and the density plotted as a function of distance down the channel in Curves 1to 30. The v

ordinates at integral values of density were read off from these curves, and plotted as isopycnals in Curve No. 33, for comparison with the isopycnals obtained interferometrically. The Central Density distribution has been plotted in Curve No. 34. For the Mach 3 Channel, ordinates of density contours were read from Curve No. 46, and plotted in Curve No. 36.

1.2 One-Dimensional Theory.

The Flow Parameters may also be predicted by one dimensional theory if the variation of parameters across the direction of flow is negligible.

If A is the area at the required section, and A^* the throat area then

$$\frac{A^*}{A} = M \left(\frac{\frac{\gamma+1}{2}}{1 + \frac{\gamma-1}{2} M^2} \right)^{\frac{\gamma+1}{2(\gamma-1)}} \quad . \quad . \quad . \quad (62)$$

The Mach Number has been read from computation curves plotting this relation(Ref.16)for both the Mach 2 and Mach 3 Channels(Tables No. 30&31).

The density is related to the Mach Number by

$$\frac{\rho_0}{\rho} = \left\{ 1 + \frac{\gamma-1}{2} M^2 \right\}^{\frac{1}{\gamma-1}} \quad . \quad . \quad . \quad (63)$$

Values of have been read from computation curves(Ref.16).

Mach Number and Density have been plotted as a function of distance down the channel in Curves Fol 34,35 and 36.

From Curve No.34 it can be seen that the results obtained by One-Dimensional and Characteristic theory correspond very well in the case of the Mach 2 Channel, being within 1% of each other. For the Mach 3 Channel(Curve No. 36)the difference is greater, amounting to as much as 6% in

some places. This is to be expected with the larger divergence of the Mach 3 Channel Walls.

1.3 Verification of Isentropic Flow.

The flow pattern obtained interferometrically for the Mach 2 Channel have been compared to the pattern predicted by Characteristic Theory in Curve No. 33, where isopycnals have been plotted. The two correspond very well, the measured flow being at a slightly lower density but within 3% of the theoretical. The interferometer involves an uncertainty of 3%(Chapter 5)so that the experimental and theoretical results agree to within the experimental error. This can also be seen from Curve No. 34, where the curves correspond to within 3% except at exit. The overcorrection at exit is due to the boundary layer thickening, discussed later.

The fact that the measured densities were lower than the theoretical is probably due to the following factors;the uncertainty in establishing the true position of the undisturbed zero fringe, and the uncertainty in measuring the reservoir conditions. These two factors together could amount at almost 3% according to the analysis of Chapter 5.

For the Mach 3 Channel, the measured densities are about 10-15% higher than the theoretical values, being at an almost constant interval above the values predicted by Characteristic Theory. Part of this is probably due to fixed error, introduced by the reference density calculated from No. 6 Pressure hole. No. 6 hole was not entirely reliable due to the fact that it was slightly chipped. The effect of chips and enlargement on pressure holes is discussed later when dealing with the Mach 3 Pressure hole tests.

Comparison of density contours obtained theoretically(Curve No. 33)with those obtained by finite fringes, infinite fringes(Fig. 38) and Contour Fringes(Fig. 45)shows that the real flow follows the somewhat uneven expansion predicted by characteristics, and the contours have the same general shape. The Mach 3 Channel has a more even expansion, as shown by both the theoretical curves(Curve No. 46)and interferograms. (Fig. 40,45) There is however quite a marked difference in the density contours, the theoretical contours beginning to curve toward the exit at about y= 0.7", while the interferograms show that the contours do not change curvature until y = 1.3". This is possibly due to the non-uniform flow in the throat,(see following section.)

1.4 Flow in the Throat.

The Method of Characteristics requires as a condition that the flow across the throat should be uniform and sonic, i.e. M=1. The corresponding density in this case is 0.2412 lbs/cu. inch. From Curve No. 33 it can be seen that the flow is not uniform for the Mach 2 channel, taking the contour labelled .24 as the sonic line, the flow has reached Mach 1 before the throat, except near the centreline. This appears to modify the flow immediately after the throat, the contours being curved more toward the throat, as for example the contours labelled .17 and.18. This is noticible also in curves 21 to 30, where there is a considerable divergence in the throat area, the curves thereafter converging. In the Mach 3 Channel the sonic line lies between the fringes labelled 21 and 22 in the infinite fringe interferogram Fig. 40; and is similar to the Mach 2 case. However here the flow appears to be modified for a much greater distance, due no

doubt to the greater divergence of the walls.

1.5 Flow in the Test Section.

The high uncertainty interval of 3% is largely due to the uncertainty in measuring the undisturbed fringe width b, which is a cumulative error, and the various fixed errors associated with measurement of reservoir conditions and undisturbed zero fringe position. If only relative changes of density taken together in the channel are to be investigated, these errors may be neglected, and the only uncertainty to be taken into account is that involved in the measurement of fringe position, which is less than 1/2% as found in Chapter 5. Thus the finite fringes as well as the infinite fringes yeild information about the details of the flow, which may involve changes of less than 3% of the density.

The area of uniform flow bounded by the last expansion waves and the exit shock waves constitutes the test section. Curves 13 to 21 show that this area has a uniform density to within 1% to 1 1/2% in the Mach 2 Channel. There is no data for the Mach 3 Channel.

The Schlieren picture of the Mach 3 Channel Fig. 46 shows a wealth of Mach lines. The Schlieren system was set for maximum sensitivity so that very weak shocks are shown clearly. An idea of the magnitude of these disturbances can be gained from the infinite fringes Fig. 38 and 39. Most of them cause only a small fraction of a fringe width distortion, one or two amounting to 1/4 fringe width. This corresponds to a 2% change in density. However the distortion is limited to the immediate area of the weak shock the density contours not being altered, so that these disturbances can be neglected.

These weak shocks originate at small imperfections in the channel walls. The Mach 2 Channel walls had been slightly roughened by prolonged use, their original polish having been removed by the abrasive action of dust in the air.

The Schlieren picture taken parallel to the glass walls(Fig. 56) shows a series of weak shock waves originating within the channel, which are strong enough to be observed by Shadowgram (Fig.55). These are absent in the #0M2 Channel (Fig. 50 and 51), which indicates that they are caused by the pressure holes in the glass walls of the #2M2 Channel. The infinte fringe interferogram shows that these are again of very small magnitude, and do not change the flow appreciably, even if it is considered that the disturbance occupies only a fraction of the channel width.

Imperfections in the glass walls of the Mach 3 Channel mark the details of the flow, so that no reliable information can be obtained either from the infinite fringes Fig. 40 to 43 or from the Schlieren Fig. 47.

2. Boundary Layer Flow.

Fringes are in sharp focus right through the boundary layer, and the interferometer is therefore ideal for boundary layer evaluation, especially since it does not in any way disturb the flow. It has been shown in Charter 5 that the errors due to refraction etc. are small in this case, so that profiles have an uncertainty of 4 or 5%.

No correlation with theory has been attempted for the following reasons. Theoretical solutions have so far been presented for a flat plate in uniform flow, with extensions to certain profiles. In this case there are severe changes of flow

parameters and wall heat conduction and roughness are difficult to assess. There is in addition the uncertainty of assigning a Reynolds Number due to the difficulty of choosing a characteristic length.

Much more meaningful results would be obtained by studying the boundary layer on a flat plate introduced into the test section, which would justify the labour involved in making a theoretical analysis of the problem. If the channels are extended to give a longer test section, and arranged to discharge into a reciever, which could be maintained at a variety of pressures the setup would be ideal for boundary layer studies over a range of Reynolds Numbers.

2.1 Boundary layer profiles.

A number of preliminary remarks can be made about the boundary layer. In both Mach 2 and Mach 3 Channels, the profiles appear to alter markedly at about 0.5" downstream of the throat, the profiles having a much steeper gradient at the wall after this point. Examination of the Mach 2 Schlieren picture(Fig. 46)shows what appears to be a boundary layer transition at about this point. The exposure of this picture was too long to show up the detail of the turbulent layer. Unfortunately all detail in the Mach 3 channel is obscured by striations. It appears to be a characteristic of the laminar layer to have a small gradient at the wall as compared to the turbulent layer.

Boundary layer development is shown clearly by the progressive profiles of Curves No. 37 and 38. The thickness estimated from these curves

for the Mach 2 Channel, are larger than those estimated from Schlieren(Curve No. 40). The curves are parallel after the boundary layer transition. The difference is due to a number of reasons. It is difficult to decide exactly where the boundary layer ends, and the corner effect discussed by Bershader(Ref. 8)would make the layer appear thicker in the interferogram. Furthermore, the exact position of the wall is masked by diffraction, and in future experiments it would be well to provide a reference mark in the focal plane of the lens so that the exact position of the wall may be determined. In the Schlieren picture, only the area of large density gradient shows up, so that the layer appears thinner. The true thickness therefore lies somewhere between the two. The boundary layer is about twice as thick as the allowance of 0.005" per inch used in the design of the channels. However it appears that this is correct, since the channels reach their design Mach Number.

The Mach 3 Channel boundary layer is considerably thicker but shows the same characteristics. On an assumption that the allowance should be about half the thickness, the allowance should be0.007" per inch. This would bring the average Mach Number measured by cones nearer the design Mach Number.(Table No. 26)

2.2 Boundary Layer Exit Shock Wave Interactions.

Curves No. 1 to 20 could have been used to plot a more detailed set of density contours in the area of the axial corner where the exit shock originates. However a better plot would have been obtained by using composite fringes, with

the fringes adjusted to be extremely narrow. However the isopycnals(Curve No. 33)and the infinite fringes (Fig. 38)show some interesting features.

Before reaching the shock the boundary layer thickens, due to the higher pressure beyond the shock being transmitted through the subsonic portion of the layer. This causes a small preliminary compression wave to be formed, which is shown clearly in several of the Schlieren pictures(Fig. 40, 58-62). The wave is also shown in Curves No. 1 to 20, just ahead of the shock wave. It may be noted here that the shock wave has been indicated by a sloping straight line inthese curves, for want of better information. Actually the shock is of course very much steeper than this, but its exact position is not shown by the interferogram.

The thickening of the boundary layer does not extend to the same extent along the glass walls, so that the boundary layer correction at the exit is a little too high. This accounts for the fact that the corrected density at exit is higher than the theoretical.

The shock wave itself appears to originate at an abrupt kink in the boundary layer a little ahead of the corner. Both the Schlieren(Fig.46) and the infinite fringes(Fig. 38)seem to show that the shock does not reach all the way to the wall, as would be expected, since a shock can only exist in supersonic flow, but originates at the point where the subsonic boundary layer changes in thickness. Almost immediately after the boundary layer is compressed by the higher pressure behind the shock.

In Curve No. 37 the boundary layer profile for the air-jet boundary is shown. The supersonic portion of this has the same shape as the profile on the brass walls at exit.

3. Instrumentation.

3.1 Interferometer.

With the different fringe configurations possible, the interferometer is a versatile instrument. For most work it appears that composite fringes will be most useful, since this method has many advantages. If very narrow fringes with the correct inclination are used, contours showing considerable dete[illegible] in [illegible] of high density gradient can [illegible] with very little effort. The composite [illegible] interferograms of Fig. 44 and 45 are not good [illegible], since the fringes were too wide. Additional important advantages are that by moving the flow and no-flow interferograms with respect to each other, contours can be moved to any portion of the field, as for example, to some reference point, and as many contours as desired may be obtained. Zero errors, as well as the evaluation error introduced by the uncertainty in measuring the original fringe width are automatically cancelled out, so that this method yields the highest accuracy. This is important when test windows of plate glass are used, and the zero fringes are slightly curved.

However, finite fringes yield information not shown by composite or infinite fringes, especially in areas of low density gradient, or where the changes in the flow involve less than one fringe distortion, such as in the test section of the channels. The complete solution using finite fringes is extremely laborious. However, since the same interferogram can be used for the com-

posite fringe method, the work can be greatly reduced by evaluating the general flow field using composite fringes, and only using the finite fringes in areas where additional information is required. Finite fringes are also most useful where density profiles are to be measured, such as in boundary layers, especially if the total density change is small.

Infinite fringes will often reveal many details not shown by other methods, and if density gradients are high and zero errors small, can often be used to advantage instead of the composite fringes, such as in the throat area. Infinite fringes also give a good deal of qualitative information about details of the flow, but have the disadvantage that all optical components in the interferometer must be of high quality to reduce zero errors.

3.2 Reference Density using Pressure Data.

Evaluation of an interferogram in terms of absolute density requires that the absolute density at some reference point in the field be known. This usually requires some independent measurement of at least one of the flow parameters, if the density at the reference point cannot be calculated theoretically. It may be noted that the densities can always be determined with respect to the density at a reference point in the field, even if the reference density is unknown, and this will often yield useful information.

For the Mach 3 Channel, the reference density was determined by measurement of the static pressure at a pressure tap in the channel wall. Curve No1 35 compares the results obtained in the Mach 3 Channel by using infinite fringes with the free air outside the jet boundaries as reference, and using infinite fringes based on a pressure tap

The curves agree within the experimental error. Densities computed from the pressure tap measurements by the isentropic relation are also plotted in this curve, and these lie almost exactly on the curve plotted from theory, demonstrating the validity of this procedure. However it should be noted that in computing the densities from the infinite fringes, the boundary layer correction was first subtracted from the pressure tap reading, and this used as reference in labelling the fringes, the corresponding boundary layer correction then being added. If this is not done, the valves near the throat where the correction is smaller, will be too high.

The wall pressures at several reservoir pressures are plotted in Curve No. 41. For the #2 Channel walls, No. 1 and 3 holes were somewhat ragged, and No. 4 and 6 holes were rather large (0.03" diameter) and the inside edges were badly chipped. The corresponding points are badly displaced from the curves, this displacement being consistent over the range of reservoir pressures, showing that the flow over these holes was disturbed and caused them to register incorrect pressures. Thus the fixed error depends on the hole shape and size, being small for small, smooth holes.

The Hoolispen picture and interferogram of the #1H2 Channel Fig. 43 and 43 show that the #1 pressure holes give rise to somewhat stronger shocks than the #2 holes, although the disturbances are still small.

The #2H2 holes were all satisfactory, and were used in tests. Unfortunately the only pressure hole available as reference in the Mach 3 Channel was also chipped, and therefore unreliable.

3.3 Probes.

Densities computed from the static probe pressures are also plotted in curve No. 35, and lie very close to the theoretical curve. Hence it may be concluded that the probe could also be used as reference for Mach interferometer, providing that the small disturbance introduced by the probe itself could be considered negligible. This disturbance is in any case small.

Curves No. 42 and 43 plot the pressures read by the probe in traverses from wall to wall, in the region near the exit of the channel. The pressures change as much as 10% in the vicinity of the wall. Examination of the Schlieren pictures(Fig. 58 to 62)shows that near the walls, the compression wave from the tip of the probe is reflected from the wall and interferes with the flow at the hole. Neglecting the readings near the walls, the pressures still vary by about 4%. This may be due to small local disturbances in the channel striking the hole, and small misalignments of the probe with the flow and shows the necessity of taking the mean of several readings.

The curves plotting total head pressure along the channel Curve No. 4 for the #1 and #2 probes are at a fixed distance of about 1.5" apart. This can be accounted for by variation in reservoir conditions for the two tests.

The Mach number computed from static and total head pressures is plotted in Curve No. 14. This is some 5% off the theoretical curve. This is probably due to an accumulation of the errors involved in the use of the probes and pressure holes, and indicates that the use of a Machmeter employing a total head probe and static pressure tap would be unreliable, except as a rough check.

3.4 Cones.

Results of the cone tests Table No. 25 and 26 agree with the theoretical Mach Number to within the 1% uncertainty interval for the Mach 2 Channel, and within 2% for the Mach 3 Channel. In the Mach 2 Channel the shock wave formed on the larger cones (Fig. 68 to 72) is strongly curved, and therefore difficult to measure, whereas the shock on the 5° and 10° cones is weak and not clearly distinguishable. The 15° and 20° cones give the best results. In the Mach 3 Channel, the 20° and 25° cones have a larger apex angle than the Mach waves in the flow, and the shock waves are strongly curved and in the case of the 25° cone slightly detached. This accounts for the low values of Mach Number obtained with these cones.

4. Points for further Research.

Anumber of interesting problems can be studied with the Mach-Zehnder interferometer which has been constructed, in conjunction with the small supersonic channels:

a) Study of various channel contours for use in supersonic wind tunnels, such as a sharp corner nozzle, or flexible and continuously variable nozzles.

b) Study of flow in supersonic diffusers of various types.

c) Study of supersonic jets in mixing, efficiency of various nozzles for ejection etc.

d) Study of boundary layers, using insulated or heat conducting flat plates, or porous or rough plates in the test section of the channels.

e) Study of shock wave-boundary layer interaction, and simple and Mach reflection of shock waves.

Conclusions

The following conclusions may be drawn from the work.

The Mach-Zehnder interferometer which has been designed and built, has proved satisfactory in the measurement of density distributions in channel flow, and boundary layer with an uncertainty interval of only a few percent. Complete theory for the formation of fringes and operation of the instrument with practical arrangements of finite aperture and spectrum width of the source has been presented, together with an analysis of the errors involved.

For the Mach 2 Channel, the flow corresponds closely predicted by characteristic theory to within the experimental error of 3%. No conclusions can be drawn from the present data forthe Mach 3 Channel, due to large zero errors associated with the plane walls, and the uncertainty of the reference density calculated from the pressure tap.

Flow in the Mach 2 test section is homogeneous and uniform to within 1 1/2%, making it suitable for use as a small wind tunnel. Again no data is available for the Mach 3 Channel.

The flow in the throat of both channels is not uniform and sonic, as assumed in the design of the channels. This does not appear to affect the flow pattern near the test section, but modifies the flow to a certain extent in the area immediately downstream of the throat.

Boundary layer profiles may be measured with a few percent uncertainty interval and boundary

layer-shock wave interactions may be studied. The boundary layer in the channels undergoes a transition at about 1/2 inch downstream of the throat.

Pressure taps give consistent and reliable results, providing the hole is smooth and less than 0.020" in diameter. Larger holes with chipped burred or ragged edges introduce large fixed errors.

The use of probes to determine the Mach Number by the Rayleigh Pitot Tube Equation, involves an uncertainty of some 5% in this case, and the use of a Machmeter with the channels is not recommended for accurate work.

Cones, using the Taylor Maccoll shock solutions to find the Mach Number give results accurate to 1%, providing that the flow over the cone may be assumed uniform.

Bibliography

Ref.No.

1 Preston T.
The Theory of Light. Macmillan & Co. London 1928

2 Hardy A.C. & Perrin F.H.
The Principles of Optics. McGraw Hill Book Co. New York 1932

3 Michelson A.A.
Studies in Optics. Univ. of Chicago Press. 1927

4 SouthallJ.P.C.
Mirrors, Prisms and Lenses. Macmillan Co. New York. 1933

5 Zobel Th.
Verwendung von Lichtinterferenzen in der Technischen Messung. V.D.I. Zeit. 81 No.1 1937

6 Winkler
The Mach Interferometer applied to studying an axially symmetric supersonic air jet. Rev.Sci.Inst.19,307 My'48

7 Ashkenas H.I. & Bryson A.E.
Design and performance of a simple Interferometer for Wind Tunnel Measurements. J.Aeronautical Sci.18 92 F '51

8 Bershader D.
An Interferometric Study of Supersonic Channel Flow. Rev.Sci.Inst.20,260 Ap'49

9 Ladenburg, van Voorhis & Winkler
Interferometric Studies of Faster than Sound Penomena.Part I ; Gas Flow around Various Objects in a free Homogeneous Supersonic Air Stream. Phys.Rev.73, 1360 Je '48

10 Ladenburg, van Voorhis & Winkler.
Interferometric Studies of Faster than Sound Phenomena. Part II.; Analysis of Supersonic Air Jets. Phys.Rev. 76 662 S '49

11 Bennet
Effect of Size and Spectral Purity of Source on Fringe Pattern of the Mach-Zehnder Interferometer. J. App. Phys.22 Je '51

12 Bennet
Optimum Source Size for the Mach-Zehnder Interferometer. J.App.Phys.22 Fe '51

13 Price.
Initial adjustment of the Mach-Zehnder Interferometer. Rev.Sci. Inst.23.162 Ap '52

14 Pope & Colclough
Unpublished Thesis Notes. University of the Witwatersrand, Johannesburg.

15 Heath.
Geometrical Optics. Cambridge 1897

16 Bailey C.L. & Wood F.C.
Computation Curves for Compressible Fluid Problems. John Wiley & Sons New York 1949

17 Liepman H.W. & Puckett A.E.
Introduction to the Aerodynamics of a Compressible Fluid. John Wiley & Sons. New York 1947

18 Gas Turbine Laboratory, M.I.T.
Aerodynamic Measurements.

19 Shapiro A.H. & Edelman G.M.
Method of Characteristics for Two-Dimensional Supersonic Flow - Graphical and Numerical Procedures. J. App. Mechanics 14, A 154, '47.

Appendix 1.

Interferograms and Plates.

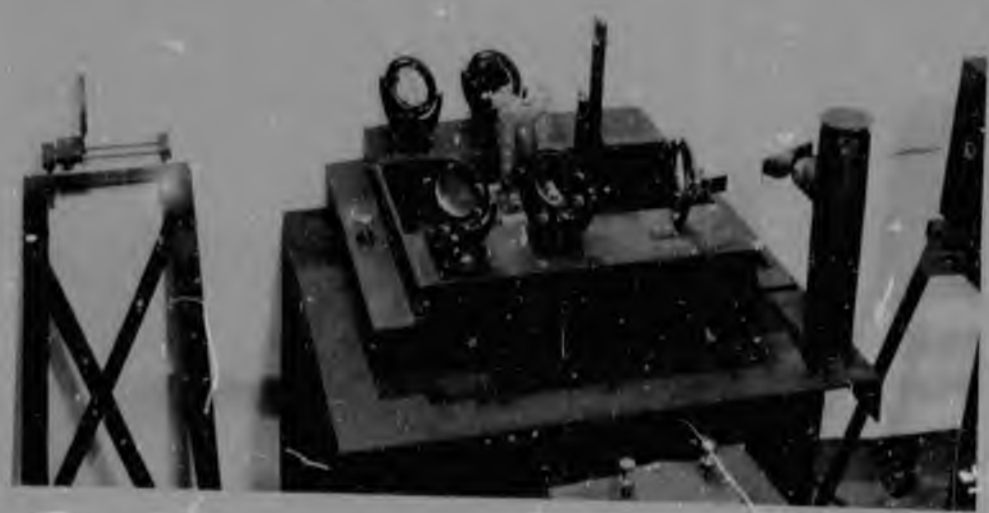

Fig. 13 General View of the Interferometer.

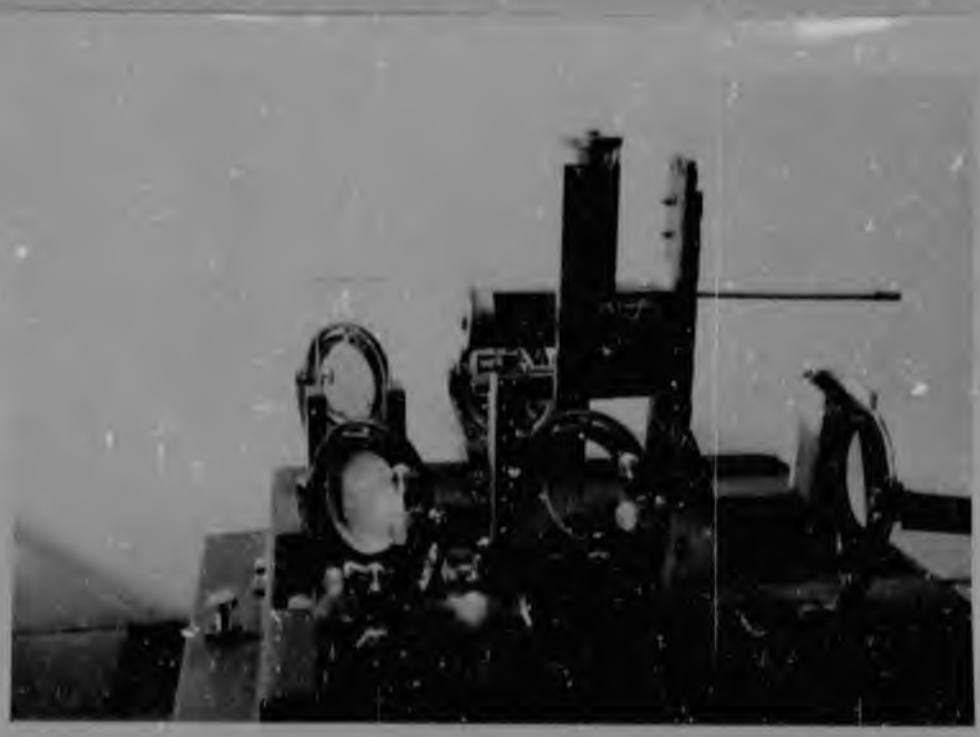

Fig.14 Closeup of the Interferometer with
Each 3 Channel.

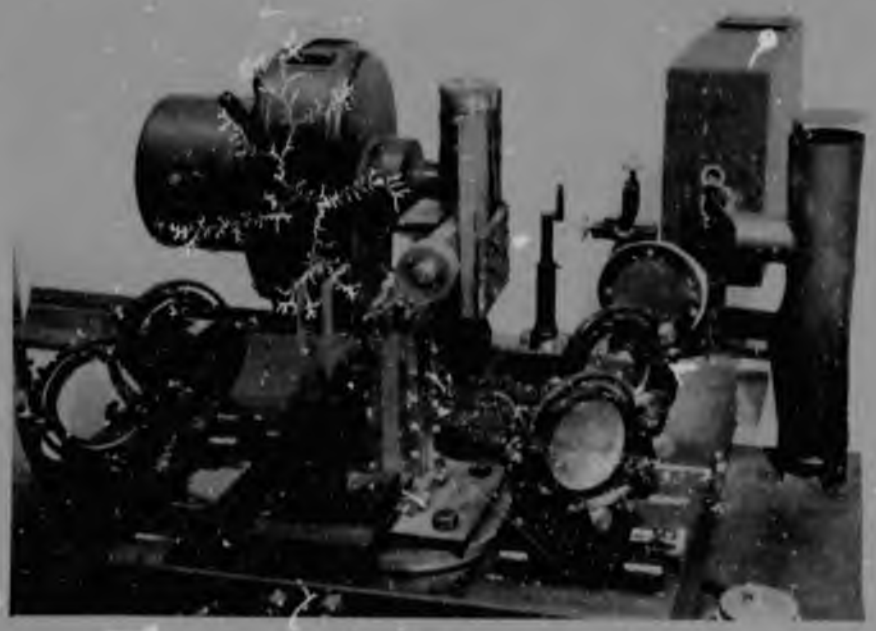

Fig 15 The Interferometer showing Arc Lamp.

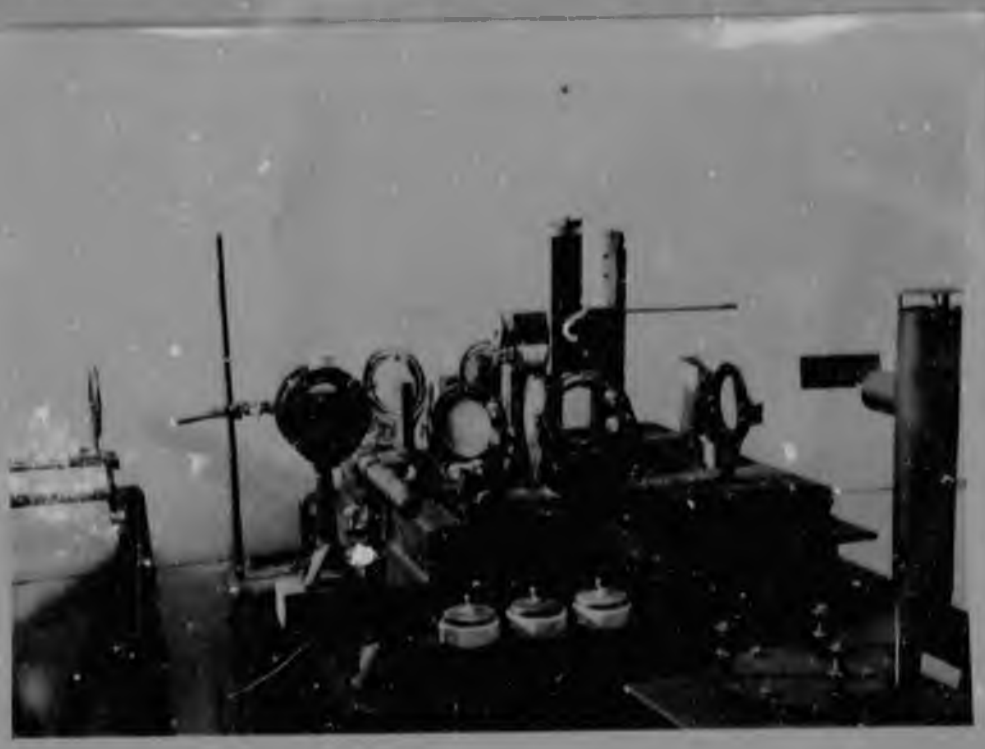

Fig. 16 Setup for Adjustment.



Fig.18 The Interferometer Plate Holders.

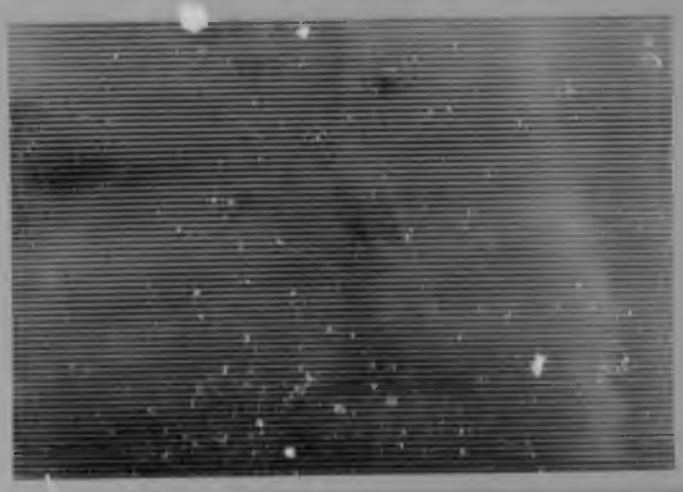

Fig.19 Fringes produced by the interferometer
lates only.



Fig.20 M2 Channel with Fringes distorted by Plate Glass.

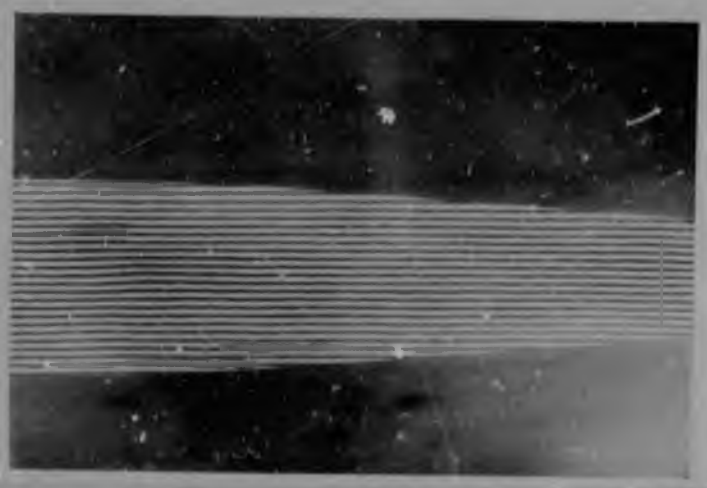

Fig.21 Zero Fringes in M2.2 Channel

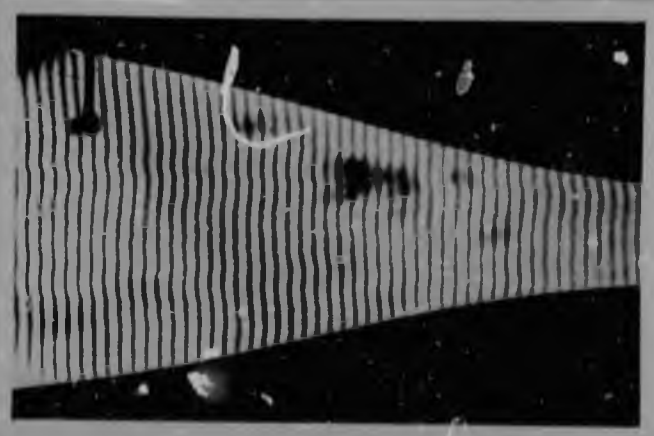

Fig.22 Zero Fringes in M3 Channel.

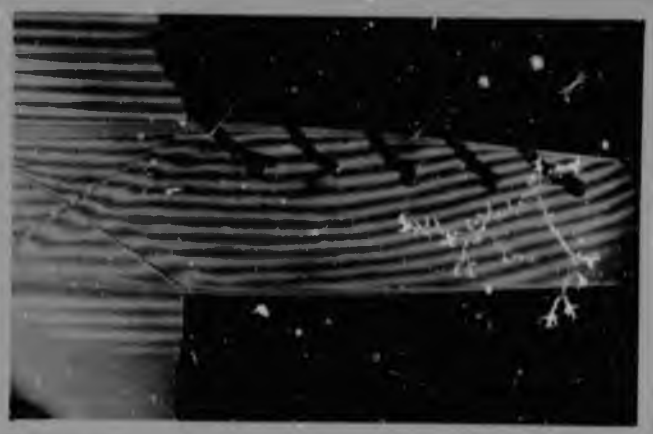

Fig. 25 -ve Vertical Fringes.



Fig. 24 Infinite Fringes.

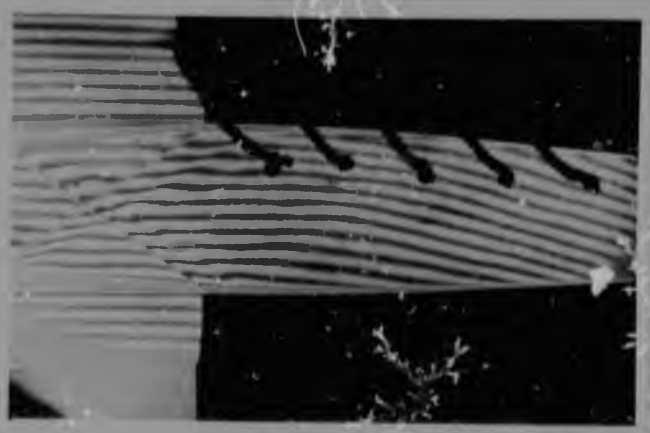

Fig. 23 +ve Vertical Fringes.



Fig.26 -ve Horiz. Fringes



Fig.27 +ve Horiz. Fringes



Fig.29 White Light Horiz. Fringes



Fig.28 Zero Horiz. Fringes



Fig.30 Mach 2 Channel.

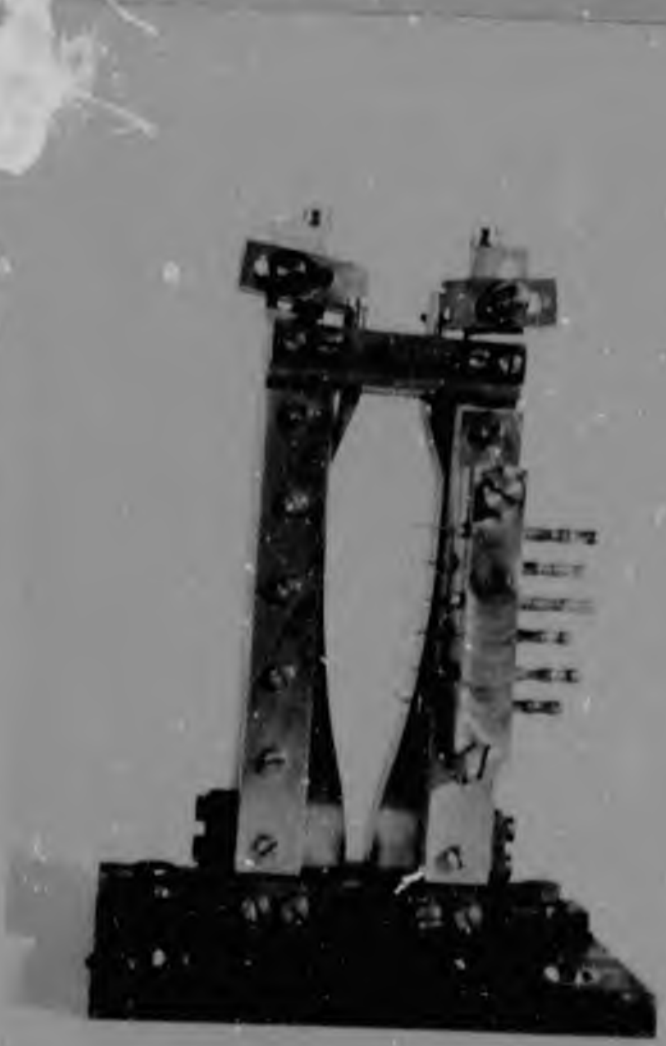

Fig.31 Mach 3 Channel.

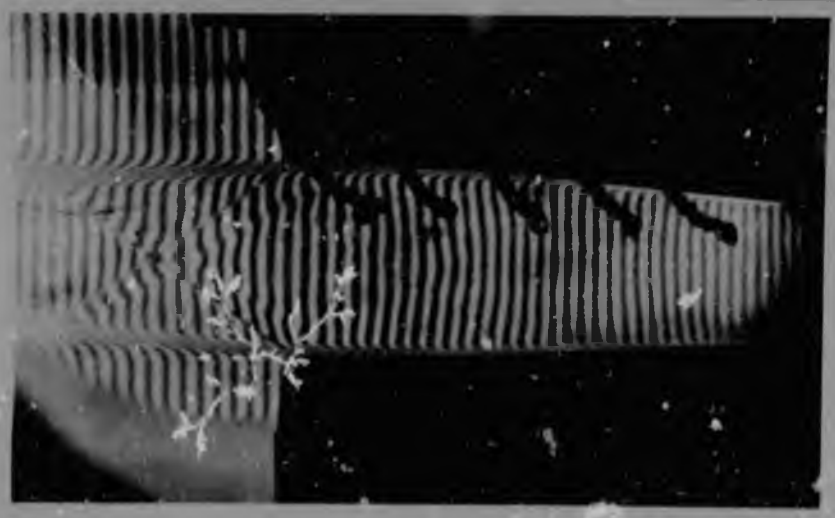

Fig.35 [illegible]



Fig.36 [illegible]

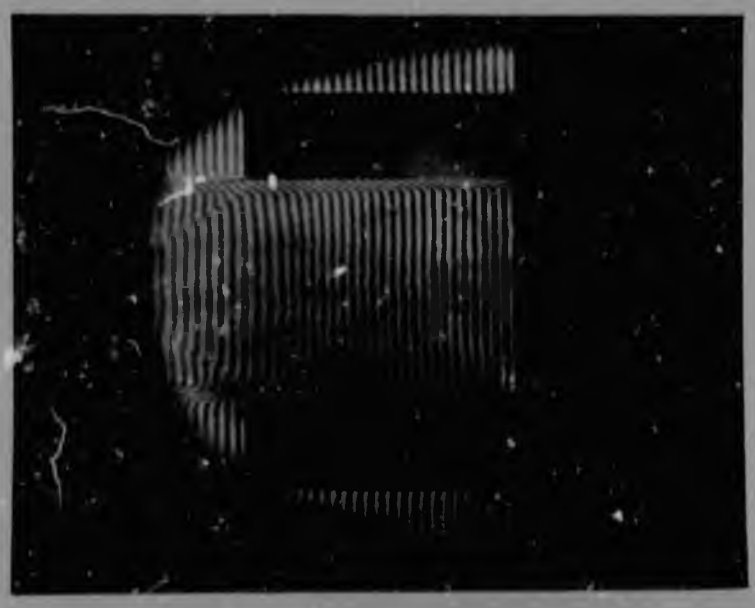

Fig.37 [illegible]

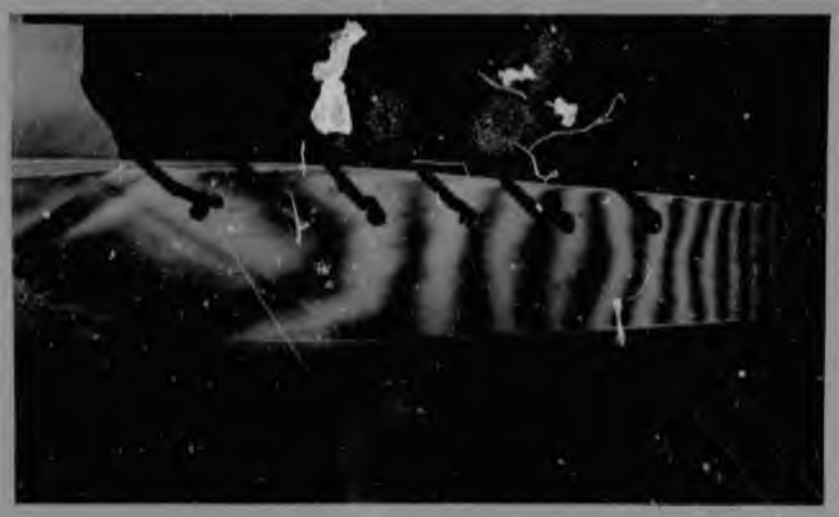

Fig.38 A2H2 Density Contours.

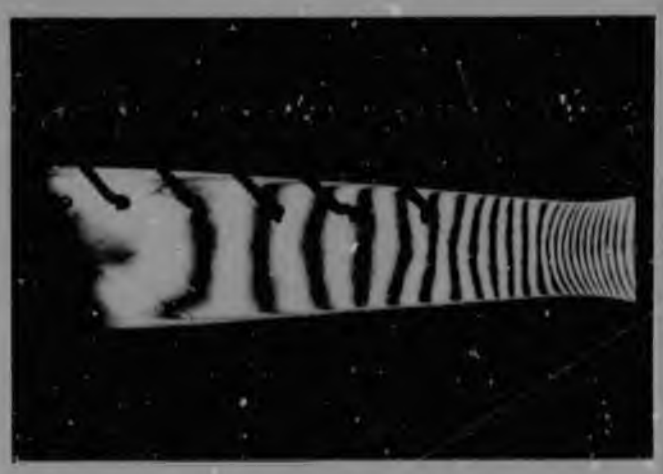

Fig.39 A2H2 Throat Density Contours.

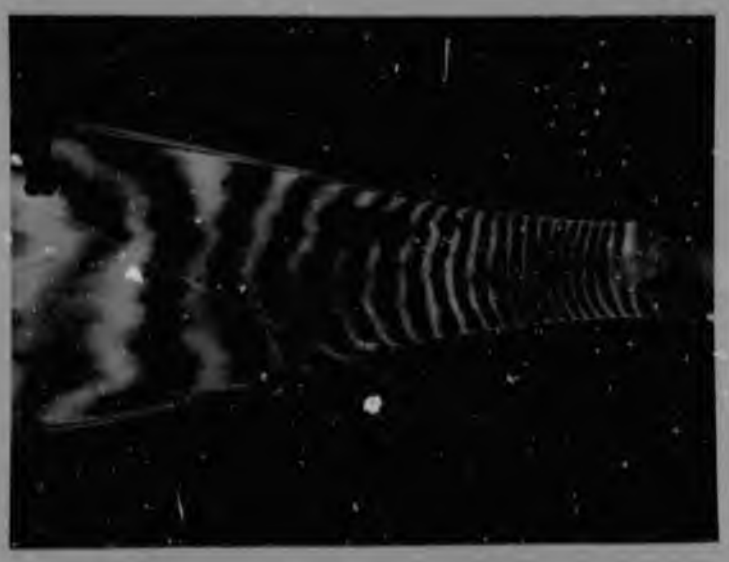

Fig.40 A3 Throat Density Contours.



Fig.36 M=2 Density Contours.

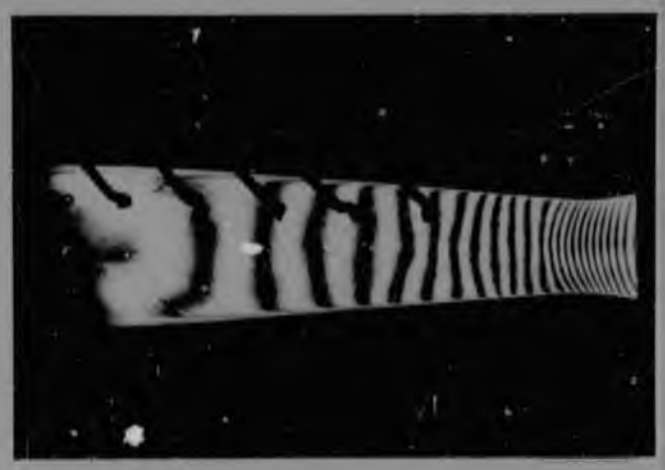

Fig.37 M=2 Throat Density Contours.

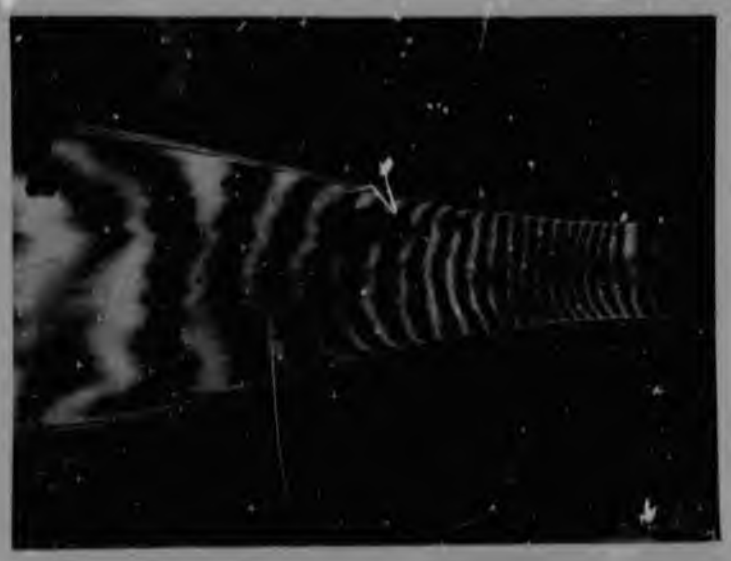

Fig.38 M Throat Density Contours.

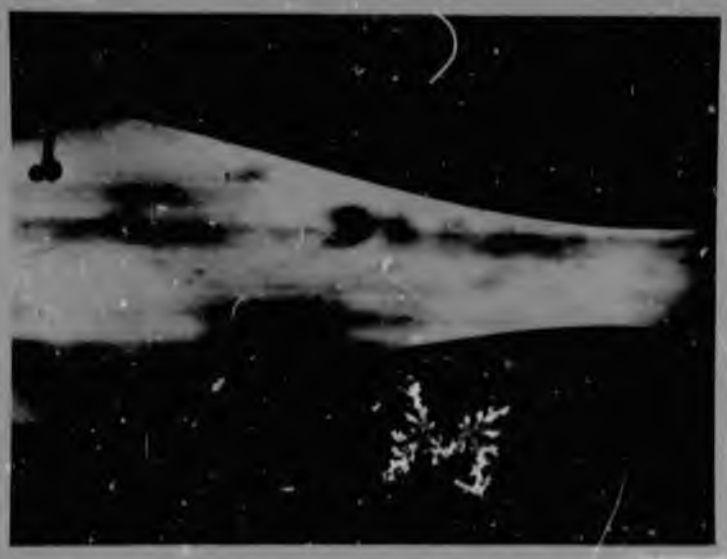

Fig.41 Zero of Fig.42 [illegible]

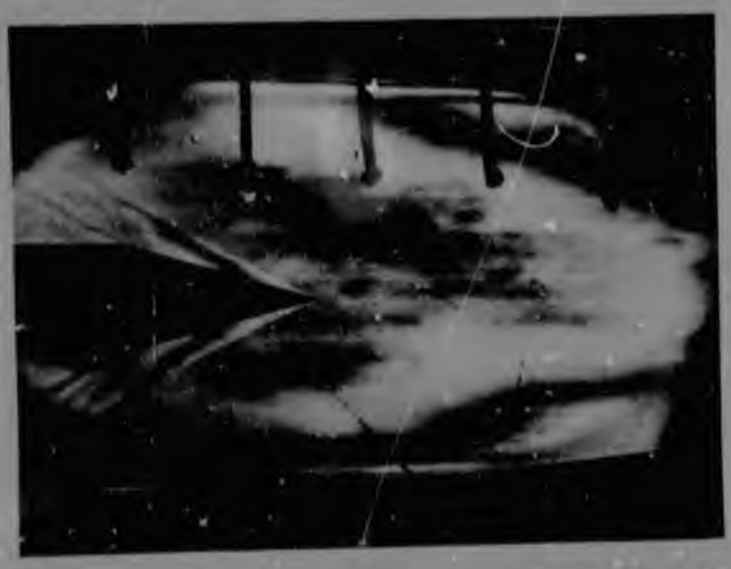

Fig.42 [illegible] Density Contours, Working Section



Fig.43 Zero of Fig.42



Fig.44 ST XP Composite Density Contours.

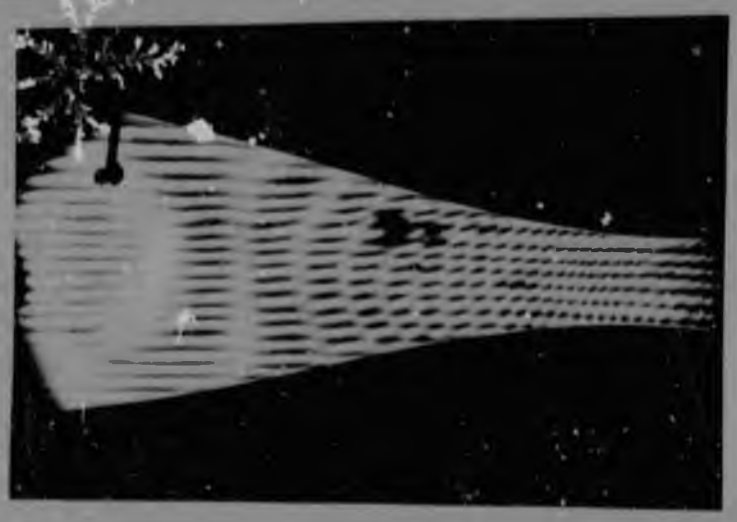

Fig.45 XP Composite Density Contours.

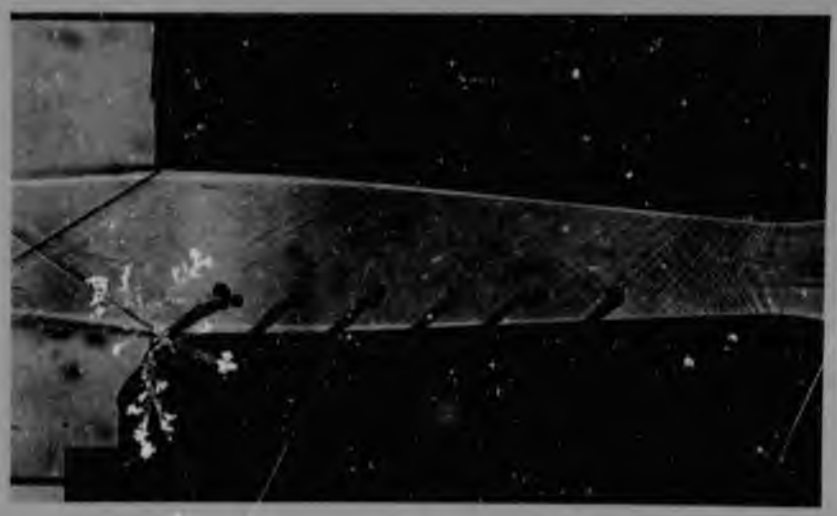

Fig.46 [illegible] Schlieren 43[illegible]



Fig.47 [illegible] Schlieren



Fig.48 [illegible] Schlieren



Fig.49 #C M2 Infinite Fringes. 3613



Fig.50 #C M2 Schlieren. 3951



Fig.51 #C M2 Infinite Fringes. 3918

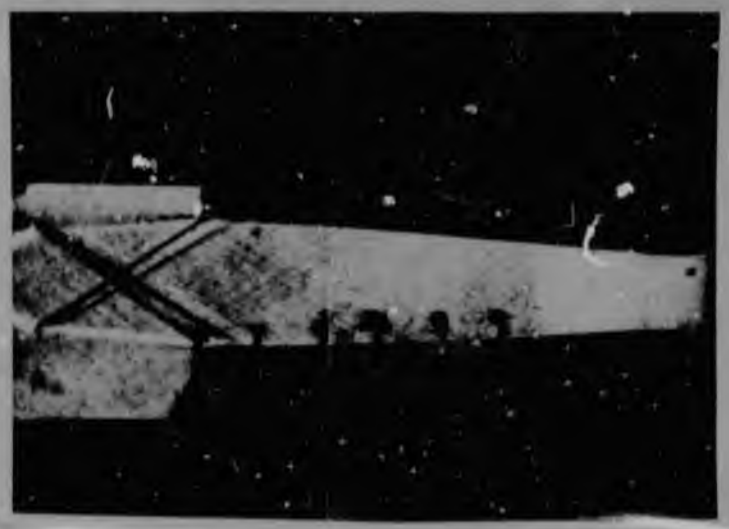

Fig.52 M_1 1.2 Schlieren P602

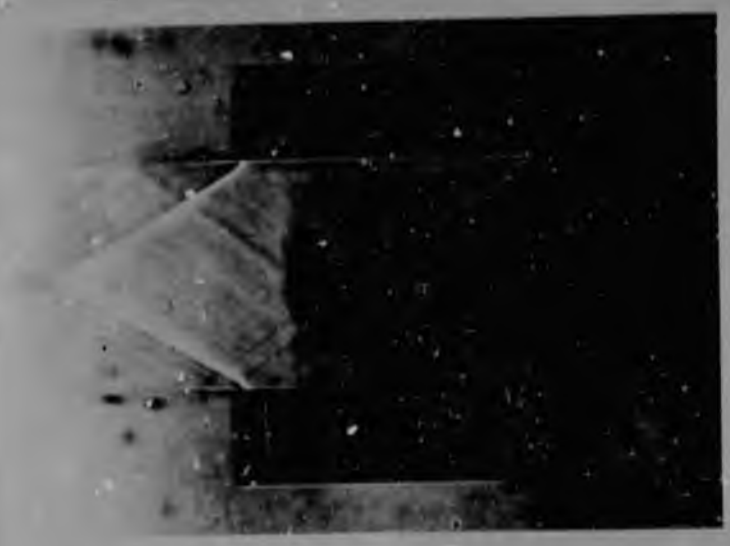

Fig.53 M_1 1.2 Schlieren 2183

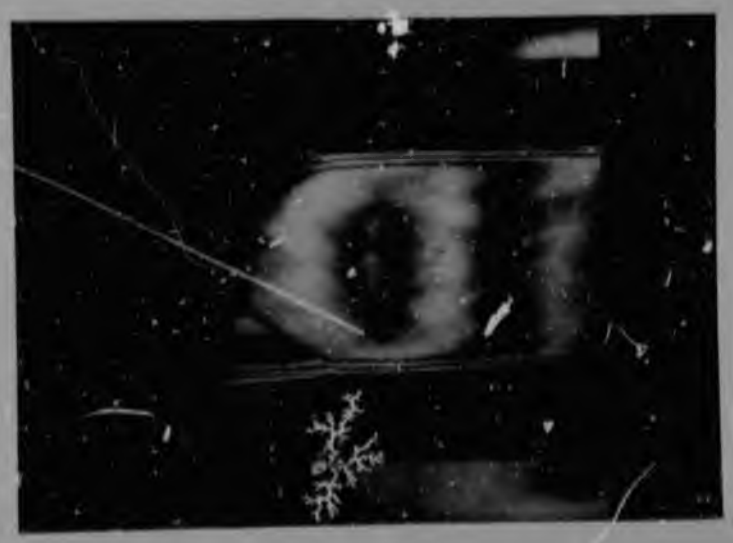

Fig.54 M_1 1.2 Infinite Fringes 3513

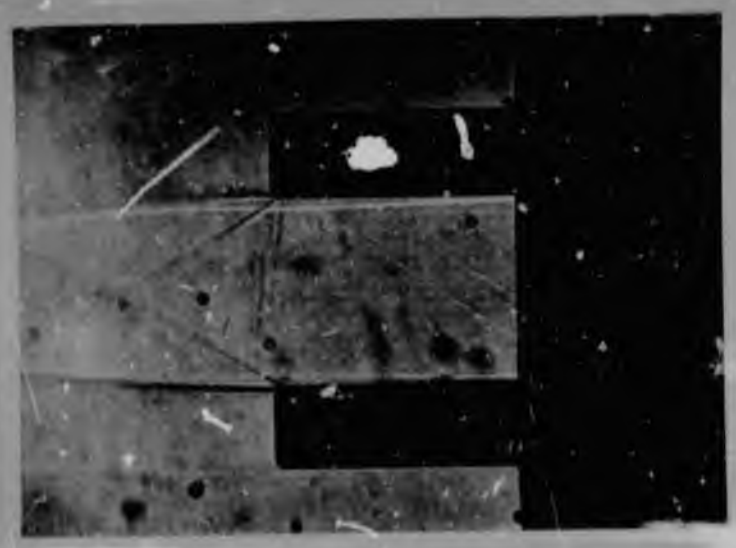

Fig.55 #2 M2 Shadowgram 4486

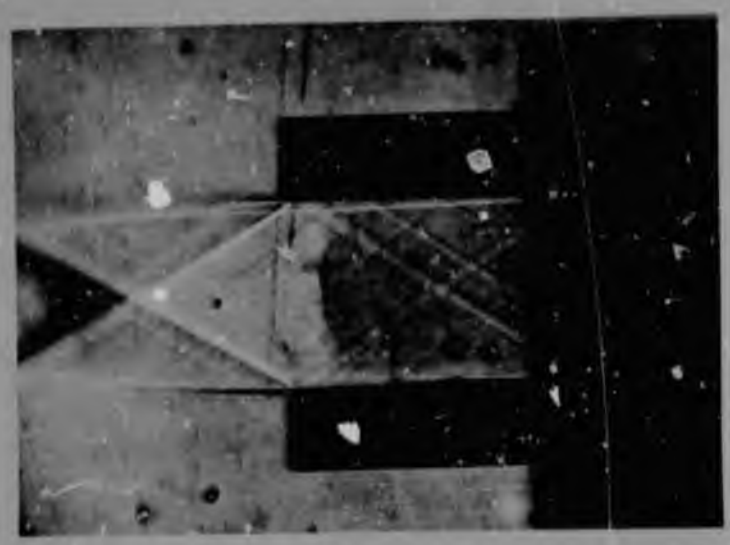

Fig.56 #2 M2 Schlieren 4486



Fig.57 #2 M2 Infinite Fringes 4813

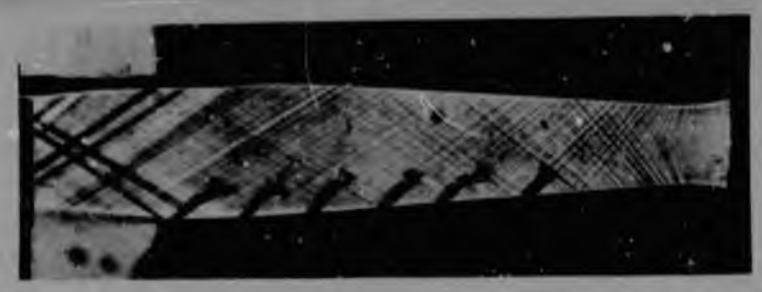

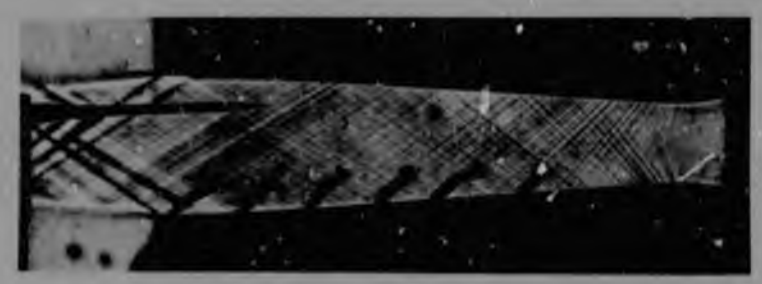







Fig.35-62 Static Probe in #2 M2 Channel

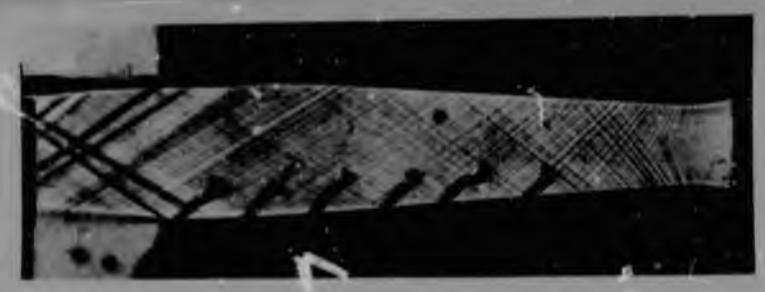

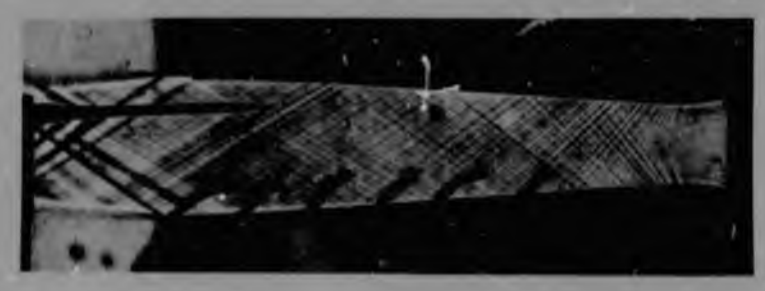





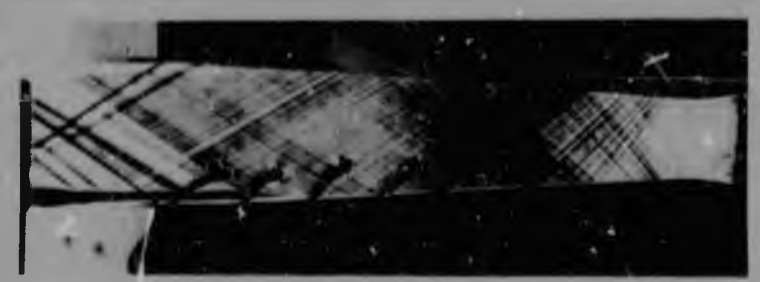

Fig.58-62 Static Probe in 12 x 2 Chennel

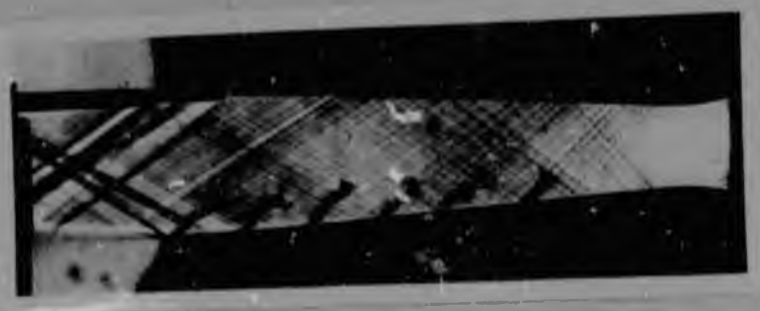

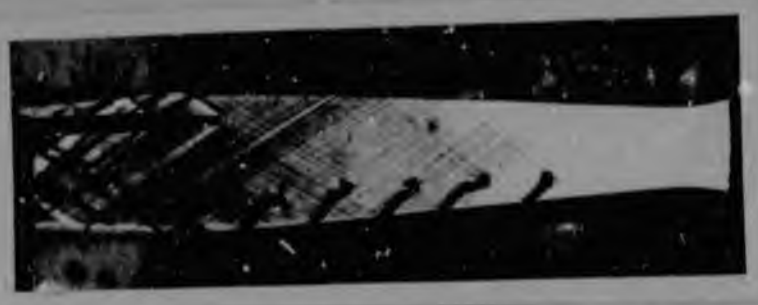



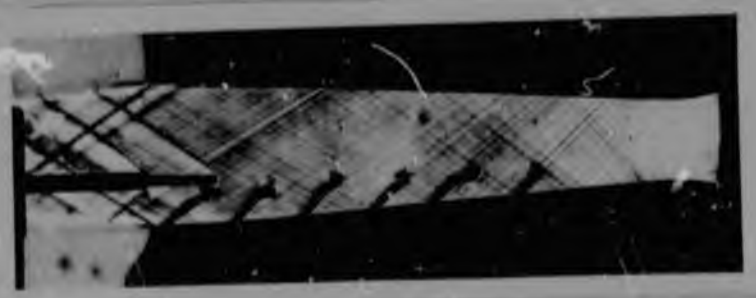



Fig.63-67 Total Head Prole in #2 M2 Channel



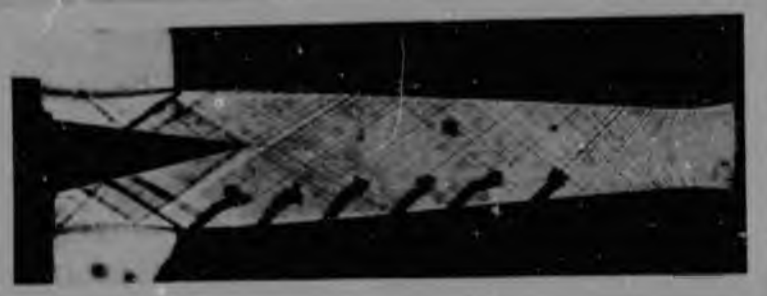

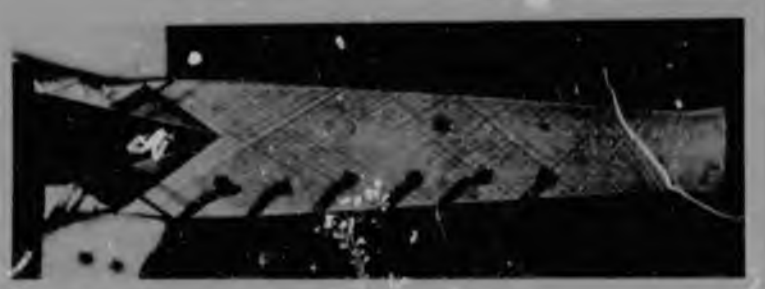



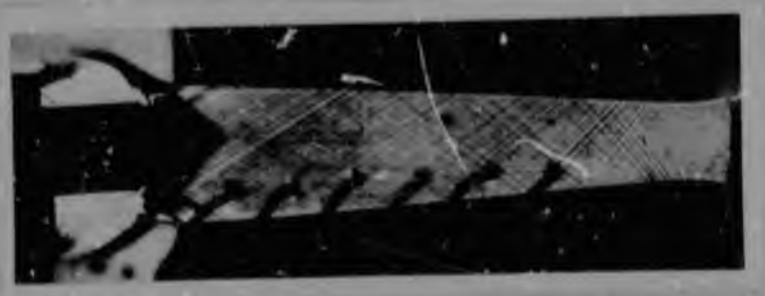

Fig. 68-72 Cones in #2 R2 Channel.

Apendix 2

Tables

Table No. 1

Mach 2 Channel Sizes

Width = .6260"

y	z	y	z
.000	.1550	.80	.2127
.05	.1563	1.00	.2278
.10	.1598	.20	.2430
.15	.1635	.40	.2547
.20	.1673	.60	.2637
.40	.1824	.80	.2688
.60	.1975	2.00	.2700

Co-ordinates of No.1 Pressure Holes

No.	x	y
1	.2211	1.989
2	.1872	1.739
3	.1220	1.456
4	.1220	1.246
5	.1240	.989
6	.1134	.742

Co-ordinates of No;2 Pressure Holes

No.	x	y
1	.159	1.765
2	.156	1.533
3	.126	1.267
4	.126	1.016
5	.120	.756
6	.120	.509

Table No.2

Mach 3 Channel Sizes.

Width = .6250

y	x	y	x
.000	.1550	.40	.5750
.05	.1565	.60	.5970
.10	.1585	.80	.6160
.20	.1654	3.00	.6337
.30	.1750	.20	.6450
.40	.1855	.40	.6560
.50	.2045	.60	.6650
.60	.2195	.80	.6700
.70	.2390	4.00	.6738
.80	.2590	.03	.6740
.90	.2820	-.00	0.1550
1.00	.3075	-.05	.1566
.20	.3575	-.10	.1580
.40	.4055	-.15	.1630
.60	.4480	-.20	.1705
.80	.4850	-.40	.2210
2.00	.5190	-.60	.2210
.20	.5490	-.80	1.13

Co-ordinates of Pressure Holes

No.	x	y
1	.3558	4.010
2	.3575	3.606
3	.3300	3.188
4	.3300	2.799
5	.2740	2.437
6	.3008	2.049

TABLE NO. 3

Mach 3 Density Distribution

From Fig. 35

Atm. Pressure: 11.93 psia. Humidity: 64%
Atm. Temperature: 58.5°F. b:0.04661"

N	y'	y	Y/b	ρ'
	x = 0.348			
-5	11.892	2.554	-.048	.0606
-4	11.618	2.508	-.094	.0608
-3	11.320	2.450	-.152	.0585
-2	11.148	2.42[illegible]	-.[illegible]	.0855
-1	10.918	2.36[illegible]	-.[illegible]	.0606
0	10.605	2.[illegible]	-.062	.0606
1	10.450	2.272	-.091	.0603
2	10.226	2.226	-.076	.0614
3	9.840	2.148	-.748	.0541
4	9.754	2.131	-.123	.0601
5	9.526	2.084	-.119	.0599
6	9.292	2.037	-.127	.0599
	x = 0.377			
-5	11.888	2.563	.145	.0624
-4	11.660	2.517	-.159	.0628
-3	11.426	2.47[illegible]	-.152	.0625
-2	11.188	[illegible]	.102	.0620
-1	10.950	[illegible].873	.073	.0617
0	10.714	2.[illegible]28	.944	.0615
1	10.488	2.879	.058	.0616
2	10.254	2.232	.051	.0615
3	10.022	2.185	.044	.0615
4	9.796	2.139	.058	.0608
5	9.540	2.087	-.055	.0605
6	9.314	2.041	-.041	.0608
	x = 0.267			
-5	11.916	2.569	.273	.0636
-4	11.700	2.525	.330	.0641
-3	11.462	2.477	.302	.0639
-2	11.220	2.428	.252	.0634
-1	11.010	2.385	.330	.0641
0	10.868	2.356	.709	.0677
1	10.542	2.290	.294	.0638
2	10.304	2.242	.264	.0635
3	10.076	2.196	.280	.0637
4	9.850	2.150	.294	.0638
5	9.638	2.107	.373	.0645
6	9.426	2.064	.451	.0653
7	9.254	2.029	.701	.0676
8	9.120	2.002	1.122	.0716
8	9.050	1.988	.822	.0687
8	8.886	1.955	.115	.0621
	x = 0.262			
5	9.708	2.121	.673	.0673
6	9.510	2.081	.815	.0687
7	9.336	2.046	1.065	.0710
8	9.200	2.018	1.465	.0748
8	8.986	1.975	.544	.0661
9	8.760	1.929	.558	.0663
10	8.568	1.890	.722	.0678
11	8.324	1.841	.672	.0673
12	8.073	1.790	.579	.0665
13	8.073	1.790	.443	.0652

N	y'	y	Y/b	p'
	x = 0.257			
-5	11.938	2.51	.359	.0644
-4	11.726	2.536	.437	.0651
-3	11.500	2.485	.473	.0655
-2	11.252	2.434	.380	.0646
-1	11.042	2.792	.480	.0655
0	10.834	2.750	.580	.0665
1	10.610	2.304	.594	.0666
2	10.382	2.258	.608	.0667
3	10.152	2.217	.730	.0679
4	9.982	2.177	.873	.0692
5	9.784	2.137	1.015	.0706
6	9.616	2.103	1.287	.0731
7	9.462	2.071	1.601	.0760
8	9.306	2.040	1.937	.0792
9	9.150	2.008	2.251	.0821
9	9.062	1.990	1.865	.0785
9	8.868	1.951	1.029	.0707
10	8.686	1.914	1.237	.0726
11	8.462	1.869	1.272	.0730
12	8.218	1.819	1.201	.0723
13	7.992	1.773	1.215	.0724
14	7.774	1.729	1.272	.0730
15	7.614	1.697	1.586	.0759
16	7.266	1.626	1.065	.0710
17	5.978	1.568	.822	.0687
18	6.728	1.517	.729	.0679
19	6.460	1.463	.572	.0664
	x = 0.252			
5	9.878	2.196	1.423	.0744
6	9.670	2.114	1.523	.0753
7	9.518	2.083	1.858	.0774
8	9.366	2.052	2.194	.0816
9	9.204	2.019	2.487	.0843
9	9.072	1.992	1.908	.0729
9	8.902	1.958	1.179	.0721
10	8.706	1.918	1.322	.0734
11	8.522	1.878	1.465	.0748
12	8.331	1.828	1.394	.0741
13	8.030	1.781	1.386	.0740
14	7.800	1.735	1.401	.0742
	x = 0.247			
-4	11.328	2.551	.887	.0694
-3	11.610	2.507	.945	.0699
-2	11.382	2.461	.959	.0700
-1	11.172	2.418	1.037	.0708
0	10.966	2.376	1.137	.0717
1	10.748	2.332	1.194	.0722
2	10.530	2.292	1.337	.0736
3	10.354	2.252	1.480	.0749
4	10.166	2.214	1.666	.0766
5	10.000	2.181	1.958	.0794
6	9.882	2.146	2.208	.0817
7	9.678	2.115	2.544	.0849
8	9.508	2.081	2.815	.0874
9	9.348	2.048	3.108	.0901
9	9.200	2.018	2.465	.0841
9	9.048	1.988	1.822	.0781
10	8.850	1.947	1.944	.0792
11	8.648	1.906	2.065	.0804
12	8.476	1.864	2.185	.0813
14	8.008	1.777	2.301	.0826
15	7.858	1.752	2.765	.0869

N	y'	y	Y/b	ρ'
16	7.564	1.687	2.372	.0833
17	7.338	1.641	2.386	.0834
18	7.088	1.590	2.293	.0825
19	6.864	1.545	2.325	.0828
20	6.630	1.497	2.300	.0826
21	6.334	1.437	2.014	.0799
22	6.012	1.372	1.621	.0762
23	5.704	1.310	1.293	.0732
	x = +1.237			
-4	11.912	2.568	1.252	.0728
-3	11.718	2.529	1.416	.0743
-2	11.508	2.486	1.494	.0750
-1	11.304	2.445	1.616	.0762
0	11.108	2.405	1.759	.0775
1	10.912	2.365	1.901	.0788
2	10.726	2.328	2.109	.0808
3	10.554	2.293	2.358	.0831
4	10.380	2.258	2.608	.0855
5	10.206	2.222	2.837	.0876
6	10.038	2.188	3.108	.0910
7	9.856	2.157	3.315	.0921
8	9.614	2.102	3.269	.0916
9	9.486	2.076	3.708	.0958
9	9.304	2.039	2.915	.0883
9	9.168	2.012	2.337	.0829
10	8.952	1.968	2.394	.0835
11	8.764	1.930	2.579	.0852
12	8.570	1.885	2.615	.0855
13	8.304	1.837	2.586	.0853
14	8.100	1.795	2.680	.0862
15	7.898	1.754	2.808	.0873
16	7.682	1.711	2.886	.0881
17	7.472	1.668	2.965	.0888
18	7.244	1.622	2.979	.0889
19	7.040	1.581	3.100	.0901
20	6.834	1.539	3.200	.0910
21	6.616	1.495	3.257	.0915
22	6.378	1.446	3.207	.0911
23	6.158	1.402	3.264	.0916
24	5.890	1.347	3.086	.0899
25	5.600	1.289	2.843	.0877
26	5.210	1.210	2.150	.0812
	x = 0.227			
-3	11.866	2.559	2.059	.0803
-2	11.666	2.518	2.180	.0815
-1	11.464	2.477	2.302	.0826
0	11.296	2.443	2.579	.0851
1	11.080	2.399	2.630	.0857
2	10.900	2.363	2.859	.0878
3	10.736	2.330	3.151	.0905
4	10.558	2.294	3.380	.0927
5	10.374	2.256	3.566	.0944
6	10.174	2.216	3.703	.0958
7	9.986	2.178	3.594	.0975
8	9.776	2.135	3.973	.0982
9	9.564	2.092	4.051	.0990
9	9.368	2.052	3.194	.0909
9	9.216	2.022	2.551	.0849
10	9.000	1.978	2.608	.0855
11	8.790	1.935	2.687	.0862
12	8.546	1.886	2.636	.0857
13	8.320	1.840	2.651	.0859

N	y'	y	V/b	p'
14	8.124	1.800	2.794	.0872
15	7.920	1.759	2.915	.0883
16	7.708	1.716	2.993	.0891
17	7.498	1.673	3.072	.0898
18	7.284	1.630	3.150	.0905
19	7.076	1.588	3.250	.0918
20	6.854	1.543	3.286	.0918
21	6.648	1.501	3.386	.0927
22	6.446	1.460	3.507	.0939
23	6.236	1.418	3.607	.0948
24	6.042	1.378	3.750	.0962
25	5.816	1.332	3.764	.0963
26	5.576	1.284	3.736	.0960
27	5.336	1.238	3.686	.0956
28	5.082	1.184	3.593	.0947
29	4.754	1.117	3.157	.0906
30	4.382	1.042	2.550	.0849
	x = 0.216			
-2	11.850	2.545	2.973	.0889
-1	11.638	2.513	3.073	.0898
0	11.460	2.476	3.280	.0918
1	11.250	2.434	3.380	.0927
2	11.062	2.396	3.566	.0944
3	10.886	2.360	3.794	.0960
4	10.686	2.320	3.937	.0979
5	10.450	2.278	3.908	.0976
6	10.242	2.230	4.008	.0986
7	10.012	2.183	4.001	.0985
8	9.880	2.156	4.423	.1024
9	9.564	2.092	4.051	.0991
9	9.342	2.047	3.087	.0899
9	9.210	2.020	2.508	.0845
10	9.000	1.978	2.608	.0855
11	8.804	1.938	2.751	.0868
12	8.530	1.883	2.572	.0851
13	8.310	1.838	2.608	.0855
14	8.108	1.797	2.729	.0866
15	7.908	1.756	2.851	.0877
16	7.790	1.734	3.379	.0927
17	7.482	1.670	3.008	.0892
18	7.274	1.628	3.108	.0901
19	7.068	1.586	3.207	.0911
20	6.848	1.542	3.265	.0916
21	6.648	1.501	3.386	.0927
22	6.448	1.461	3.529	.0941
23	6.236	1.418	3.607	.0948
24	6.046	1.379	2.771	.0963
25	5.828	1.335	3.829	.0969
26	5.620	1.293	3.928	.0978
27	5.410	1.250	4.007	.0986
28	5.188	1.205	4.043	.0989
29	4.962	1.159	4.057	.0990
30	4.730	1.116	4.135	.1007
31	4.500	1.066	4.064	.0991
32	4.244	1.014	3.950	.0980
33	3.776	0.919	2.914	.0883
	x = 0.206			
-2	12.024	2.591	3.745	.0961
-1	11.754	2.536	3.566	.0944
0	11.574	2.500	3.794	.0960
1	11.374	2.459	3.916	.0977

N	y'	y	Y/D	p'
2	11.134	2.414	3.952	.0980
3	10.940	2.371	4.080	.0988
4	10.720	2.326	4.066	.0991
5	10.488	2.279	4.058	.0991
6	10.242	2.230	4.004	.0986
7	10.012	2.183	4.001	.0985
8	9.782	2.136	3.994	.0984
9	9.572	2.094	4.094	.0994
9	9.378	2.058	3.322	.0921
9	9.214	2.022	2.551	.0849
10	9.014	1.981	3.672	.0961
11	8.788	1.935	2.687	.0862
12	8.518	1.880	2.508	.0845
13	8.314	1.839	2.629	.0857
14	8.108	1.797	2.729	.0866
15	7.902	1.755	2.829	.0875
16	7.682	1.711	2.886	.0881
17	7.472	1.668	2.965	.0888
18	7.210	1.615	2.829	.0875
19	7.[illegible]	1.563	3.143	.0905
20	[illegible]	1.539	3.200	.0910
21	[illegible]	1.499	3.343	.0923
22	6.486	1.458	3.464	.0935
23	6.228	1.416	3.884	.0944
24	6.032	1.376	3.707	.0957
25	5.818	1.333	3.786	.0965
26	5.608	1.290	3.864	.0972
27	5.408	1.250	4.007	.0986
28	5.198	1.207	4.086	.0993
29	5.000	1.167	4.228	.1006
30	4.798	1.126	4.350	.1018
31	4.600	1.086	4.492	.1031
32	4.390	1.043	4.571	.1030
33	4.200	1.005	4.751	.1055
34	3.970	.958	4.749	.1055
35	3.730	.910	4.721	.1052
	x = .196			
0	11.640	2.513	4.073	.0993
1	11.426	2.480	4.152	.0999
2	11.198	2.423	4.359	.1019
3	10.954	2.374	4.094	.0994
4	10.726	2.328	4.109	.0995
5	10.492	2.280	4.050	.0992
6	10.250	2.231	4.030	.0988
7	10.020	2.185	4.044	.0989
8	9.796	2.139	4.058	.0990
9	9.[illegible]	2.096	4.137	.0998
9	9.486	2.076	3.708	.0958
9	9.280	2.024	2.594	.0853
10	9.034	1.985	2.758	.0869
11	8.768	1.931	2.601	.0854
12	8.428	1.862	2.551	.0849
13	8.320	1.840	2.651	.0859
14	8.104	1.796	2.708	.0860
15	7.890	1.753	2.786	.0871
16	7.672	1.709	2.843	.0877
17	7.462	1.666	2.922	.0884
18	7.260	1.625	3.043	.0895
19	7.048	1.582	3.122	.0903
20	6.834	1.539	3.200	.0910
21	6.632	1.498	3.322	.0921
22	6.428	1.456	3.422	.0931
23	6.222	1.415	3.543	.0942
24	6.026	1.375	3.750	.0962

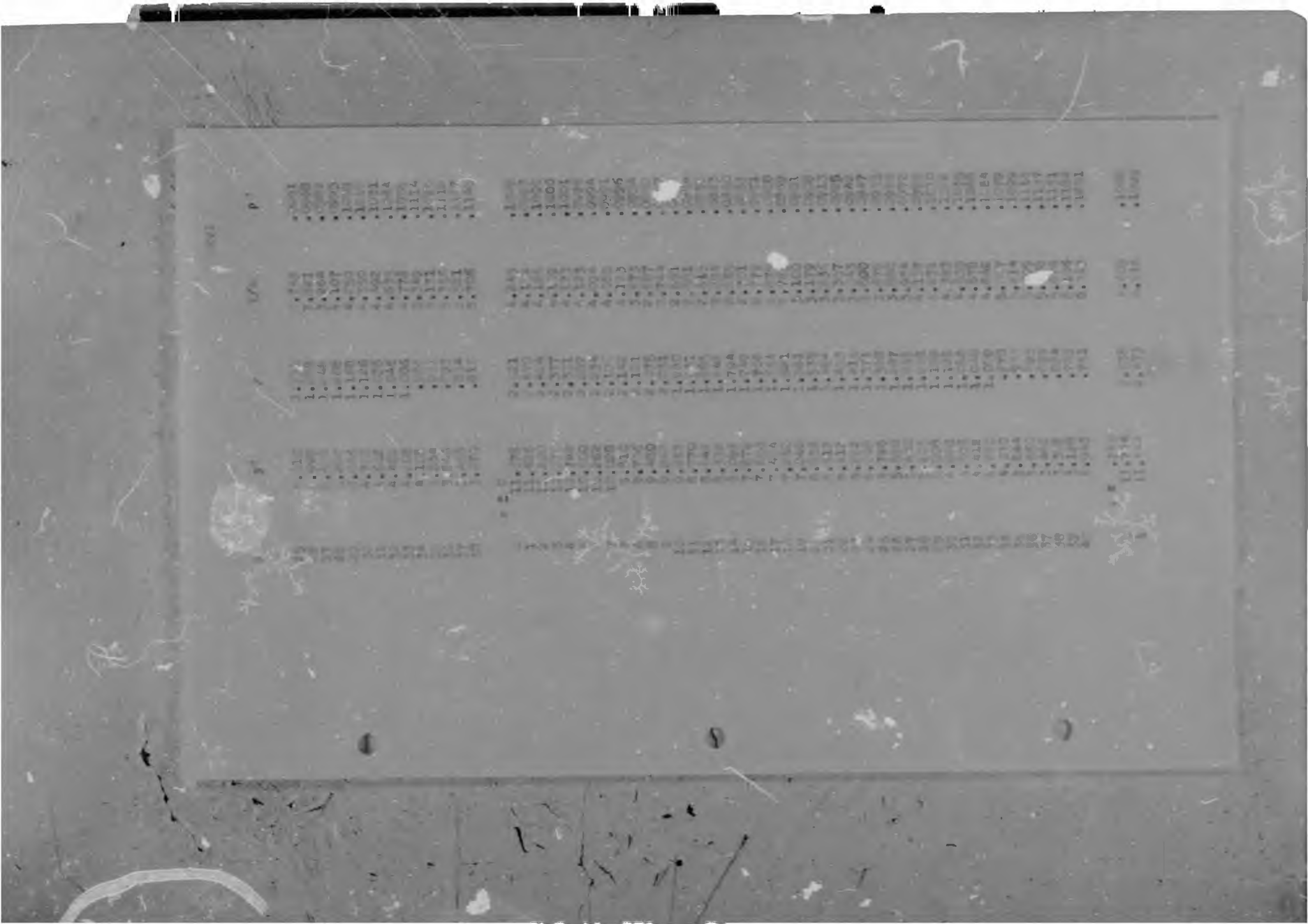

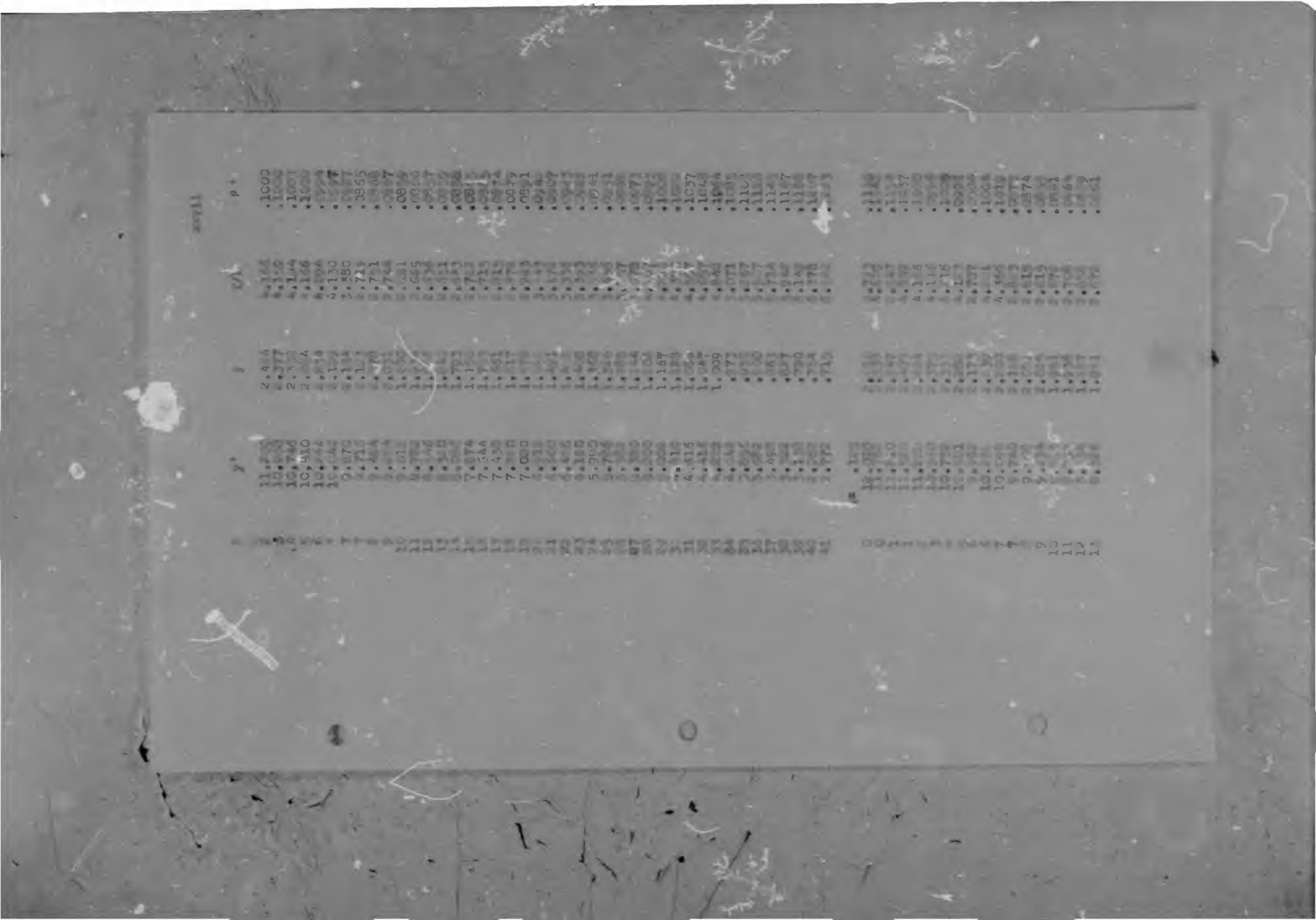

N	y'	y	Y/b	p'
14	8.100	1.795	2.686	.0862
15	7.866	1.748	2.679	.0861
16	7.642	1.703	2.715	.0865
17	7.432	1.660	2.793	.0872
18	7.232	1.619	2.915	.0883
19	7.913	1.575	2.972	.0889
20	6.722	1.533	3.050	.0896
21	6.608	1.493	3.214	.0911
22	6.408	1.469	3.700	.0957
23	6.130	1.396	3.136	.0904
24	5.978	1.365	3.472	.0933
25	5.790	1.327	3.637	.0953
26	5.592	1.287	3.700	.0966
27	5.400	1.248	3.964	.0982
28	5.210	1.210	4.150	.0999
29	5.020	1.176	4.314	.1014
30	4.822	1.151	4.457	.1028
31	4.634	1.[illegible]	4.642	.1045
32	4.428	[illegible]	4.742	.1054
33	4.240	1.013	4.928	.1072
34	4.060	.976	5.135	.1091
35	3.870	.938	5.321	.1109
36	3.688	.901	5.528	.1128
37	3.516	.866	5.778	.1151
38	3.342	.831	6.028	.1175
39	3.152	.792	6.192	.1190
40	2.968	.755	6.399	.1209
	x = 0.105			
0	12.024	2.591	5.745	.1148
1	11.820	2.549	5.845	.1158
1	11.582	2.501	4.816	.1161
2	11.260	2.436	4.423	.1024
3	10.930	2.369	3.987	.0984
4	10.762	2.335	4.259	.1009
5	10.580	2.298	4.466	.1029
6	10.300	2.241	4.244	.1008
6	10.172	2.215	3.987	.0956
6	9.980	2.176	2.851	.0877
7	9.748	2.129	2.844	.0877
8	9.486	2.076	2.708	.0864
9	9.248	2.028	2.680	.0861
10	9.018	1.981	2.672	.0861
11	8.798	1.937	2.729	.0866
	x = .085			
0	12.030	2.592	5.766	.1150
1	11.814	2.548	5.823	.1156
2.	11.590	2.504	5.880	.1161
2	11.446	2.474	5.237	.1101
2	11.310	2.446	4.637	.1045
3	10.998	2.383	4.287	.1012
4	10.748	2.334	4.194	.1003
5	10.536	2.289	4.273	.1010
6	9.998	2.228	2.966	.0888
6	9.998	2.180	2.937	.0875
7	9.736	2.127	2.901	.0873
8	9.496	2.078	2.851	.0868
9	9.262	2.031	2.744	.0867
10	9.031	1.984	2.737	.0867
11	8.804	1.938	2.751	.0868
12	8.584	1.889	2.701	.0863

N	y'	y	Y/b	P'
13	8.330	1.842	2.694	.0863
14	8.100	1.795	2.686	.0862
15	7.870	1.749	2.701	.0863
16	7.638	1.702	2.693	.0863
17	7.416	1.657	2.729	.0866
18	7.210	1.615	2.829	.0875
19	7.008	1.574	2.950	.0887
20	6.792	1.530	3.007	.0892
21	6.576	1.486	3.064	.0898
22	6.370	1.445	3.186	.0909
23	6.180	1.406	3.350	.0924
24	5.980	1.366	3.493	.0937
25	5.786	1.326	3.636	.0951
26	5.600	1.289	3.843	.0970
27	5.406	1.249	3.986	.0984
28	5.216	1.211	4.171	.1001
29	5.022	1.171	4.314	.1014
30	4.832	1.133	4.500	.1032
31	4.638	1.094	4.664	.1047
32	4.448	1.055	4.828	.1062
33	4.260	1.017	5.014	.1080
34	4.072	.979	5.199	.1097
35	3.890	.942	5.407	.1118
36	3.714	.906	5.635	.1138
37	3.532	.869	5.842	.1157
38	3.348	.832	6.049	.1187
39	3.170	.796	6.278	.1198
40	2.982	.758	6.463	.1215
41	2.804	.722	6.692	.1237
	x = 0.064			
0	12.036	2.593	5.787	.1152
1	11.804	2.546	5.780	.1152
2	11.592	2.503	5.859	.1159
3	11.370	2.458	5.894	.1152
3	11.[illegible]	2.446	5.637	.1138
3	11.062	2.396	4.566	.1038
4	10.746	2.332	4.194	.1003
5	10.562	2.296	4.380	.1020
5	10.468	2.275	3.973	.0982
5	10.232	2.228	2.966	.0888
6	10.010	2.183	3.001	.0891
7	9.726	2.125	2.758	.0869
8	9.498	2.079	2.772	.0870
9	9.262	2.031	2.744	.0867
10	9.020	1.982	2.694	.0863
	x = 0.044			
0	12.042	2.594	5.809	.1154
1	11.812	2.548	5.823	.1156
2	11.584	2.501	5.816	.1155
3	11.370	2.456	5.894	.1162
3	11.202	2.424	5.1[illegible]	.1094
3	11.084	2.400	4.652	.1046
4	10.852	2.349	4.5[illegible]	.1037
4	10.628	2.308	3.680	.0955
4	10.468	2.275	2.97[illegible]	.0889
5	10.246	2.230	3.008	.0892
6	9.912	2.163	2.573	.0851
7	9.722	2.124	2.757	.0867
8	9.498	2.079	2.772	.0870
9	9.264	2.031	2.744	.0867

n	y'	y	Y/b	p'
10	9.028	1.983	2.715	.0867
11	8.792	1.936	2.708	.0854
12	8.554	1.887	2.658	.0859
13	8.332	1.842	2.694	.0863
14	8.098	1.795	2.686	.0862
15	7.863	1.747	2.656	.0859
16	7.626	1.699	2.629	.0857
17	7.412	1.656	2.708	.0854
18	7.176	1.608	2.679	.0861
19	6.960	1.564	2.736	.0867
20	6.752	1.522	2.586	.0876
21	6.664	1.484	3.022	.0893
22	6.358	1.442	3.122	.0903
23	6.168	1.404	3.307	.0920
24	5.972	1.364	3.450	.0933
25	5.784	1.326	3.636	.0951
26	5.582	1.285	3.757	.0962
27	5.400	1.248	3.964	.0982
28	5.202	1.208	4.107	.0995
29	5.010	1.169	4.271	.1010
30	4.822	1.131	4.457	.1028
31	4.634	1.093	4.642	.1045
32	4.442	1.054	4.807	.1060
33	4.264	1.018	5.035	.1082
34	4.088	0.982	5.264	.1103
35	3.896	.943	5.428	.1119
36	3.712	.906	5.635	.1138
37	3.520	.867	5.799	.1153
38	3.334	.829	5.985	.1171
39	3.160	.794	6.235	.1194
40	2.984	.758	6.463	.1215
41	2.898	.741	7.099	.1275
	x = 5.300 = 0.024			
0	12.030	2.592	5.766	.1150
1	11.804	2.546	5.780	.1152
2	11.572	2.499	5.773	.1151
3	11.356	2.455	5.830	.1156
4	11.138	2.411	5.887	.1162
4	11.020	2.387	5.373	.1113
4	10.862	2.355	4.687	.1049
4	10.768	2.336	4.280	.1022
4	10.476	2.277	3.016	.0893
5	10.192	2.219	2.775	.0870
6	9.962	2.173	2.787	.0871
7	9.736	2.127	2.801	.0873
8	9.504	2.080	2.794	.0872
9	9.214	2.021	2.830	.0847
10	9.026	1.983	2.715	.0868
	x = .002			
0	12.022	2.590	5.723	.1146
1	11.804	2.546	5.780	.1152
2	11.574	2.500	5.795	.1153
3	11.380	2.464	5.809	.1154
4	11.132	2.410	5.866	.1160
4	10.947	2.371	5.030	.1081
4	10.542	2.290	3.294	.0919
5	10.178	2.215	2.687	.0862
6	9.962	2.173	2.787	.0871
7	9.748	2.129	2.844	.0877
8	9.508	2.079	2.772	.0870
9	9.266	2.032	2.765	.0869
10	9.024	1.983	2.715	.0868

N	y'	y	Y/h	p'
11	8.894	1.956	3.137	.0904
12	8.546	1.886	2.636	.0857
13	8.314	1.839	2.629	.0857
14	8.084	1.792	2.622	.0856
15	7.860	1.747	2.658	.0859
16	7.644	1.703	2.715	.0865
17	7.410	1.656	2.708	.0864
18	7.180	1.609	2.700	.0863
19	6.946	1.561	2.672	.0861
20	6.746	1.521	2.815	.0874
21	6.548	1.481	2.957	.0887
22	6.354	1.441	3.100	.0901
23	6.162	1.403	3.286	.0918
24	5.972	1.364	3.450	.0933
25	5.782	1.326	3.636	.0951
26	5.592	1.287	3.800	.0966
27	5.393	1.246	3.921	.0978
28	5.200	1.208	4.108	.0995
29	5.012	1.169	4.271	.1010
30	4.834	1.133	4.500	.1032
31	4.642	1.094	4.664	.1047
32	4.460	1.058	4.893	.1068
33	4.278	1.021	5.100	.1086
34	4.100	0.985	5.328	.1109
35	3.912	.946	5.492	.1125
36	3.726	.909	5.599	.1144
37	3.534	.870	5.864	.1159
38	3.350	.833	6.071	.1179
39	3.158	.794	6.285	.1184
40	2.968	.755	6.399	.1209
41	2.800	.721	6.671	.1225

TABLE No. 4

Mach 2 Densit Distribution

From Fig. 36

Atm Pressure: 11.91 psia. Humidity: 69%
Atm. Temperature: 71.4°F. b:0.03754

N	y'	y	Y/b	ρ'
	x = 0.191			
0	8.020	.831	5.77	.1146
1	7.842	.795	5.81	.1149
2	7.654	.757	5.79	.1147
3	7.462	.718	5.75	.1144
4	7.296	.684	5.84	.1152
5	6.982	.620	5.14	.1087
	x = 0.181			
0	8.022	.831	5.76	.1145
1	7.882	.803	6.01	.1168
2	7.738	.774	6.24	.1190
3	7.590	.744	6.44	.1208
4	7.456	.717	6.72	.1234
5	7.316	.688	6.95	.1256
6	7.164	.657	7.12	.1272
7	6.990	.622	7.19	.1278
8	6.800	.584	7.18	.1278
9	6.608	.545	7.14	.1274
10	6.344	.491	6.70	.1233
	x = 0.171			
0	8.034	.834	5.84	.1152
1	7.890	.805	6.07	.1174
2	7.744	.775	6.27	.1192
3	7.602	.746	6.50	.1214
4	7.462	.718	6.75	.1237
5	7.324	.691	7.03	.1264
6	7.188	.662	7.26	.1285
7	7.048	.634	7.51	.1308
8	6.910	.606	7.76	.1332
9	6.768	.577	7.99	.1353
10	6.630	.549	8.25	.1378
11	6.461	.515	8.34	.1386
12	6.298	.482	8.46	.1397
13	6.176	.457	8.79	.1428
14	6.010	.423	8.89	.1438
15	5.890	.399	9.25	.1471
16	5.744	.369	9.45	.1490
	x = 0.161			
0	8.038	.835	5.87	.1155
1	7.892	.805	6.07	.1174
2	7.750	.776	6.30	.1195
3	7.604	.747	6.52	.1216
4	7.458	.717	6.72	.1234
5	7.328	.691	7.03	.1264

N	y'	y	Y/b	p'
6	7.190	.668	7.28	.1287
7	7.048	.634	7.51	.1308
8	6.912	.608	7.76	.1332
9	6.780	.579	8.02	.1359
10	6.634	.550	8.27	.1380
11	6.498	.523	8.53	.1404
12	6.362	.495	8.81	.1430
13	6.224	.467	9.06	.1454
14	6.092	.440	9.34	.1480
15	5.948	.411	9.57	.1501
16	5.810	.383	9.82	.1522
17	5.662	.353	10.02	.1543
18	5.522	.324	10.25	.1565
19	5.412	.302	10.66	.1603
20	5.310	.281	11.10	.1644
21	5.194	.258	11.49	.1681
	x = 0.151			
16	5.822	.385	9.86	.1530
17	5.668	.356	10.16	.1556
18	5.512	.322	10.20	.1560
19	5.448	.309	10.35	.1621
20	5.336	.287	11.26	.1659
21	5.226	.264	11.65	.1696
22	5.122	.243	12.09	.1737
23	5.010	.221	12.50	.1778
24	4.898	.198	12.89	.1812
25	4.774	.173	13.23	.1841
26	4.660	.150	13.61	.1870
27	4.538	.125	13.95	.1911
28	4.410	.099	14.25	.1934
29	4.300	.077	14.67	.1979
30	3.566	-.072	19.70	.2445
39	3.512	-.082	20.43	.2518
40	3.452	-.094	21.11	.2581
41	3.380	-.109	21.71	.2638
42	3.314	-.122	22.36	.2698
43	3.246	-.136	22.99	.2757
44	3.176	-.150	23.63	.2815
45	3.096	-.167	24.[illegible]	.2867
46	3.098	-.167	24.63	.2911
0	8.050	.837	5.92	.1160
1	7.902	.807	6.12	.1178
2	7.756	.777	6.32	.1197
3	7.608	.747	6.52	.1216
4	7.470	.719	6.78	.1246
5	7.324	.690	7.00	.1461
6	7.180	.661	7.23	.1282
7	7.046	.633	7.48	.1306
8	6.910	.606	7.76	.1332
9	6.774	.578	8.02	.1356
10	6.636	.550	8.27	.1380
11	6.498	.522	8.53	.1404
12	6.362	.495	8.87	.1430
13	6.224	.467	9.06	.1454
14	6.086	.439	9.31	.1477
15	5.946	.410	9.54	.1498
16	5.822	.385	9.88	.1530
17	5.698	.360	10.21	.1561
18	5.564	.333	10.49	.1587

N	y'	y	Y/b	ρ'
19	5.450	.310	10.88	.1624
20	5.340	.287	11.26	.1659
21	5.232	.266	11.70	.1701
22	5.126	.244	12.12	.1740
23	5.014	.221	12.50	.1776
24	4.902	.199	12.92	.1815
25	4.800	.178	13.36	.1856
26	4.784	.175	14.28	.1932
27	4.568	.131	14.11	.1926
28	4.450	.107	14.47	.1960
29	4.330	.083	14.83	.1998
30	4.224	.061	15.24	.2032
31	4.128	.041	15.71	.2076
32	4.040	.024	16.25	.2127
33	3.966	.009	16.85	.2183
34	3.890	-.006	17.46	.2240
35	3.804	-.021	18.00	.2290
36	3.738	-.036	18.64	.2352
38	3.672	-.050	19.28	.2410
38	3.600	-.064	19.91	.2469
39	3.538	-.077	20.56	.2530
40	3.476	-.090	21.22	.2592
41	3.402	-.105	21.82	.2648
42	3.334	-.118	22.47	.2709
43	3.266	-.133	23.07	.2765
44	3.188	-.148	23.67	.2821
45	3.108	-.164	24.24	.2874
46	3.018	-.182	24.74	.2923
	x = 0,110			
0	8.062	.849	5.97	.1164
1	7.918	.810	6.20	.1186
2	7.764	.779	6.38	.1203
3	7.608	.747	6.52	.1216
4	7.454	.716	6.70	.1233
5	7.322	.689	6.98	.1259
6	7.176	.660	7.20	.1279
7	7.036	.631	7.43	.1301
8	6.900	.604	7.71	.1327
9	6.782	.576	7.97	.1351
10	6.628	.549	8.25	.1378
11	6.492	.521	8.50	.1401
12	6.356	.493	8.75	.1425
13	6.222	.466	9.03	.1451
14	6.084	.438	9.29	.1475
15	5.950	.411	9.57	.1501
16	5.828	.386	9.90	.1532
17	5.706	.362	10.26	.1566
18	5.594	.338	10.62	.1600
19	5.484	.313	10.96	.1631
20	5.370	.290	11.32	.1665
21	5.260	.267	11.73	.1700
22	5.148	.244	12.12	.1740
23	5.038	.222	12.53	.1776
24	4.928	.202	13.00	.1832
25	4.817	.181	13.44	.1863
26	4.698	.157	13.88	.1897
27	4.598	.137	14.27	.1941
28	4.478	.113	14.63	.1975
29	4.374	.092	15.07	.2016
30	4.282	.073	15.56	.2062
31	4.194	.055	16.04	.2111
32	4.108	.038	16.63	.2168

N	y'	y	Y/b	ρ'
33	4.028	.021	17.17	.2213
34	3.460	.006	17.83	.2274
35	3.872	-.009	18.38	.2326
36	3.800	-.024	18.98	.2382
37	3.780	-.028	19.87	.2465
38	3.662	-.052	20.23	.2499
39	3.590	-.066	20.86	.2558
40	3.522	-.080	21.48	.2616
41	3.446	-.096	22.06	.2670
42	3.382	-.109	22.71	.2731
43	3.310	-.223	23.04	.2790
44	3.246	-.140	23.78	.2841
45	3.148	-.156	24.46	.2895
46	3.068	-.172	25.82	.2948
47	2.982	-.190	25.97	.2997
	x = 0.070			
J	9.070	.541	6.03	.1170
1	7.928	.872	6.25	.1191
2	7.772	.741	6.43	.1207
3	7.618	.749	6.58	.1221
4	7.472	.730	6.80	.1242
5	7.320	.680	6.98	.1259
6	7.178	.660	7.20	.1279
7	7.032	.631	7.43	.1301
8	6.898	.603	7.68	.1324
9	6.762	.576	7.97	.1351
10	6.622	.547	8.19	.1372
11	6.490	.521	8.50	.1401
12	6.354	.493	8.75	.1425
13	6.218	.466	9.03	.1451
14	6.100	.442	9.39	.1484
15	5.972	.416	9.78	.1513
16	5.850	.391	10.04	.1545
17	5.730	.367	10.40	.1579
18	5.602	.341	10.70	.1607
19	5.498	.319	11.12	.1646
20	5.380	.296	11.50	.1682
21	5.258	.271	11.84	.1714
22	5.142	.247	12.20	.1747
23	5.032	.228	12.61	.1786
24	4.912	.201	12.97	.1819
25	4.822	.182	13.47	.1866
26	4.720	.162	13.93	.1909
27	4.600	.137	14.27	.1941
28	4.492	.115	14.68	.1980
29	4.400	.097	15.20	.2028
30	4.322	.081	15.77	.2082
31	4.246	.066	16.37	.2138
32	4.166	.049	16.92	.2189
33	4.090	.034	17.51	.2245
34	4.018	.019	18.12	.2302
35	3.932	.002	18.67	.2353
36	3.858	-.012	19.30	.2412
37	3.788	-.040	20.51	.2470
38	3.720	-.040	20.55	.2529
39	3.646	-.055	21.15	.2585
40	3.580	-.068	21.80	.2646
41	3.500	-.085	22.35	.2697
42	3.430	-.098	22.98	.2756
43	3.372	-.115	23.55	.2810
44	3.270	-.131	24.12	.2864
45	3.198	-.146	24.72	.2919

N	y'	Z	Y/b	f'
46	3.108	-.164	25.21	.2968
47	3.026	-.181	25.79	.3019
48	2.930	-.200	26.28	.3065
	x = 0.019			
0	8.082	.844	6.11	.1177
1	7.924	.811	6.23	.1189
2	7.778	.782	6.46	.1210
3	7.620	.750	6.60	.1223
4	7.468	.719	6.78	.1240
5	7.322	.689	6.98	.1259
6	7.172	.659	7.18	.1278
7	7.026	.629	7.38	.1296
8	6.882	.600	7.61	.1318
9	6.746	.573	7.89	.1344
10	6.604	.544	8.11	.1365
11	6.472	.517	8.39	.1391
12	6.346	.491	8.70	.1420
13	6.226	.467	9.07	.1454
14	6.104	.442	9.39	.1484
15	5.982	.418	9.75	.1518
16	5.862	.393	10.09	.1550
17	5.742	.369	10.45	.1584
18	5.624	.345	10.81	.1617
19	5.444	.319	11.12	.1646
20	5.380	.293	11.50	.1682
21	5.262	.272	11.86	.1716
22	5.142	.247	12.20	.1743
23	5.038	.226	12.64	.1789
24	4.930	.204	13.05	.1827
25	4.816	.187	13.44	.1863
26	4.710	.160	13.88	.1905
27	4.606	.139	14.32	.1946
28	4.508	.119	14.79	.1990
29	4.420	.101	15.31	.2039
30	4.340	.085	15.88	.2092
31	4.264	.069	16.45	.2145
32	4.194	.055	17.08	.2204
33	4.118	.040	17.68	.2260
34	4.046	.025	18.28	.2317
35	3.966	.009	18.85	.2370
36	3.893	-.004	19.51	.2432
37	3.819	-.020	20.08	.2485
38	3.743	-.034	20.71	.2544
39	3.676	-.047	21.31	.2600
40	3.602	-.064	21.91	.2656
41	3.522	-.080	22.48	.2710
42	3.443	-.095	23.08	.2766
43	3.374	-.110	23.68	.2822
44	3.296	-.126	24.26	.2876
45	3.210	-.144	24.78	.2925
46	3.134	-.159	25.38	.2981
47	3.042	-.178	25.87	.3027
48	2.948	-.199	26.36	.3073
	x = -0.019			
0	8.086	.844	6.11	.1177
1	7.933	.813	6.28	.1193
2	7.778	.782	6.46	.1210
3	7.623	.751	6.63	.1226
4	7.480	.721	6.83	.1255
5	7.330	.691	7.03	.1264
6	7.176	.660	7.20	.1279

N	y'	y	Y/b	p'
7	7.022	.629	7.38	.1296
8	6.876	.599	7.58	.1315
9	6.738	.571	7.83	.1338
10	6.604	.544	8.11	.1365
11	6.472	.517	8.39	.1391
12	6.346	.491	8.70	.1420
13	6.222	.466	9.03	.1451
14	6.102	.442	9.39	.1484
15	5.992	.420	9.81	.1524
16	5.864	.394	10.12	.1553
17	5.842	.369	10.45	.1584
18	5.624	.345	10.81	.1617
19	5.500	.320	11.14	.1648
20	5.382	.296	11.49	.1681
21	5.270	.273	11.89	.1718
22	5.152	.249	12.25	.1752
23	5.042	.227	12.66	.1790
24	4.426	.204	13.05	.1827
25	4.816	.181	[illegible].44	.1863
26	4.714	.160	13.88	.1905
27	4.610	.139	14.32	.1946
28	4.530	.121	14.84	.1995
29	4.456	.104	15.39	.2046
30	4.358	.089	15.96	.2096
31	4.274	.071	16.51	.2151
32	4.200	.056	17.11	.2207
33	4.132	.042	17.73	.2265
34	4.054	.027	18.33	.2321
35	3.984	.012	18.93	.2377
36	3.908	-.002	19.56	.2436
37	3.830	-.018	20.14	.2491
38	3.760	-.032	20.76	.2549
39	3.686	-.047	21.[illegible]6	.2605
40	3.620	-.060	22.02	.2667
41	3.542	-.076	22.59	.2720
42	3.462	-.092	23.18[illegible]	.2773
43	3.390	-.107	23.76	.2829
44	3.308	-.124	24.31	.2881
45	3.232	-.139	24.91	.2937
46	3.146	-.155	25.46	.2989
47	3.055	-.174	25.98	.3037
48	2.952	-.196	26.39	.3076

N	y'	y	Y/b	ρ'
7	7.022	.629	7.38	.1296
8	6.876	.599	7.58	.1315
9	6.738	.571	7.83	.1338
10	6.604	.544	8.11	.1365
11	6.472	.517	8.39	.1391
12	6.346	.491	8.70	.1420
13	6.222	.466	9.03	.1451
14	6.102	.442	9.39	.1484
15	5.992	.420	9.81	.1524
16	5.864	.394	10.12	.1553
17	5.842	.369	10.45	.1584
18	5.624	.345	10.81	.1617
19	5.500	.320	11.14	.1648
20	5.382	.296	11.49	.1681
21	5.270	.273	11.89	.1718
22	5.152	.249	12.25	.1752
23	5.038	.227	12.66	.1790
24	4.428	.204	13.05	.1827
25	4.816	.181	13.44	.1863
26	4.710	.160	13.88	.1905
27	4.610	.139	14.32	.1946
28	4.520	.121	14.84	.1995
29	4.436	.104	15.39	.2046
30	4.358	.088	15.96	.2096
31	4.274	.071	16.51	.2151
32	4.200	.056	17.11	.2207
33	4.132	.042	17.73	.2265
34	4.064	.027	18.33	.2321
35	3.984	.012	18.93	.2377
36	3.908	-.002	19.56	.2436
37	3.830	-.018	20.14	.2491
38	3.760	-.032	20.76	.2549
39	3.686	-.047	21.36	.2605
40	3.620	-.060	22.02	.2667
41	3.542	-.076	22.59	.2720
42	3.462	-.092	23.184	.2773
43	3.390	-.107	23.76	.2829
44	3.308	-.124	24.31	.2881
45	3.232	-.139	24.91	.2937
46	3.146	-.158	25.46	.2989
47	3.058	-.174	25.98	.3037
48	2.952	-.196	26.39	.3076

TABLE NO. 5

Mach 2 Density Distribution Along the Light Path Fig. 37

Atm. Pressure: 11.95 psia. Humidity: 69%
Atm. Temperature: 71.4°F.

z'	z	y'	y	y_o	Y/b	ρ'
3.600	-0.4062	4.330	.1047			
3.800	- .3657	4.342	.1072			
4.000	- .3252	4.350	.1088			
4.200	- .2848	4.350	.1088			
4.324	- .2597	4.348	.1084			
5.612	.0008	4.312	.1011	.1180	0.521	.0662
5.650	.0084	4.202	.0788	.1182	1.216	.0728
5.700	.0186	4.074	.0530	.1187	2.028	.0804
5.725	.0236	4.020	.0432	.1188	2.334	.0832
5.750	.0287	4.000	.0380	.1188	2.495	.0847
5.775	.0337	3.998	.0376	.1189	2.510	.0849
6.000	.0793	3.998	.0376	.1205	2.560	.0854
6.300	.1399	4.032	.0445	.1225	2.099	.0810
6.600	.2006	4.040	.0461	.1245	2.421	.0841
6.900	.2613	4.040	.0461	.1256	2.479	.0846
7.200	.3220	4.050	.0481	.1284	2.479	.0846
7.500	.3827	4.062	.0505	.1304	2.467	.0845
7.800	.4434	4.072	.0525	.1320	2.454	.0843
8.100	.5041	4.078	.0538	.1342	2.482	.0846
8.400	.5648	4.084	.0550	.1360	2.500	.0848
8.500	.5850	4.086	.0558	.1367	2.497	.0848
8.550	.5951	4.100	.0582	.1370	2.432	.0848
8.575	.6002	4.128	.0639	.1371	2.259	.0825
8.600	.6052	4.170	0.0736	.1373	1.966	.0798
8.625	.6103	4.234	.0853	.1375	1.611	.0765
8.650	.6153	4.294	.0975	.1377	1.241	.0730
8.675	.6204	4.356	.1100	.1378	1.167	.0713
8.704	.6263	4.420	.1224	.1380	0.466	.0657
9.940	.8763	4.536	.1464			
10.400	.9644	4.544	.1480			
10.200	.9289	4.540	.1472			

TABLE NO. 6

Mach 2 Central Density Distribution
from Finite Prandtl Eqs. 36 & 38

Atm. Pressure: 11.93 psia
Atm. Temperature: 68.6°F.

Humidity = 64%
ρ_o = 0.3820

S	ρ'	Correction	ρ	ρ/ρ$_o$	M
2	.0865	.0110	.0975	3.917	1.905
1.415	.09	.0050	.0950	4.021	1.955
1.319	.095	.0038	.0988	3.866	1.895
1.190	.1	.0032	.1032	3.701	1.827
1.081	.105	.0028	.1078	3.543	1.814
.999	.11	.0025	.1125	3.395	1.771
.800	.12	.0020	.1220	3.131	1.701
.618	.13	.0015	.1315	2.904	1.631
.510	.14	.0011	.1411	2.707	1.562
.432	.15	.0010	.1510	2.529	1.494
.360	.16	.0009	.1609	2.374	1.438
.286	.17	.0008	.1708	2.236	1.370
.219	.18	.0007	.1807	2.114	1.32[illegible]
.120	.20	.0003	.2005	1.909	1.222
.052	.22		.2200	1.736	1.045
.003	.24		.2400	1.591	1.011
-.048	.26		.2600	1.469	.911
-.100	.28		.2800	1.364	.812
-.168	.30		.3000	1.273	.712

EL

TABLE NO. 7

Mach 2 Central Density Distribution
from Infinite Fringes Fig. 38

Atm. Pressure: 11.93 psia
Atm. Temperature: 68.6°F.

Humidity = 64%
ρ = 0.009363 lbs/cu ft

N	y'	y	ρ'
0	1.32	1.411	.0975
1	1.85	1.174	.1069
2	2.21	1.013	.1162
3	2.61	0.833	.1256
4	3.00	0.659	.1349
5	3.26	0.542	.1443
6	3.44	0.461	.1537
7	3.62	0.381	.1630
8	3.78	0.310	.1724
9	3.915	0.251	.1818
10	4.038	0.199	.1911

TABLE NO. 8

Mach 2 Central Density Distribution
from Infinite Fringes Fig. 39

Atm. Pressure: 11.95 psia Humidity = 69%
Atm. Temperature: 71.4°F. ∂ρ = .009363 lbs/cu ft

No.	y' above bottom	y	ρ'
0	2.53	1.140	0.1019
1	2.36	1.050	.1112
2	2.04	0.879	.1206
3	1.72	.709	.1299
4	1.45	.565	.1393
5	1.285	.477	.1487
6	1.16	.410	.1581
7	1.03	.341	.1674
8	0.905	.274	.1780
9	.800	.218	.1862
10	.700	.165	.1955
11	.615	.120	.2049
12	.580	.101	.2142
13	.505	.061	.2236
14	.462	.038	.2329
15	.415	.013	.2423
16	.375	-.007	.2517
17	.325	-.034	.2611
18	.285	-.055	.2704
19	.235	-.082	.2798
20	.190	-.106	.2892
21	.120	0.143	.2985
22	.085	-.162	.3079

TABLE NO. 9

Mach 2 Central Density Distribution
from Composite Fringes Fig. 44

Atm. Pressure: 11.956 psia
Atm. Temperature: 58.6°F.
Humidity: 62%

N	y'	y	p'
0	1.24	1.356	.0968
1	1.67	1.133	.1062
2	1.99	.967	.1155
3	2.37	.770	.1249
4	2.63	.635	.1342
5	2.81	.541	.1436
6	2.95	.468	.1530
7	3.08	.401	.1623
8	3.22	.328	.1717
9	3.33	.271	.1811
10	3.42	.224	.1904
11	3.49	.188	.1998
12	3.56	.152	.2091
13	3.61	.126	.2185

TABLE NO. 10

Mach 3 Central Density Distribution

from Infinite Fringes Fig. 40
(based on pressure taps)

Atm. Pressure: 11.934 psia Humidity: 76%
Atm. Temperature: 68.8°F. ρ_o = 0.3828 lbs/cu ft.

N	y'	y	ρ'	Corr.	ρ	ρ_o/ρ	M
0	.2	1.942	.0381	.0076	.0457	8.37	2.538
1	.75	1.649	.0474	.0065	.0539	7.11	2.441
2	1.13	1.446	.0568	.0056	.0624	6.14	2.310
3	1.43	1.285	.0662	.0049	.0711	5.38	2.190
4	1.67	1.157	.0755	.0042	.0797	4.81	2.092
5	1.94	1.013	.0849	.0035	.0884	4.33	1.999
6	2.14	.906	.0943	.0031	.0974	3.93	1.909
8	2.32	.810	.1046	.0026	.1072	3.57	1.822
8	2.47	.730	.1130	.0023	.1153	3.31	1.752
9	2.61	.656	.1223	.0018	.1241	3.08	1.686
10	2.73	.591	.1327	.0016	.1343	2.85	1.610
11	2.87	.516	.1411	.0012	.1423	2.69	1.552
12	2.94	.478	.1504	.0010	.1514	2.515	1.492
13	3.04	.425	.1598	.0008	.1606	2.383	1.442
14	3.115	.385	.1692	.0005	.1697	2.258	1.390
15	3.185	.347	.1785	.0003	.1788	2.142	1.334
16	3.284	.310	.1879	.	.1879	2.042	1.283
17	3.335	.267	.1973		.1973	1.940	1.232
18	3.410	.227	.2066		.2066	1.851	1.195
19	3.495	.182	.2160		.2160	1.782	1.145
20	3.590	.131	.2253		.2253	1.700	1.095
21	3.720	.062	.2347		.2347	1.631	1.045
22	3.840	-.002	.3441		.2441	1.568	0.992

TABLE NO. 11

Mach 3 Central Density Distribution
from Composite Fringes Fig. 45

Atm. Pressure: 11.934 psia
Atm. Temperature: 68.8°F.

Humidity: 76%
$\delta\rho = .009363$

N	y'	y	ρ'
0	.32	1.869	.0457
1	.89	1.548	.0550
2	1.26	1.340	.0644
3	1.54	1.182	.0738
4	1.78	1.047	.0831
5	2.01	.918	.0925
6	2.18	.822	.1019
7	2.32	.743	.1112
8	2.45	.670	.1206
9	2.58	.597	.1299
10	2.67	.546	.1393
11	2.77	.490	.1487
12	2.86	.439	.1580
13	2.95	.389	.1674
14	3.01	.355	.1768
15	3.08	.315	.1861
16	3.13	.287	.1955
17	3.21	.242	.2049
18	3.29	.197	.2142
19	3.37	.142	.2236
20	3.48	.092	.2329

TABLE NO. 12

Mach 2 Boundary Layers
from Figs. 35 and 36

	x'	x	x/δ	y'	y	Y/b	ρ'	ρ'/ρ₁
N = 5	6.700	.306		9.512	2.082	-.163	.0596	
	6.65	.295		9.512	2.082	-.163	.0596	
	6.6	.285		9.512	2.082	-.163	.0596	
	6.55	.275		9.528	2.085	-.099	.0602	
	6.5	.265		9.612	2.102	-.265	.0635	
	6.45	.225		9.792	2.138	1.037	.0708	
	6.425	.250		9.886	2.157	1.444	.0746	
	6.4	.245		9.998	2.180	1.937	.0792	
	4.775	.240		10.108	2.202	1.408	.0836	
	6.35	.235		10.194	2.220	2.794	.0872	
	6.325	.230		10.288	2.239	3.201	.0910	
	6.3	.225		10.358	2.253	3.501	.0938	
	6.275	.220		10.432	2.268	3.823	.0968	
	6.25	.214		10.464	2.275	3.973	.0982	
	6.225	.209		10.470	2.276	3.994	.0984	
	6.2	.204		10.490	2.280	4.080	.0992	
	6.15	.194		10.502	2.282	4.123	.0996	
	6.1	.184		10.498	2.281	4.101	.0994	
	6.0	.164		10.502	2.282	4.123	.0996	
N = 10	6.00	.101		9.814	1.981	2.672	.0861	
	6.1	.081		9.032	1.984	2.737	.0867	
	6.15	.071		9.032	1.984	2.737	.0861	
	6.2	.061		9.020	1.982	2.694	.0863	
	6.25	.051		9.006	1.979	2.629	.0857	
	6.3	.040	.800	8.992	1.976	2.565	.0851	.989
	6.35	.030	.600	8.954	1.968	2.394	.0835	.971
	6.375	.025	.500	8.906	1.959	2.201	.0817	.950
	6.4	.020	.400	8.838	1.945	1.901	.0788	.916
	6.425	.015	.300	8.776	1.932	1.622	.0762	.886
	6.45	.010	.200	8.694	1.916	1.279	.0730	.849
	6.475	.005	.100	8.608	1.898	0.894	.0694	.867
	6.5	.0	.0	8.460	1.868	0.251	.0634	.737
N = 15	6	.099		8.872	1.749	2.701	.0863	
	6.1	.079		7.882	1.757	2.743	.0867	
	6.2	.059		7.898	1.764	2.808	.0873	
	6.3	.038		7.902	1.755	2.829	.0875	
	6.35	.028	.84	7.900	1.753	2.829	.0875	.996
	6.375	.023	.69	7.866	1.748	2.679	.0861	.981
	6.4	.018	.54	7.784	1.731	2.315	.0827	.942
	6.425	.013	.39	7.692	1.718	1.929	.0791	.901
	6.45	.007	.24	7.582	1.690	1.436	.0745	.848
	6.475	.003	.09	7.402	1.666	0.922	.0697	.794
	6.492	0	.0	7.354	1.644	0.450	.0653	.744
N = 20	6.2	.051		6.834	1.539	3.200	.0910	
	6.25	.041		6.838	1.540	3.222	.0912	
	6.3	.036		6.840	1.540	3.222	.0912	
	6.325	.025	1	6.848	1.542	3.265	.0916	1
	6.35	.020	.800	6.834	1.549	3.200	.0910	.993
	6.375	.015	.600	6.800	1.532	3.050	.0896	.978

	x'	x	x/δ	y'	y	Y/b	p'	p'/p₁
	6.4	.010	.400	6.702	1.512	2.622	.0856	.934
	6.425	.005	.200	6.546	1.485	2.043	.0802	.875
	6.45	.0	.0	6.378	1.446	1.207	.0723	.789
N = 25	6.2	.039		5.802	1.330	3.721	.0959	
	6.25	.029		5.812	1.332	3.764	.0963	
	6.275	.023		5.816	1.332	3.764	.0963	1
	6.3	.018	.782	5.802	1.330	3.721	.0959	.995
	6.325	.013	.565	5.772	1.323	3.571	.0945	.981
	6.35	.008	.347	5.694	1.308	3.250	.0915	.950
	6.375	.003	.130	5.448	1.258	2.178	.0814	.845
	6.392	.0	.0	5.302	1.228	1.536	.0754	.782
N' = 0	5.900	.032		8.030	.833	5.81	.1089	
	5.950	.022		8.022	.831	5.76	.1145	
	6.000	.012	.012	8.008	.829	5.71	.1140	.995
	6.025	.007	.437	7.948	.816	5.36	.1107	.966
	6.050	.002	.125	7.770	.780	4.40	.1014	.885
	6.06	.0	.0	7.702	.766	4.03	.0983	.858
N' = 5	5.9	.024		7.320	.689	6.98	.1259	
	5.95	.014	.823	7.318	.689	6.98	.1259	.999
	5.96	.012	.705	7.310	.687	6.92	.1253	.994
	5.975	.009	.529	7.300	.685	6.87	.1249	.991
	5.99	.006	.352	7.266	.678	6.68	.1231	.976
	6	.004	.235	7.186	.662	6.26	.1126	.945
	6.01	.002	.117	7.060	.636	5.56	.1126	.893
	6.02	.0	.0	7.000	.624	5.28	.1096	.869
N' = 10	5.8	.036		6.624	.548	8.22	.1405	
	5.9	.016	.888	6.626	.548	8.22	.1405	.997
	5.925	.011	.611	6.606	.544	8.11	.1365	.969
	5.95	.006	.333	6.542	.531	7.77	.1331	.931
	5.98	.0	.0	6.442	.513	7.23	.1256	.910
N' = 15	5.8	.025		5.942	.410	9.54	.1498	.
	5.85	.015	.833	5.942	.410	9.54	.1498	.998
	5.86	.013	.722	5.936	.409	9.49	.1494	.996
	5.875	.010	.555	5.922	.406	9.41	.1486	.990
	5.89	.007	.388	5.916	.404	9.38	.1480	.986
	5.9	.005	.277	5.900	.401	9.30	.1476	.984
	5.91	.003	.166	5.884	.398	9.22	.1468	.978
	5.925	.0	.0	5.868	.345	9.14	.1461	.974
N' = 20	5.800	.017	.944	5.442.	.308	11.82	.1712	.999
	5.825	.012	.666	5.434	.307	11.80	.1710	.998
	5.850	.007	.388	5.412	.302	11.66	.1697	.990
	5.875	.002	.110	5.396	.299	11.58	.1689	.985
	5.884	.0	.0	5.334	.286	11.24	.1658	.960
N' = 25	5.750	.015	.833	4.798	.178	13.36	.1856	.999
	5.775	.010	.555	4.786	.175	13.28	.1849	.996
	5.800	.005	.277	4.764	.191	13.18	.1838	.990
	5.825	.0	.0	4.746	.167	13.07	.1823	.982
N' = 30	5.825	.015	.833	4.234	.063	15.29	.2037	.998
	5.850	.010	.555	4.220	.060	15.21	.2029	.994
	5.875	.005	.277	4.202	.057	15.13	.2022	.991
	5.900	.0	.0	4.196	.055	15.08	.2017	.988

TABLE NO. 13

Mach 3 Boundary Layers

	x'	x	x/δ	y'	y	Y/b	p'	p'/p₁
N = 7	1.75	.0535	.823	8.816	3.174	-2.323	.0392	.980
	1.70	.0432	.664	8.770	3.165	-2.499	.0375	.937
	1.65	.0329	.506	8.712	3.153	-2.734	.0353	.882
	1.60	.0226	.347	8.660	3.142	-2.949	.0333	.832
	1.55	.0124	.190	8.592	3.128	-3.222	.0307	.767
	1.50	.0021	.032	8.500	3.109	-3.593	.0273	.682
	1.49	0	0	8.446	3.098	-3.808	.0253	.632
N = 15	1.95	.0629		6.928	2.786	-1.905	.0431	
	1.90	.0526	.992	6.936	2.788	-1.866	.0434	.997
	1.85	.0423	.748	6.914	2.783	-1.964	.0425	.977
	1.80	.0321	.605	6.854	2.771	-2.199	.0403	.926
	1.75	.0218	.411	6.788	2.757	-2.472	.0378	.868
	1.70	.0115	.216	6.706	2.741	-2.785	.0348	.800
	1.644	0	0	6.590	2.717	-3.254	.0304	.698
N = 25	2.15	.0561		4.50	2.287	-1.657	.0454	
	2.10	.0458	.916	4.508	2.289	-1.618	.0458	.995
	2.05	.0345	.690	4.448	2.277	-1.852	.0436	.947
	2.00	.0223	.446	4.356	2.258	-2.224	.0401	.871
	1.95	.010	.200	4.212	2.228	-2.810	.0346	.752
	1.916	0	0	4.148	2.215	-3.064	.0322	.700
N = 25	2.45	0.0379	.789	2.122	1.799	-1.193	.0497	.984
	2.40	0.0247	.514	2.048	1.783	-1.506	.0468	.926
	2.35	0.0114	.237	1.868	1.746	-2.229	.0400	.792
	2.324	0	0	1.738	1.720	-2.737	.0353	.699
N' = 0	6.15	.0530		11.936	2.0897	-1.870	.0434	
	6.20	.0415	.830	11.918	2.0859	-1.948	.0427	.981
	6.25	.0280	.560	11.862	2.0762	-2.189	.0404	.928
	6.30	.0155	.310	11.732	2.0469	-2.752	.0351	.825
	6.35	.0	0	11.558	2.010	-3.513	.0280	.643
N' = 10	2.00	.0435		9.752	1.6313	-1.322	.0488	
	1.95	.0348		9.764	1.6338	-1.271	.0490	
	1.925	.0295	.893	9.760	1.6330	-1.287	.0489	.998
	1.90	.0223	.675	9.706	1.6216	-1.522	.0467	.951
	1.875	.0080	.242	9.596	1.598	-2.009	.0384	.782
	1.870	.0	0	9.362	1.549	-3.011	.0327	.665
N' = 20	2.45	.0346		7.718	1.2027	-0.160	.0594	
	2.40	.0241	.964	7.702	1.2010	-0.195	.0591	.999
	2.384	.0188	.752	7.682	1.1968	-0.281	.0583	.986
	2.372	.0132	.528	7.608	1.1813	-0.601	.0553	.937
	2.366	.0080	.320	7.514	1.1615	-1.009	.0515	.872
	2.366	.0	0	7.368	1.1309	-1.640	.0455	.771
N' = 30	2.814	.0277	.989	6.042	.8526	2.620	.0857	.999
	2.770	.0175	.625	6.020	.8479	2.573	.0845	.985
	2.750	.0093	.332	5.960	.8354	2.265	.0821	.957
	2.746	.0064	.228	5.892	.8211	1.971	.0793	.925
	2.744	0	0	5.706	.7820	1.164	.0718	.837

	x'	x	x/δ	y'	y	Y/b	ρ'	ρ'/ρ₁
N' = 40	3.048	.0322		4.718	.5747	6.890	.1254	
	3.000	.0202	.686	4.702	.5713	6.820	.1247	.993
	2.986	.0172	.593	4.682	.5671	6.733	.1239	.987
	2.970	.0139	.479	4.648	.5600	6.587	.1226	.976
	2.904	0	0	4.600	.5499	6.378	.1206	.960
N' = 50	3.188	.0159	.395	3.554	.3303	11.850	.1718	.998
	3.160	.0100	.500	3.548	.3291	11.826	.1716	.997
	3.140	.0059	.290	3.534	.3261	11.764	.1710	.994
	3.112	0	0	3.522	.3236	11.712	.1705	.991

Table No. 14

Boundary Layer Correction Factors

y	M2 Area $\times 10^{-3}$	Corr.	y	M3 Area $\times 10^{-3}$	Corr.
1.9	3.775	.01205	3.15	3.180	.01015
1.7	2.435	.00777	2.75	2.800	.00[illegible]
1.5	1.[illegible]	.00[illegible]	2.25	2.[illegible]	.00[illegible]
1.3	1.270	.00405	2.05	2.[illegible]	.00847
.8	.730	.00233	1.75	2.[illegible]	.00823
.675	.625	.00[illegible]	1.[illegible]	2.[illegible]	.00[illegible]
.525	.520	.00166	1.18	1.270	.00405
.4	.[illegible]	.00076	.82	1.015	.00324
.3	.165	.000526	.56	.[illegible]05	.00288
.175	.235	.000750	.325	.075	.00023
.060	.2[illegible]	.000700			

Table No. 15

Boundary Layer Thickness

#2M2 Interferometer y*	Thick*	#2M2 Schlieren y*	Thick*	M3 Interferometer y*	Thick*
1.9	.03	1.[illegible]1	.0271	3.15	.055
1.7	.025	1.778	.0179	2.75	.0[illegible]
1.5	.015	1.536	.010[illegible]	2.[illegible]	.0[illegible]
1.3	.012	1.[illegible]	.0082	2.05	.0[illegible]
.8	.010	1.052	.007[illegible]	1.75	.0[illegible]
.675	.010	.810	.0058	1.6[illegible]	.0[illegible]
.525	.012	.[illegible]	.00[illegible]	1.18	.0[illegible]
.4	.012	.325	.00[illegible]	.82	.0[illegible]
.3	.012	.0[illegible]3	.0030	.56	.0[illegible]
.175	.012			.325	.0[illegible]
.060	.012				

Table No. 16

[illegible] Density Distribution From Wall Tap

Atm. Pressure: [illegible] atm. Humidity: [illegible]
Atm. Temperature: [illegible] F.

Hole No.	[illegible]	[illegible]
1	10.[illegible]	.[illegible]
2	10.52	.[illegible]
3	11.[illegible]	.[illegible]
4	12.[illegible]	.1[illegible]
5	13.[illegible]	.12[illegible]
6	1[illegible].30	.1[illegible]

Table No. 17

M3 Density Distribution From Wall Taps

Atm. Pressure: 11.[illegible] psia. Humidity: [illegible]
Atm. Temperature: [illegible] °F.

Hole No.	P	
1	1.71	[illegible]
2	1.[illegible]	[illegible]
3	1.[illegible]	[illegible]
4	2.[illegible]	[illegible]
5	2.[illegible]	[illegible]
6	3.[illegible]	[illegible]

Table No. 18

M2 Wall Pressures

Atm. Pressure : 12.[illegible] psia. Humidity: [illegible]
Atm. Temperature: [illegible] °F

Reservoir Pressure		Hole No. 1	2	3	4	5	6
#2	67	[illegible]	[illegible]	[illegible]	11.71	[illegible]	[illegible]
	75	[illegible]	[illegible]	[illegible]	12.[illegible]	15.[illegible]	[illegible]
	77	[illegible]	[illegible]	11.66	13.72	16.[illegible]	[illegible]
#1	67	[illegible]	[illegible]	[illegible]	[illegible]	11.[illegible]	14.02
	75	[illegible]	[illegible]	[illegible]	[illegible]	13.[illegible]	15.75
	77	[illegible]	[illegible]	11.[illegible]	[illegible]	[illegible]	[illegible]

Table No. 21

M2 Central Density Distribution From Static Probes

Atm.Pressure :11.98psia. Humidity: 69%
Atm.Temperature:71.[illegible] °F. ρ_o : 0.3828 lb/cu. ft

y	P_1	ρ_1
1.834	10.34	.0929
1.634	10.28	.0926
1.434	10.49	.0939
1.234	11.16	.0975
1.034	12.12	.1041

Table No. 19

#1 #2 Static Probe Test

Atm. Pressure: 11.[illegible] psia. Humidity : 52%
Atm. Temperature: 71.[illegible]°F 1 unit = [illegible]"
Res. Pressure: 63 psig.

Zero Co-ordinates of probe hole
x = [illegible]" y = [illegible].111"

y	x	p psig.	p psia.	y	x	p psig.	p psia.
0	0	-[illegible]	11.6[illegible]		4	-2.11	[illegible]
	2	-1.23	10.73		6	-2.[illegible]	9.04
	4	-2.12	[illegible]		8	-1.92	10.04
	6	-1.96	9.99		10	-1.[illegible]	10.04
	8	-1.99	9.97		11	-2.[illegible]	9.7[illegible]
	10	-.[illegible]	11.37				
	11	-.[illegible]	11.[illegible]	1[illegible]	1	-1.92	10.0[illegible]
					2	-2.31	[illegible]
2	0	-0.02	11.04		4	-2.02	9.0[illegible]
	2	-1.42	10.54		6	-2.[illegible]	9.04
	4	-1.90	10.02		8	-1.[illegible]	10.0[illegible]
	6	-1.[illegible]	[illegible]		10	-2.[illegible]	9.04
	8	-2.02	[illegible]				
	10	-1.54	11.42	[illegible]	1	-0.[illegible]	11.[illegible]
	11	-0.[illegible]	11.57		2	-1.13	10.[illegible]
					4	-1.13	10.[illegible]
5	0	-1.82	10.14		6	-1.[illegible]	10.[illegible]
	2	-1.[illegible]	10.14		8	-1.[illegible]	10.[illegible]
					10	-1.0[illegible]	10.[illegible]

Table No. 20

#2 #2 Static Probe Test

Atm. Pressure: 12.[illegible] psia. Humidity: [illegible]
Atm. Temperature: 60.[illegible]°F. 1 unit = .[illegible]"
Res. Pressure: 63 psig.

Zero Co-ordinates of Probe Hole:
x = [illegible].631" y = 1.[illegible]

y	x	p psig.	p psia.	y	x	p psig.	p psia.
0	0	-1.[illegible]	10.7[illegible]		4	-1.[illegible]	10.33
	2	-1.39	10.[illegible]		6	-1.92	10.[illegible]
	4	-1.82	10.18		8	-1.[illegible]	10.[illegible]
	6	-1.72	10.[illegible]		10	-1.[illegible]	10.[illegible]
	8	-1.77	10.22				
	10	-1.[illegible]	10.24	15	1	-0.5[illegible]	11.[illegible]
					3	-0.[illegible]	11.[illegible]
5	0	-1.23	[illegible].77		5	-1.03	10.[illegible]
	2	-1.[illegible]	[illegible]		7	-1.03	10.[illegible]
	4	-1.[illegible]	[illegible]		9	-1.[illegible]	10.[illegible]
	6	-1.[illegible]	[illegible]				
	8	-1.[illegible]	10.[illegible]	20	3	0.[illegible]	12.[illegible]
10	0	-1.03	10.57		5	0.[illegible]	12.2[illegible]
	2	-1.[illegible]	10.[illegible]		7	0.[illegible]	12.3[illegible]
					9	0.[illegible]	11.80

Table No. 22

P1 M7 Total Head Probe Test

Atm. Pressure : 11.[illegible] psia. Humidity: [illegible]
Atm. Temperature: 71.[illegible]°F. 1 unit = 0.04"
Rec. Pressure : 63 psia.

Zero Co-ordinates:
x = 0.237" y = 1.825"

y	x	pt
0	0	52.0
	2	53.2
	4	53.0
	6	52.4
	8	53.0
	10	54.6
	12	52.1
5	1	53.5
	4	52.1
	6	52.0
	9	52.4
	11	54.0
10	1	55.1
	3	56.3
	5	57.3
	7	57.5
	9	53.2
	11	54.1
15	1	55.0
	3	55.9
	4	54.8
	4	54.6
	6	56.8
	10	55.0
20	2	57.0
	4	57.0
	6	57.1
	8	57.1
	10	56.8

y	x	pt
25	2	59.6
	4	58.5
	6	59.1
	8	59.2
	10	59.0
30	2	62.0
	4	62.0
	6	62.0
	8	61.8
	10	61.7
35	3	64.8
	5	65.0
	7	65.0
	9	64.8
40	3	66.0
	5	67.0
	7	67.4
	9	67.0
45	3	69.4
	5	68.0
	7	68.5
	9	68.2
50	3	69.0
	5	69.3
	7	69.6
	9	69.2

Pressures along the Centreline

y"	pt
1.682	51.5
1.382	53.2
1.082	53.7
.782	54.2
.482	55.8
.182	58.0

y"	pt
-.118	60.5
-.418	63.3
-.718	66.2
-1.018	68.1
-1.318	70.2
-1.618	70.8

Table No. 23

Ø2 M2 Intel Head Probe Test

Atm.Pressure :12.[illegible]m. Resistyt 6/8
Atm.Temperature:[illegible] 1 unit = 0.04"
Bas.Pressure :63 m/m.

Zero Co-ordinates
x = 0.220" y = 1.062"

y	x	pA	y	x	pB
0	0	45.0	30	1	59.9
	2	47.0		3	60.8
	4	46.0		5	60.0
	6	47.5		7	60.6
	8	51.8		9	61.2
	10	49.8	35	1	59.5
5	0	51.5		3	63.0
	2	51.0		5	62.0
	4	51.8		7	63.3
	6	51.2		9	62.8
	8	51.0	40	2	66.8
	10	53.5		4	66.1
10	0	54.0		6	66.2
	2	55.5		8	66.6
	4	53.0	45	2	68.4
	6	52.7		4	68.6
	8	53.0		6	68.6
	10	54.0		8	68.1
15	0	54.8	50	3	70.5
	2	54.0		5	70.8
	4	53.5		7	70.8
	6	53.8		9	70.0
	8	53.0	55	3	71.0
	10	56.0		5	70.9
20	0	56.0		7	70.6
	2	54.8		9	71.5
	4	55.2			
	6	55.5			
	8	55.6			
	10	55.7			

Pressures along the Centreline

x"	pA	x"	pB
1.[illegible]	52.7	.625	62.2
1.625	52.7	.425	64.1
1.425	53.8	.225	67.4
1.225	54.8	.025	69.3
1.025	57.0	-.175	59.8
.825	50.3		

Table No 24

Mach Number from Rayleigh Pitot Tube Equation

Wall Taps and Impact Probe.

Tap No.	P	p1	po'	P1/Po'	M
1	1.[illegible]	10.[illegible]	52.5	.2028	1.85
2	1.[illegible]	10.52	52.0	.[illegible]	1.86
3	1.276	11.30	54.4	.2[illegible]03	1.82
4	1.018	12.8[illegible]	57.0	.2256	1.75
5	0.756	15.86	60.3	.2[illegible]10	1.60
6	0.609	18.30	63.9	.2820	1.57

Static and Impact Probes.

P	P1	p'	P1/p'	M
1.234	10.[illegible]4	52.6	.1965	1.805
1.[illegible]34	10.28	52.6	.1954	1.800
1.[illegible]34	10.40	53.0	.1964	1.805
1.234	11.16	54.7	.2040	1.845
1.034	12.12	56.8	.2133	1.895

Table No. 25

M2 Cone Tests

Atm.pressure :11.98 psia. Humidity: 70%
Atm.Temperature:70.0°F Run.Pressure: 65 psig.

Cone Semi-Angle#0	Shock Semi-Angle #1	#2	Mean	M
5	30.8	30.7	30.75	
10		31.4	31.4	1.99
15	34.7	34.2	34.4	2.07
20	37.9	38.4	38.1	1.995
25	42.7	42.0	42.3	1.98

Table No. 26

M3 Cone Tests

Atm.Pressure :11.924psia. Humidity: 77%
Atm.Temperature:[illegible].8 F Run.Pressure: 65 psig.

Cone Semi-Angle	Shock Semi-Angle	M
15	24.8	3.09
20	29.0	2.64
25	33.1	2.86
20*	29.7	

*Schadowgraph

Table No. 27

M2 Cone Tests with various Pressures

Atm.Pressure :11.[illegible]psia. Humidity :70%
Atm.Temperature:71.4°F Cone Semi-Angle:20°

Run. Press.	Shock Semi-Angle#2	Shock Semi-Angle#1
61	38.5	38.7
63	38.2	38.4
64*	37.8	38.0
65	38.2	37.8

Table No. [illegible]

Constants for Characteristics Theory

ω	α	M	ρ/ρ_0	ρ
0	90.00	1.000	.633	.2418
0.5	72.89	1.050	.607	.2318
1	67.57	1.081	.591	.2257
1.5	64.47	1.108	.577	.2204
2	61.99	1.132	.564	.2154
2.5	59.95	1.155	.553	.2112
3	58.18	1.176	.542	.2070
3.5	56.61	1.197	.532	.2032
4	55.20	1.217	.522	.1994
4.5	53.92	1.237	.512	.1950
5	52.73	1.256	.503	.1921
5.5	51.64	1.275	.494	.1887
6	50.68	1.293	.485	.1853
6.5	49.65	1.312	.477	.1822
7	48.75	1.330	.468	.1787
7.5	47.89	1.347	.460	.1757
8	47.08	1.365	.452	.1726
8.5	46.30	1.383	.445	.1699
9	45.56	1.400	.437	.1669
9.5	44.85	1.417	.429	.1638
10	44.17	1.434	.422	.1612
10.5	43.52	1.452	.415	.1585
11	42.89	1.469	.407	.1554
11.5	42.28	1.486	.401	.1532
12	41.70	1.503	.393	.1501
12.5	41.13	1.520	.387	.1478
13	40.58	1.537	.380	.1451
13.5	40.05	1.554	.373	.1425
14	39.53	1.571	.367	.1402
14.5	39.03	1.587	.360	.1375
15	38.54	1.604	.354	.1352
15.5	38.07	1.621	.347	.1325
16	37.61	1.638	.341	.1302
16.5	37.16	1.655	.335	.1279
17	36.72	1.672	.329	.1257
17.5	36.29	1.689	.323	.1234
18	35.87	1.706	.317	.1211
18.5	35.46	1.723	.311	.1188
19	35.06	1.740	.306	.1169
19.5	34.67	1.757	.300	.1146
20	34.29	1.775	.294	.1123
20.5	33.91	1.792	.289	.1104
21	33.54	1.809	.284	.1085
21.5	33.18	1.826	.278	.1062
22	32.83	1.844	.273	.1043
22.5	32.48	1.861	.268	.1024
23	32.14	1.879	.263	.1005
23.5	31.81	1.896	.258	.0985
24	31.48	1.914	.253	.0966
24.5	31.16	1.932	.248	.0947
25	30.84	1.950	.243	.0928
25.5	30.53	1.968	.238	.0909
26	30.22	1.986	.233	.0890

w	a	M	P/P₀	P
28	29.05	2.059	.215	.0821
30	27.94	2.134	.198	.0756
32	26.99	2.210	.182	.0695
34	25.91	2.289	.167	.0638
36	24.96	2.369	.152	.0581
38	24.06	2.452	.139	.0531
40	23.30	2.537	.126	.0482
42	22.38	2.626	.114	.0435
44	21.59	2.717	.104	.0398
46	20.83	2.812	.093	.0356
48	20.09	2.910	.084	.0321
50	19.39	3.012	.075	.0287

Table No. 29

M2 Central Density Distribution from Characteristics Theory

Res. Pressure : 75 psia. Res. Density: 0.38201 lbs/cu.ft.
Res. Temperature: 70° F.

ω	y	ρ	N
26	2.000	.0890	1.9862
25.5	1.515	.0909	1.9682
25	1.430	.0928	1.9502
24.5	1.395	.0947	1.9324
24	1.281	.0966	1.9146
23.5	1.219	.0985	1.8969
23	1.179	.1005	1.8793
22.5	1.145	.1024	1.8618
22	1.109	.1043	1.8443
21	1.050	.1085	1.8095
20	.984	.1123	1.7750
19	.913	.1169	1.7406
18	.834	.1211	1.7065
17	.750	.1257	1.6725
16	.600	.1302	1.6385
14	.536	.1402	1.5709
12	.457	.1501	1.5032
10	.366	.1612	1.4349
8	.242	.1726	1.3655
6	.178	.1853	1.2938
4	.141	.1994	1.2177
2	.091	.2154	1.1326
1	.065	.2257	1.0818
0	0.000	.2418	1.0000

Table No. 30

M2 Central Density Distribution from One-Dimensional Theory

Same conditions as above

y	x	Effective x	$\frac{A^*}{A}$	N	$\frac{\rho_0}{\rho}$	ρ
0.0	.1550	.1550	1.0000	1.000	1.578	.2420
.05	.1563	.1561	.9929	1.087	1.60	.2065
.1	.1598	.1593	.9830	1.186	1.05	.2065
.15	.1635	.1628	.9720	1.256	1.98	.1929
.2	.1673	.1663	.9670	1.312	2.09	.1828
.4	.1824	.1804	.8502	1.480	2.48	.1600
.6	.1975	.1945	.7969	1.607	2.83	.1349
.8	.2127	.2087	.7426	1.714	3.16	.1208
1.0	.2278	.2238	.6925	1.804	3.50	.1091
1.2	.2430	.2378	.6540	1.879	3.79	.10079
1.4	.2547	.2477	.6257	1.936	4.04	.09450
1.6	.2637	.2557	.6061	1.971	4.21	.09073
1.8	.2688	.2596	.5966	1.983	4.31	.08863
2.0	.2700	.2600	.5961	1.995	4.32	.08842

Table No. 31

MB Control Density Distribution
From One-Dimensional
Theory

Res. Pressure : 75 psia.
Res. Temperature: 70° F.

Res. Density: 0.38201
lbs./cu.ft.

y	z	Effective R	A^*/A	M	ρ_0/ρ	ρ
0.0	.1550	.1550	1.0000	1.000	1.478	.24207
.0	.1565	.1565	.9916	1.092	1.700	.2247
.1	.1585	.1580	.9810	1.152	1.79	.2134
.2	.1654	.1644	.9428	1.284	2.03	.1881
.3	.1750	.1735	.8933	1.407	2.30	.1661
.4	.1855	.1835	.8446	1.512	2.56	.1490
.5	.2045	.2020	.7673	1.661	3.00	.1273
.6	.2195	.2165	.7159	1.760	3.34	.1143
.7	.2300	.2355	.6581	1.872	3.77	.1013
.8	.2500	.2550	.6078	1.970	4.19	.0911
.9	.2820	.2775	.5585	2.071	4.71	.0811
1.0	.3075	.3025	.5123	2.171	5.26	.0726
1.2	.3575	.3515	.4409	2.338	6.33	.0603
1.4	.4035	.3985	.3880	2.472	7.37	.0518
1.6	.4480	.4400	.3522	2.516	8.25	.0463
1.8	.4850	.4760	.3256	2.611	9.07	.0421
2.0	.5190	.5090	.3045	2.732	9.81	.0389
2.2	.5490	.5380	.2881	2.783	10.40	.0367
2.4	.5750	.5630	.2753	2.832	11.00	.0347
2.6	.5970	.5840	.2654	2.880	11.55	.0330
2.8	.6160	.6020	.2574	2.902	11.82	.0323
3.0	.6330	.6180	.2508	2.930	12.17	.0313
3.2	.6460	.6300	.2460	2.950	12.41	.0307
3.4	.6560	.6740	.2425	2.966	12.62	.0302
3.6	.6650	.6470	.2395	2.981	12.85	.0297
3.8	.6700	.6520	.2380	2.987	12.91	.0295
4.0	.6738	.6330	.2370	2.990	13.05	.0292

Table No.12

M3 Central Density Distribution

From Characteristic Theory

Res.Pressure :752psia. Res.Density: 0.38201
Res.Temperature:70°F. lbs./cu.ft.

ω	y	P	W
0	0	.2420	1.000
2	.100	.2181	1.132
4	.172	.1995	1.217
6	.241	.1857	1.293
8	.296	.1732	1.365
10	.351	.1612	1.435
12	.403	.1505	1.503
14	.453	.1402	1.571
16	.504	.1301	1.638
18	.550	.1211	1.706
20	.608	.1128	1.775
22	.659	.1042	1.844
24	.702	.0966	1.914
26	.773	.0859	1.986
28	.841	.0821	2.059
30	.908	.0756	2.134
32	.978	.0695	2.210
34	1.052	.0638	2.288
36	1.183	.0581	2.369
38	1.281	.0531	2.452
40	1.421	.0482	2.537
42	1.578	.0435	2.626
44	1.810	.0398	2.717
46	1.912	.0356	2.812
48	2.210	.0321	2.910
50	2.500	.0287	3.012

Appendix 3

Curves


CURVE No. 1
x = 0.148"

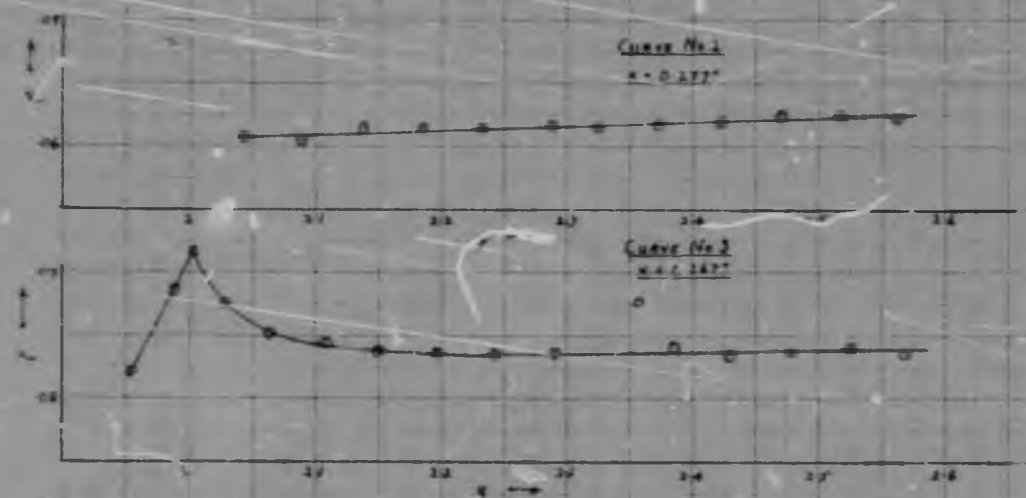
CURVE No. 2
x = 0.272"
CURVE No. 3
x = 0.362"

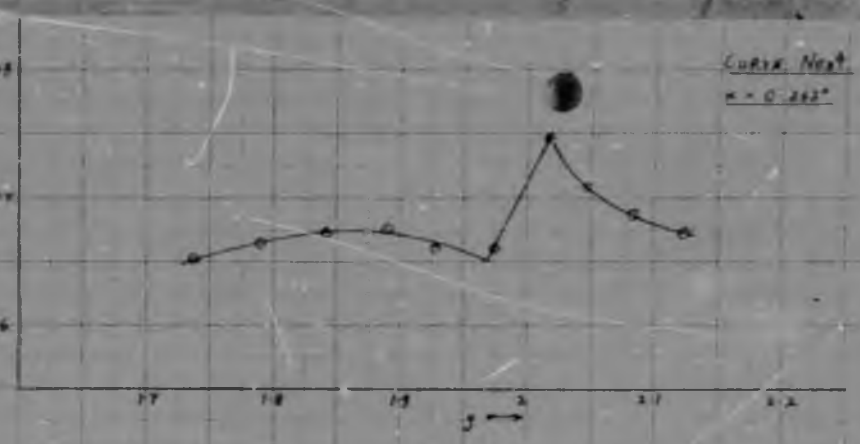
CURVE No. 4
x = 0.262"

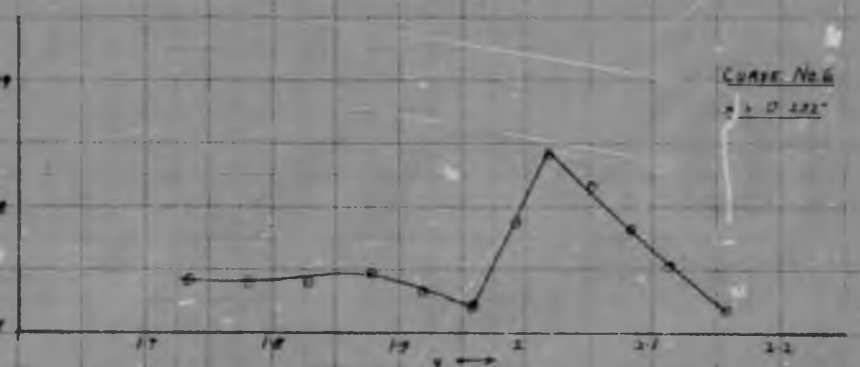
CURVE No. 6
x = 0.222"

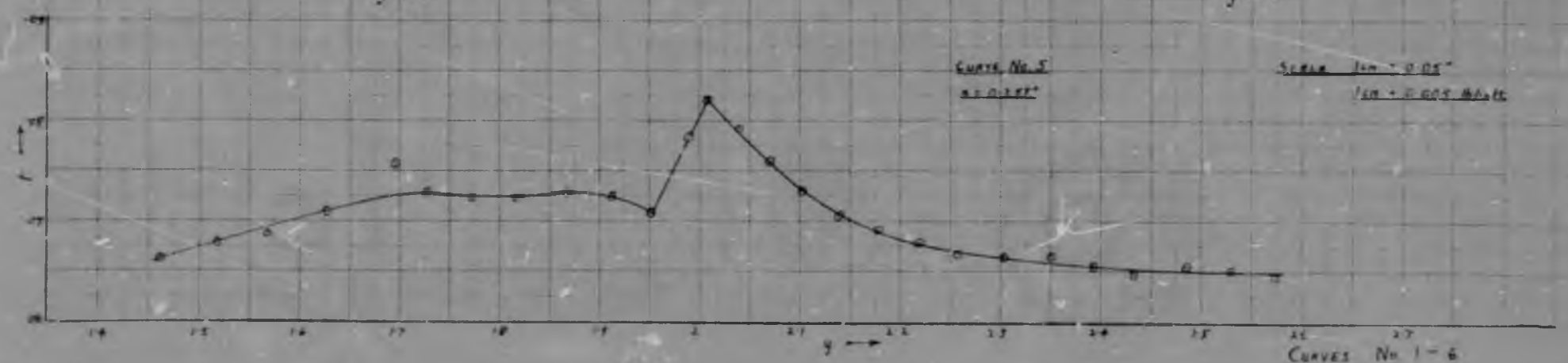
CURVE No. 5
x = 0.322"
SCALE 1cm = 0.05"
1cm = 0.005 VOLTS

CURVES No. 1 – 6

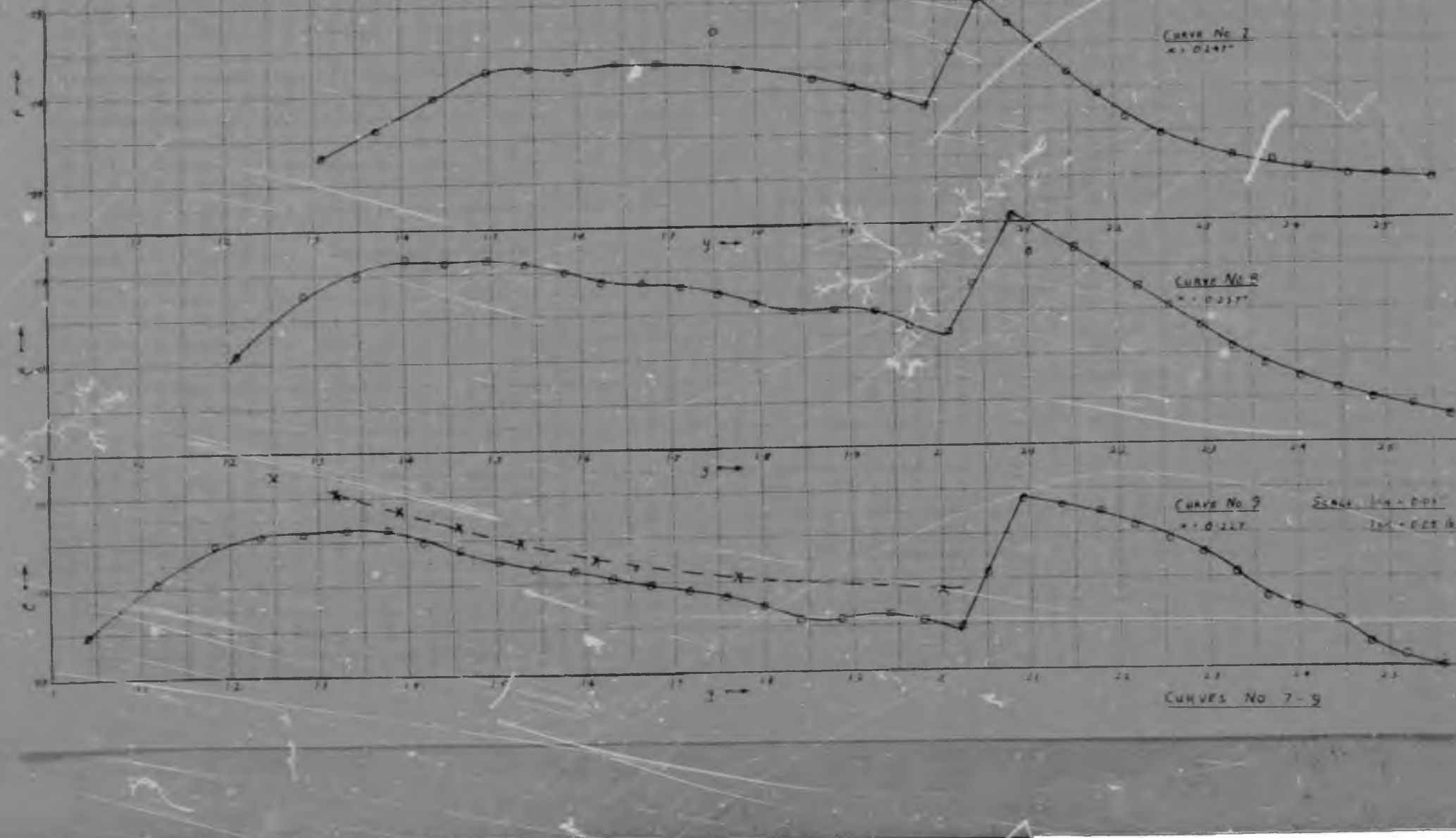
CURVE No 7
CURVE No 8
CURVE No 9
CURVES No 7-9

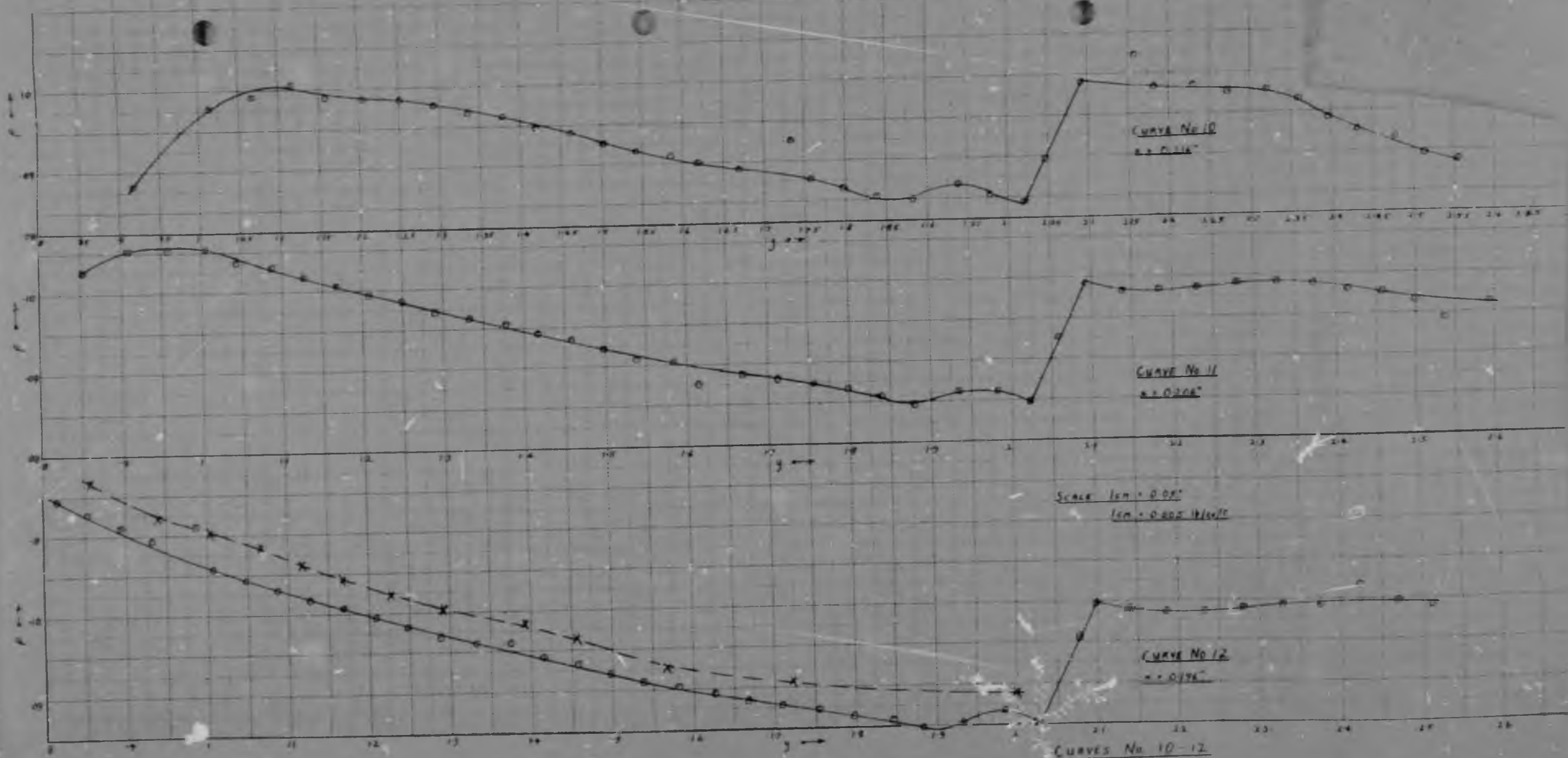
Curve No 10
Curve No 11
Scale 1cm = 0.05"
Curve No 12
Curves No 10 - 12

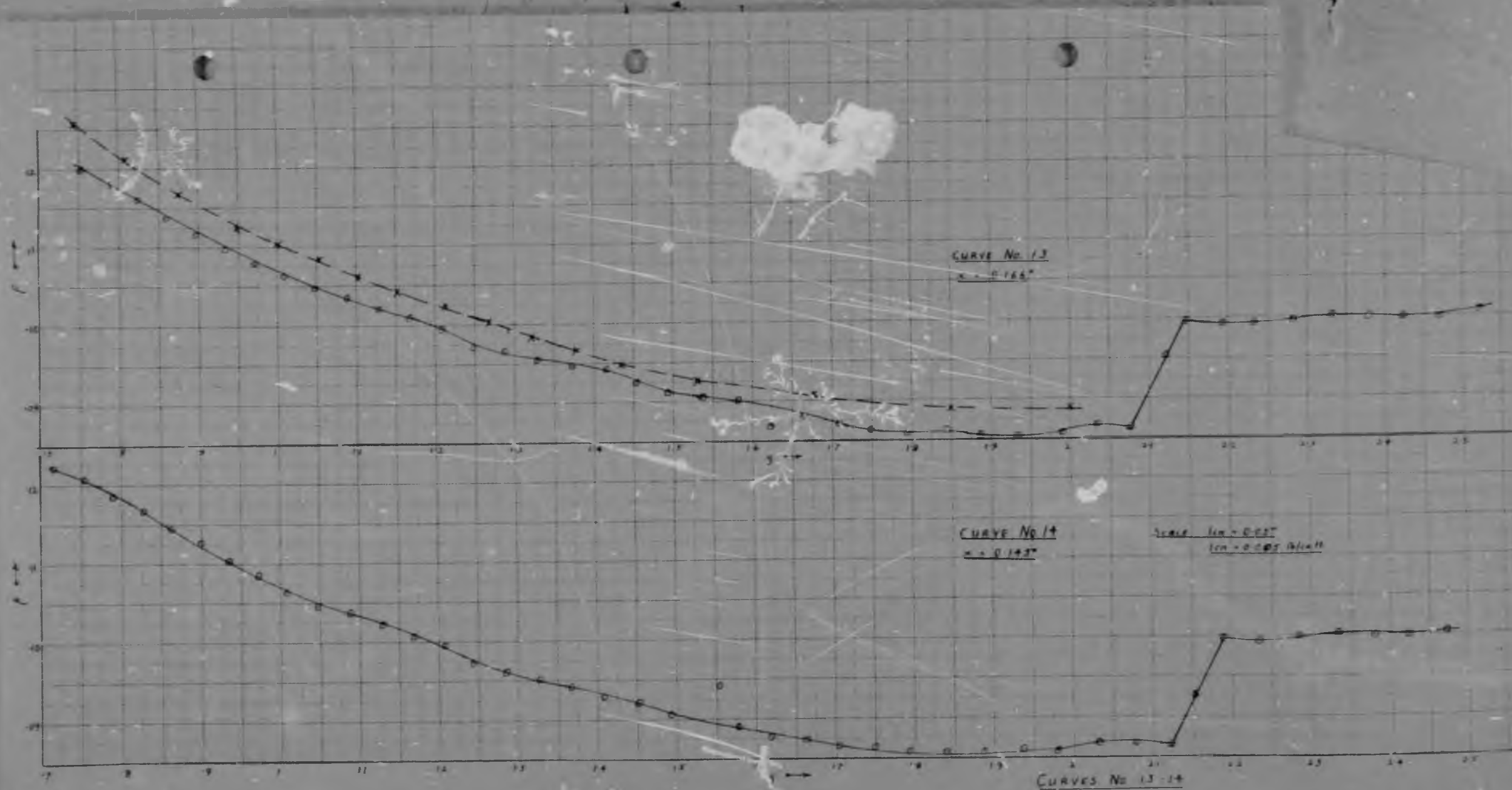
CURVE No. 13
CURVE No 14
CURVES No 13-14

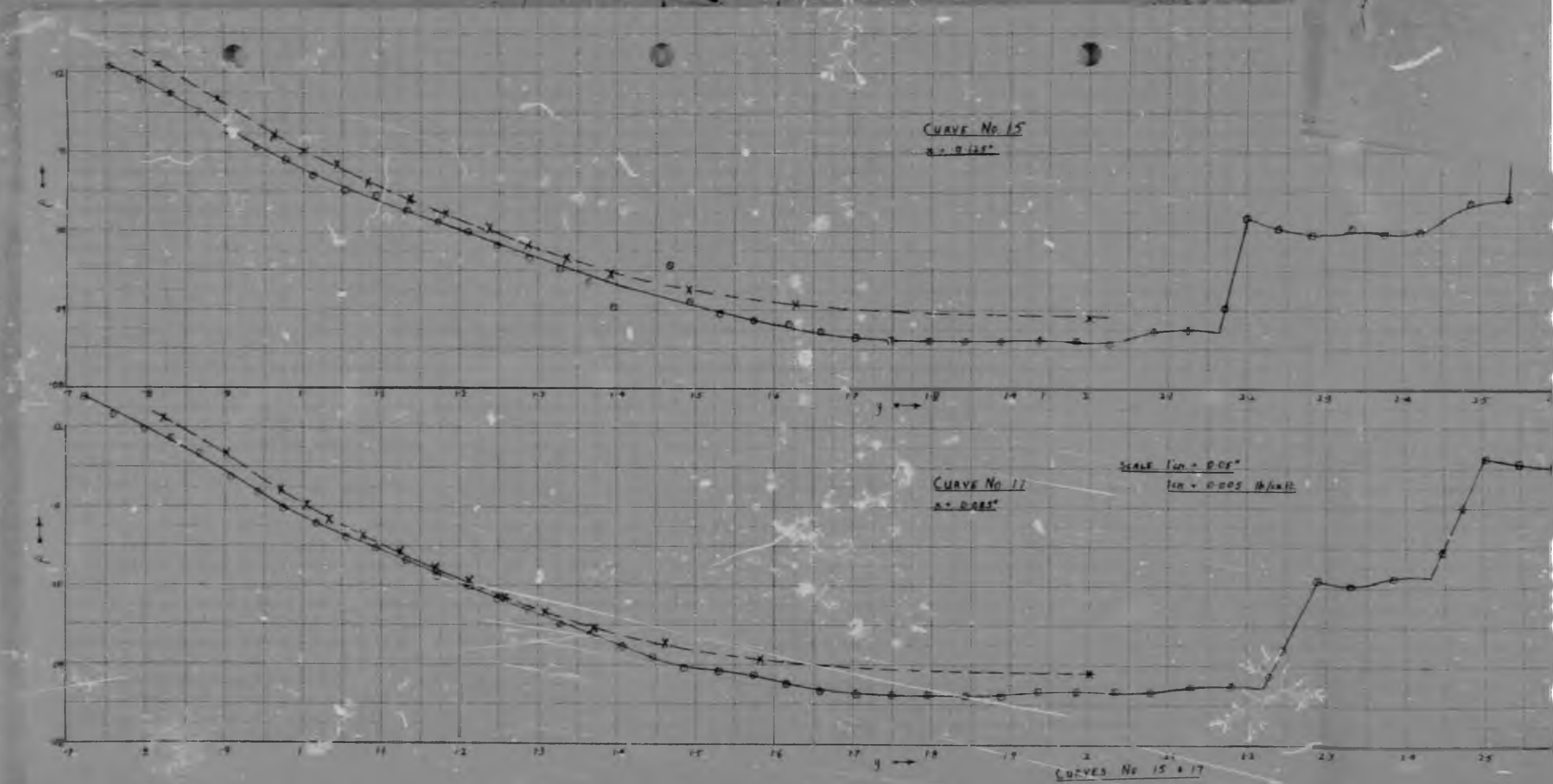
CURVE No 15
x = 0.125"
CURVE No 17
x = 0.085"
SCALE 1cm = 0.05"
1cm = 0.005 lb/cu ft
y →
ρ →
CURVES No 15 & 17

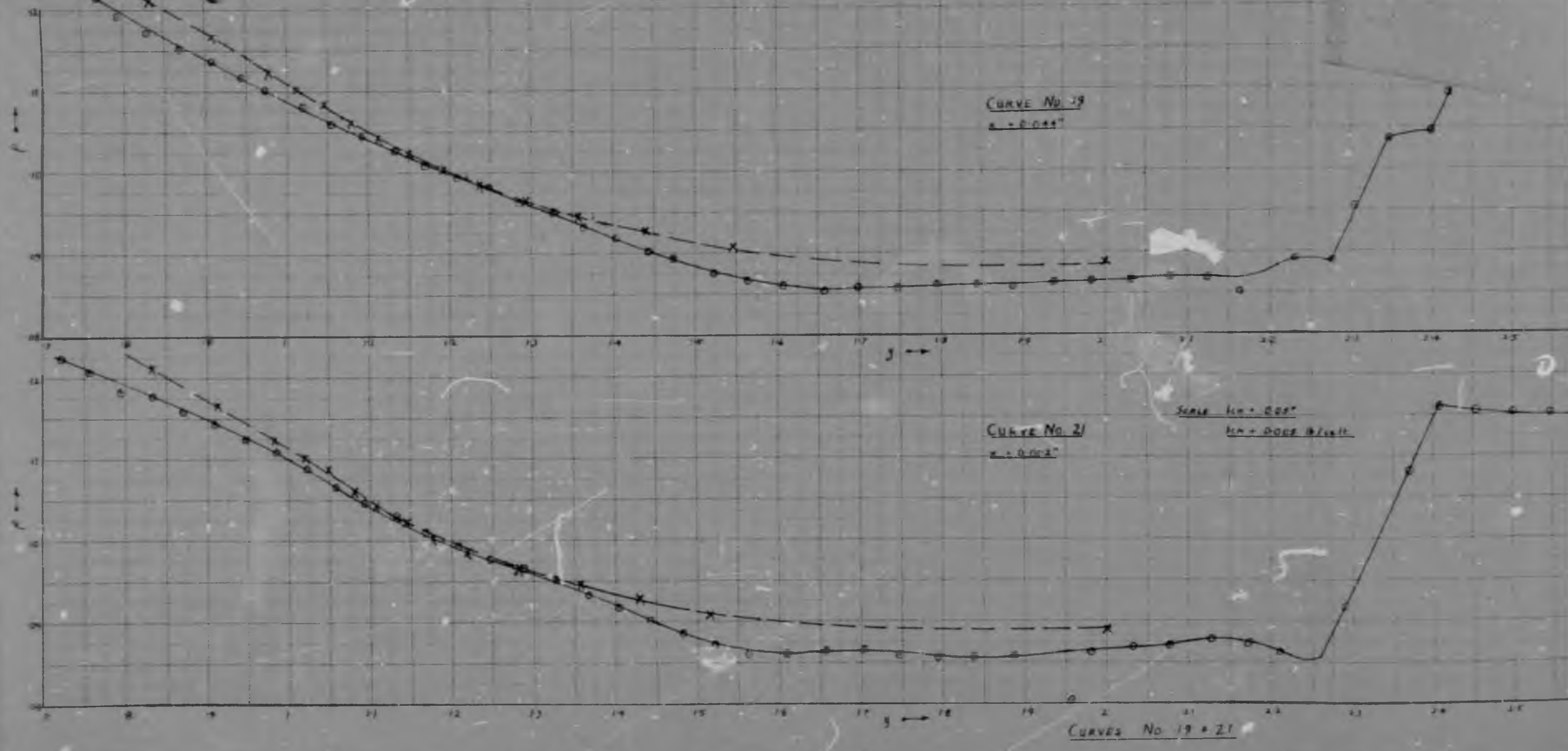
Curve No. 19
Curve No. 21
Curves No. 19 + 21

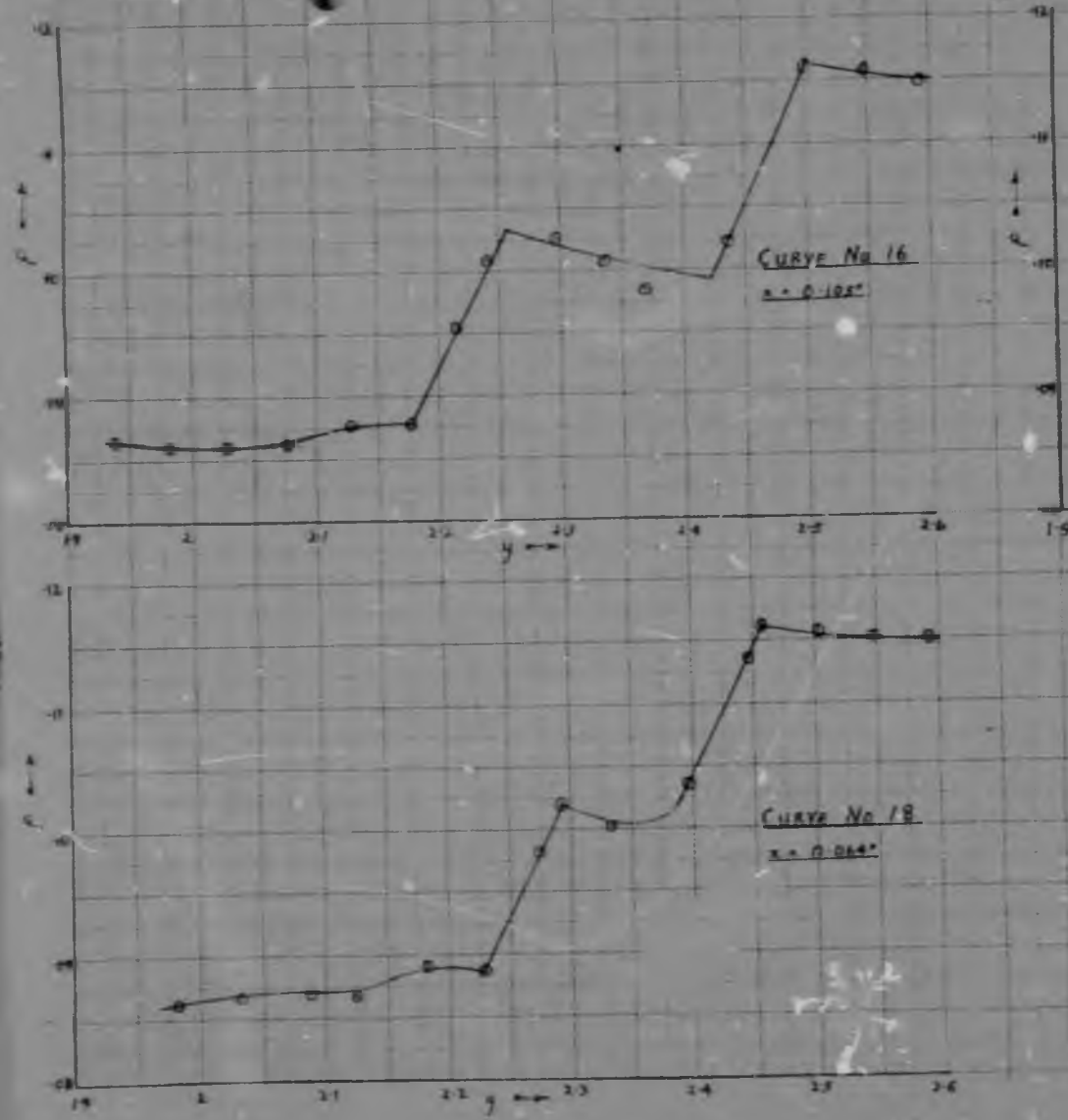

SCALE 1cm = 0·05"
1cm = 0·005 lb/sq ft

CURVES No 1 to 20
M2 EAST. DENSITIES FROM FIG 35 TABLE No 3

OBSERVED DENSITY —o—
THEORETICAL " —x—

CURVES No 16, 18 & 20

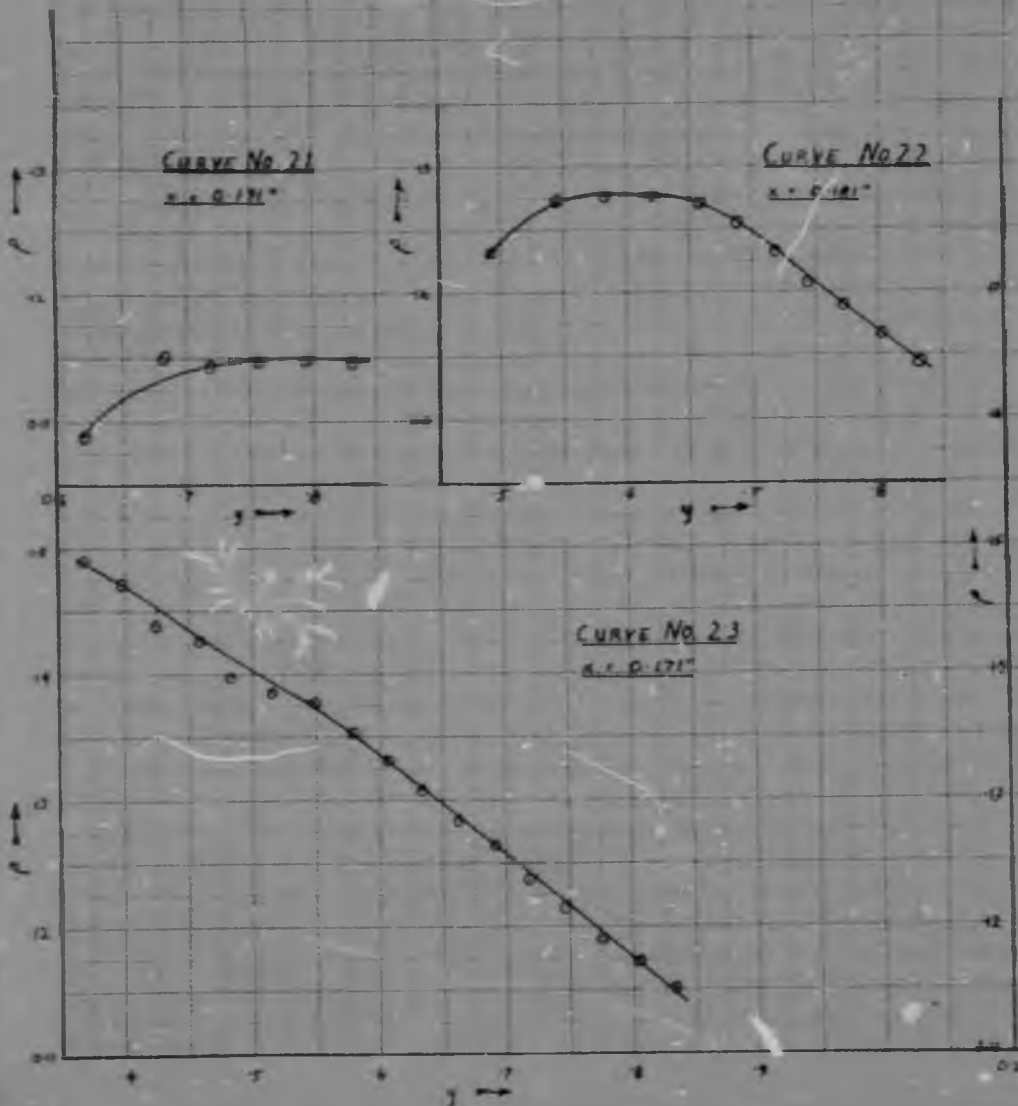

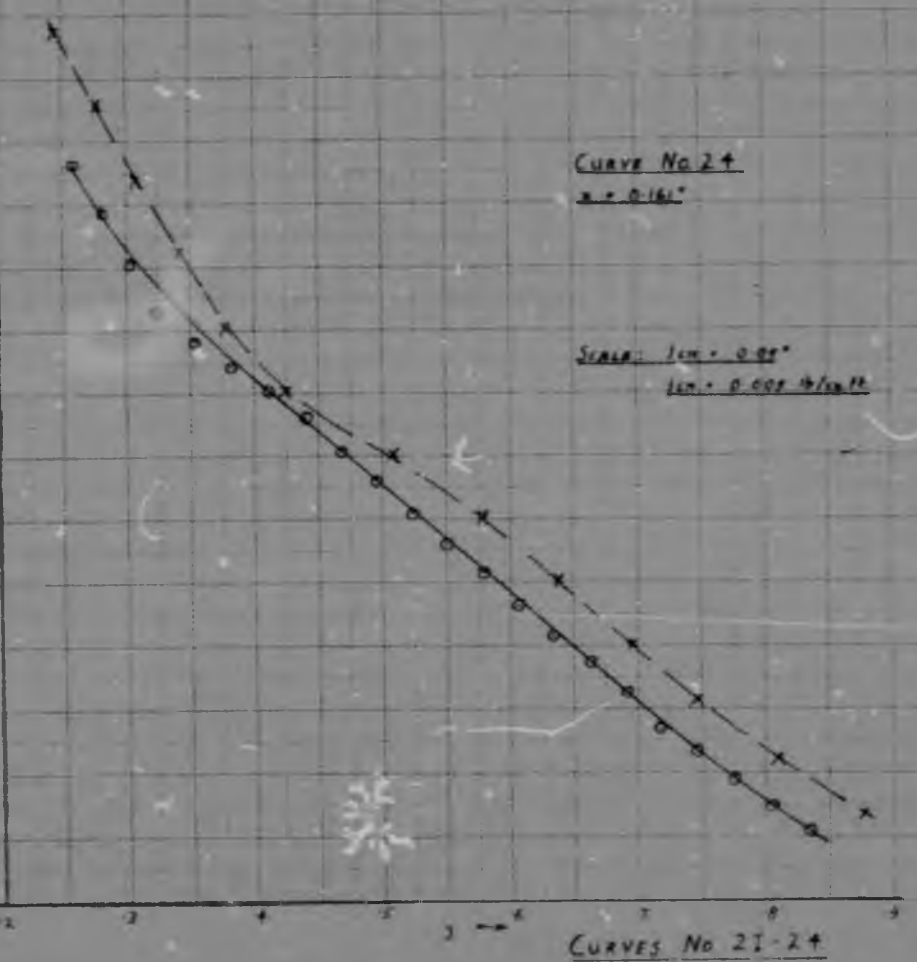

Curves No 21-24

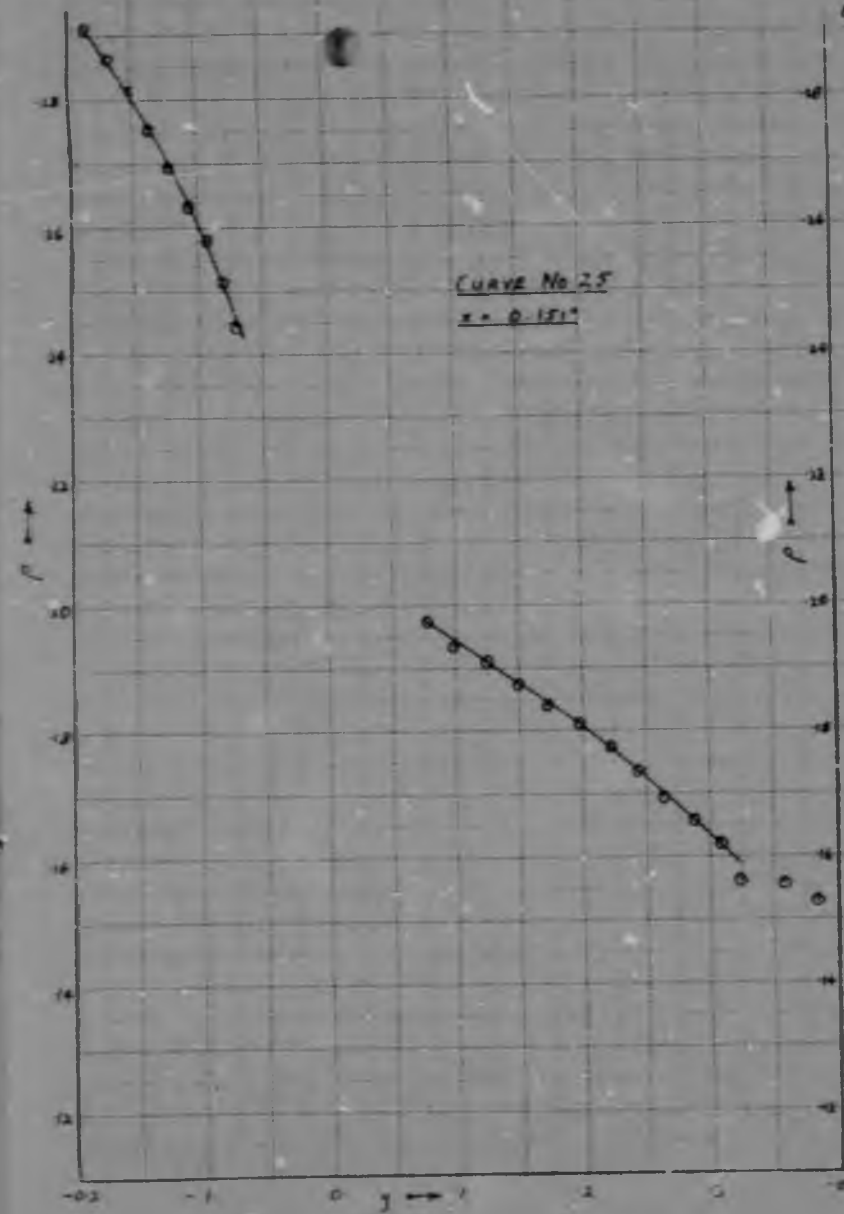

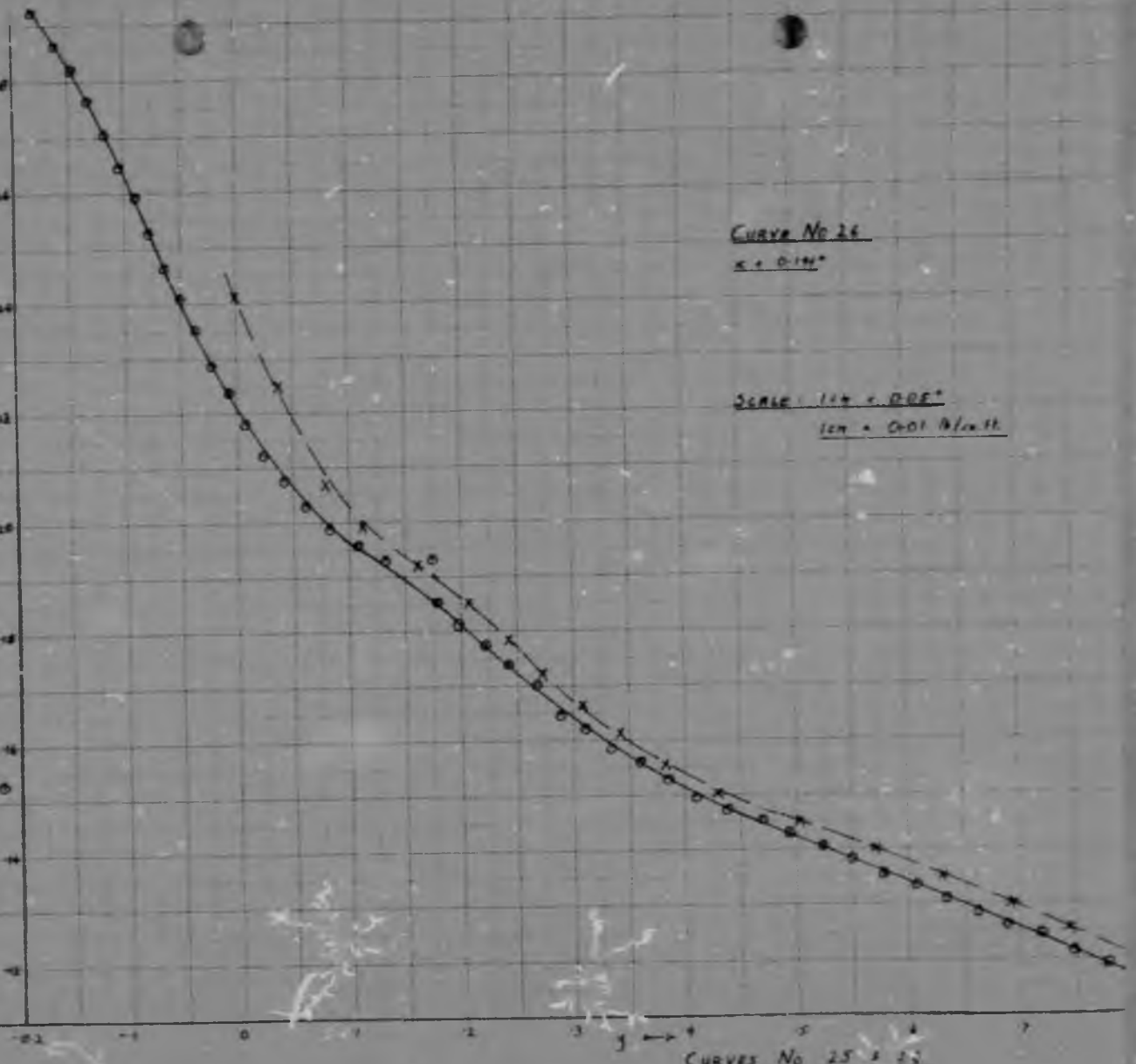

Curves No 25 & 26

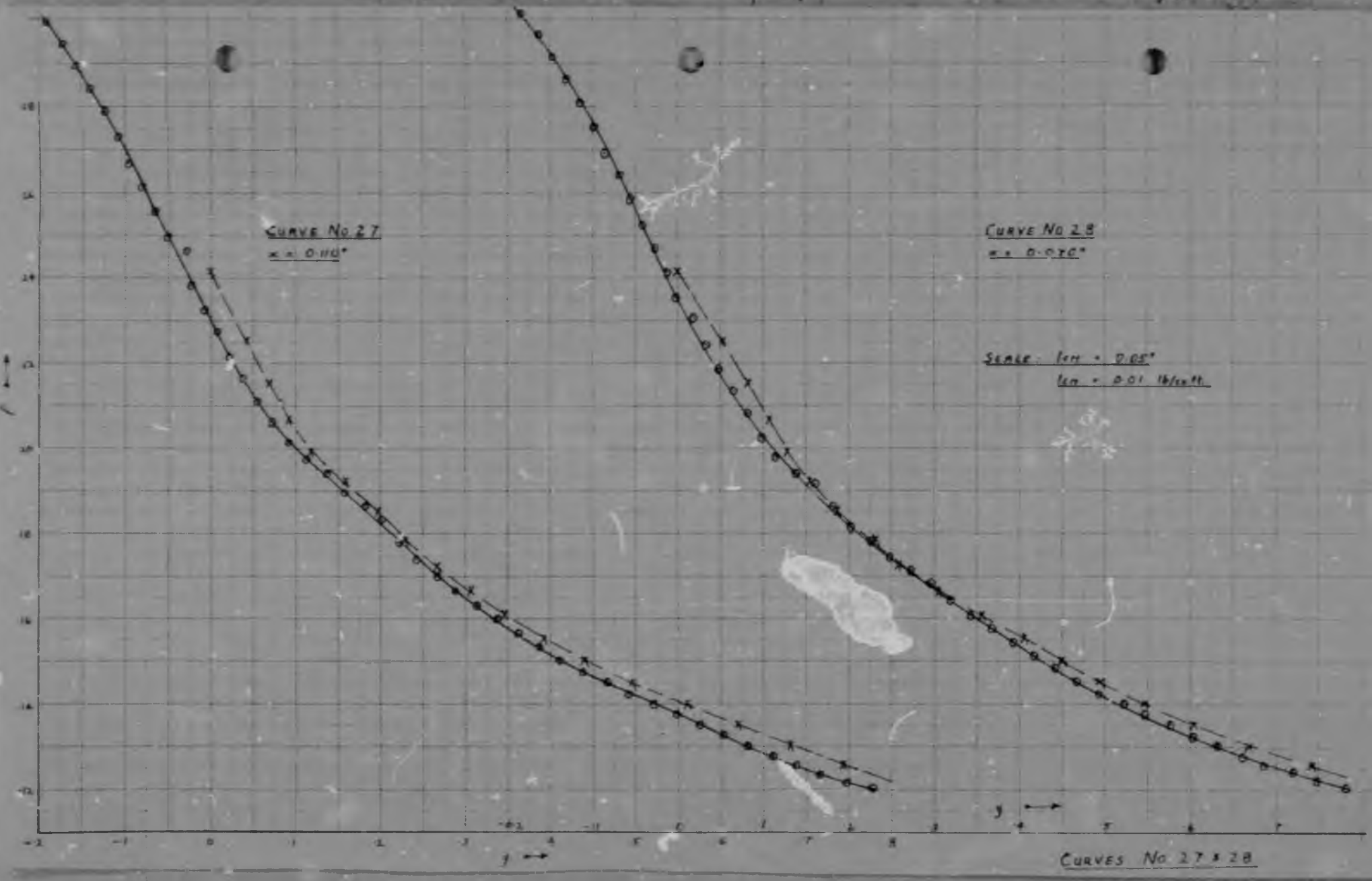

CURVES No 27 & 28

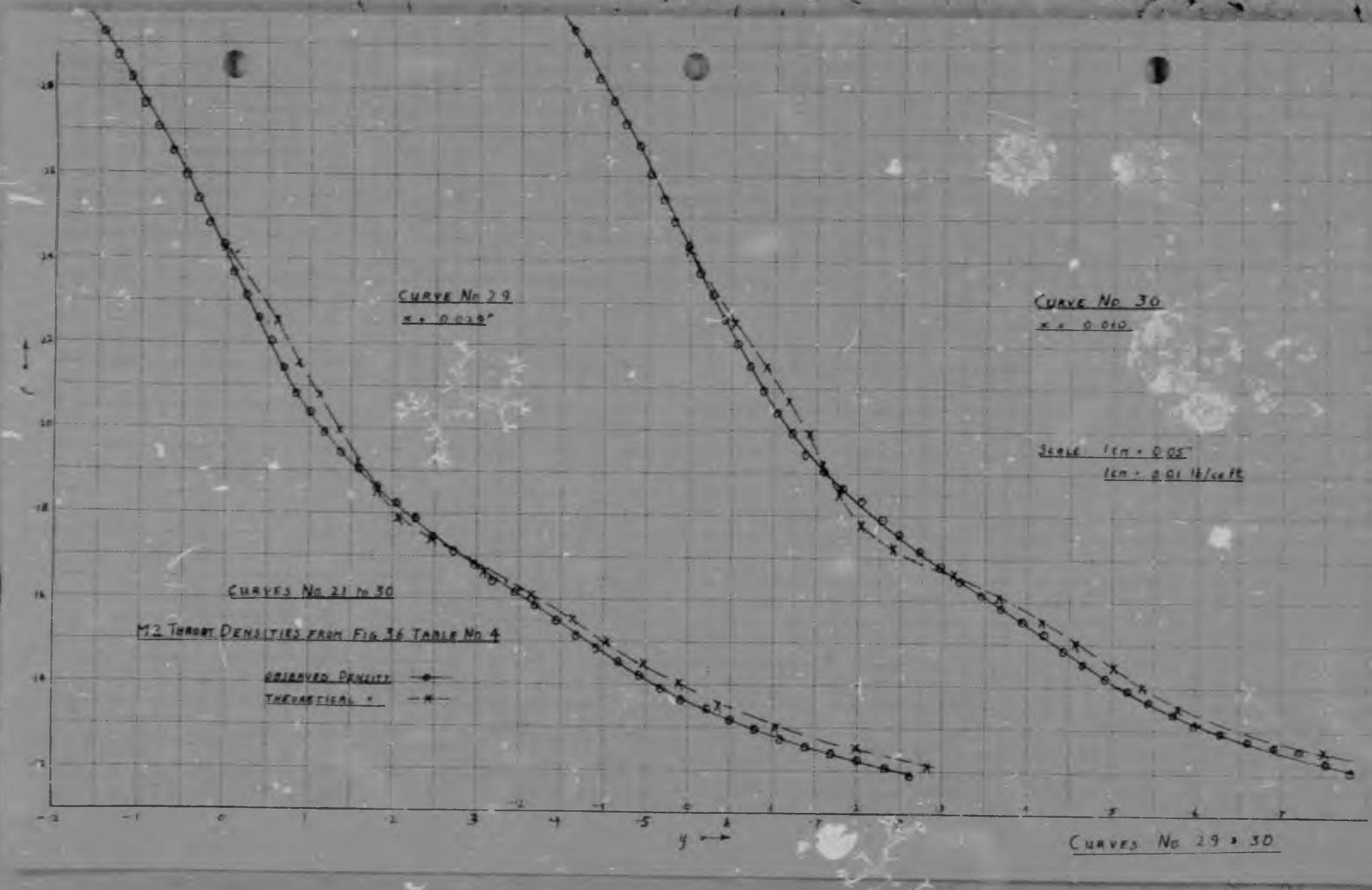
CURVE No 29
x = 0.020"
CURVE No 30
x = 0.010
SCALE 1cm = 0.05"
1cm = 0.01 lb/cu ft
CURVES No 21 to 30
M2 THROAT DENSITIES FROM FIG 36 TABLE No 4
OBSERVED DENSITY
THEORETICAL "
y
CURVES No 29 & 30

CORRECTION CURVE
FOR FIG 32

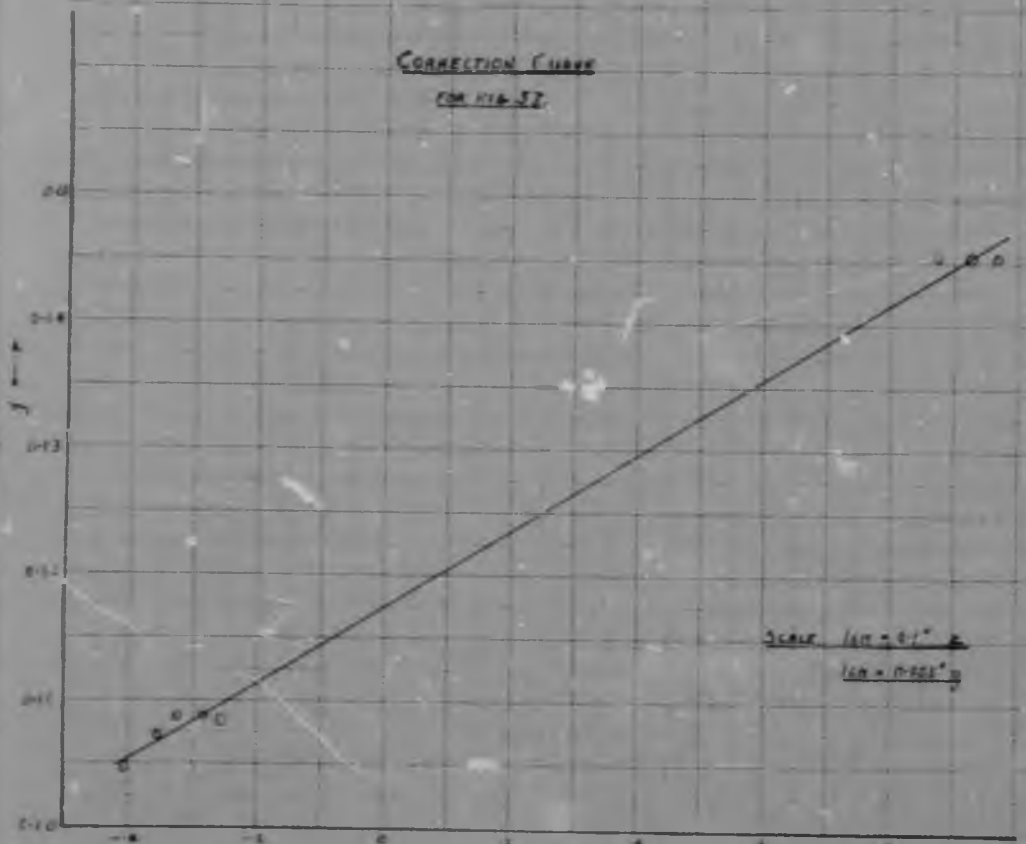

SCALE 1cm = 0·1" &
1cm = 0·025" y

CURVE NO 31

DENSITY DISTRIBUTION ALONG
THE LIGHT PATH.
FIG 32 TABLE NO 5

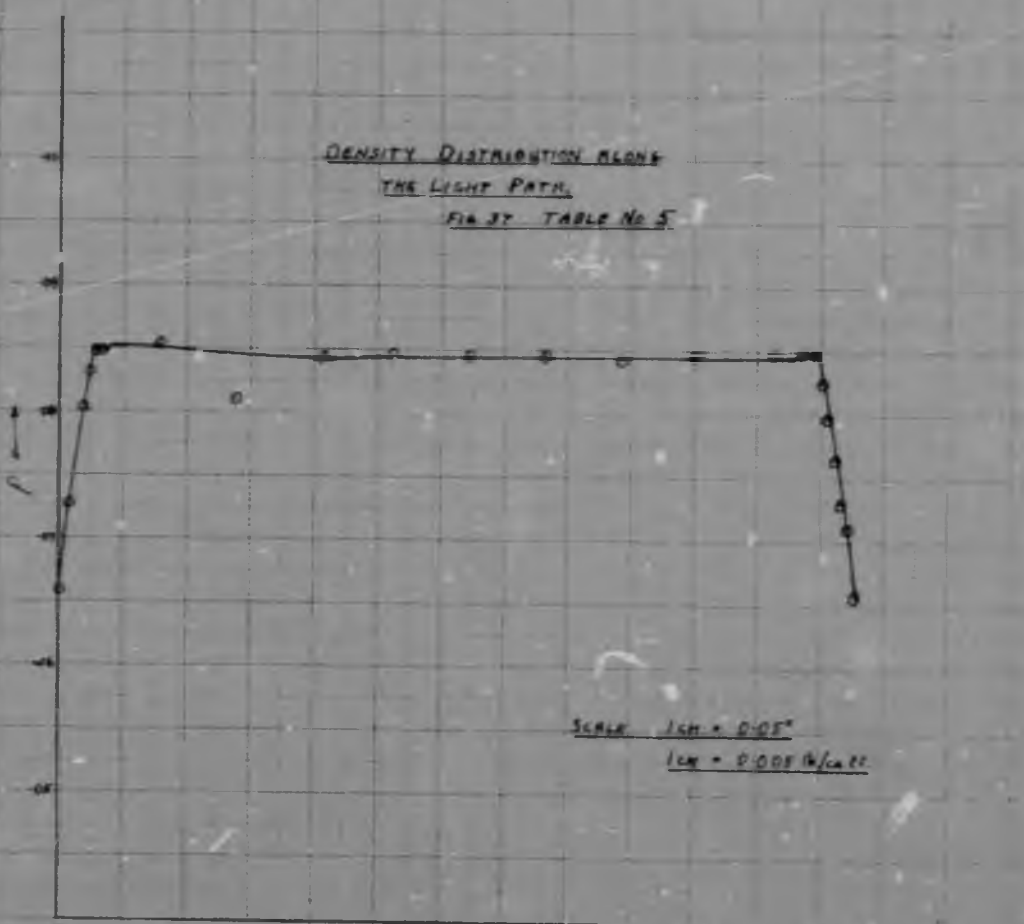

SCALE 1cm = 0·05"
1cm = 0·005 gm/cm²

CURVE NO 32

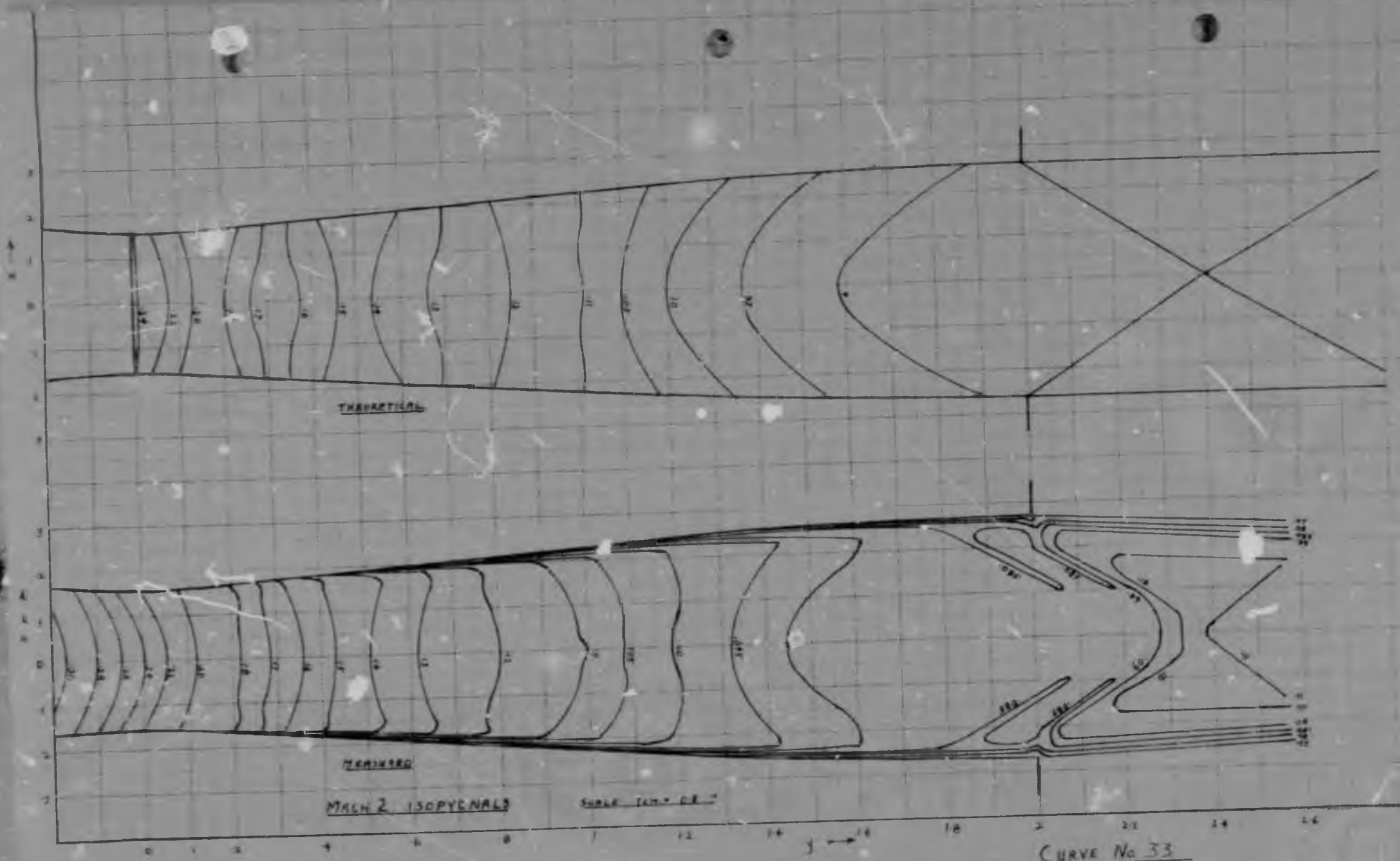

CURVE No 33

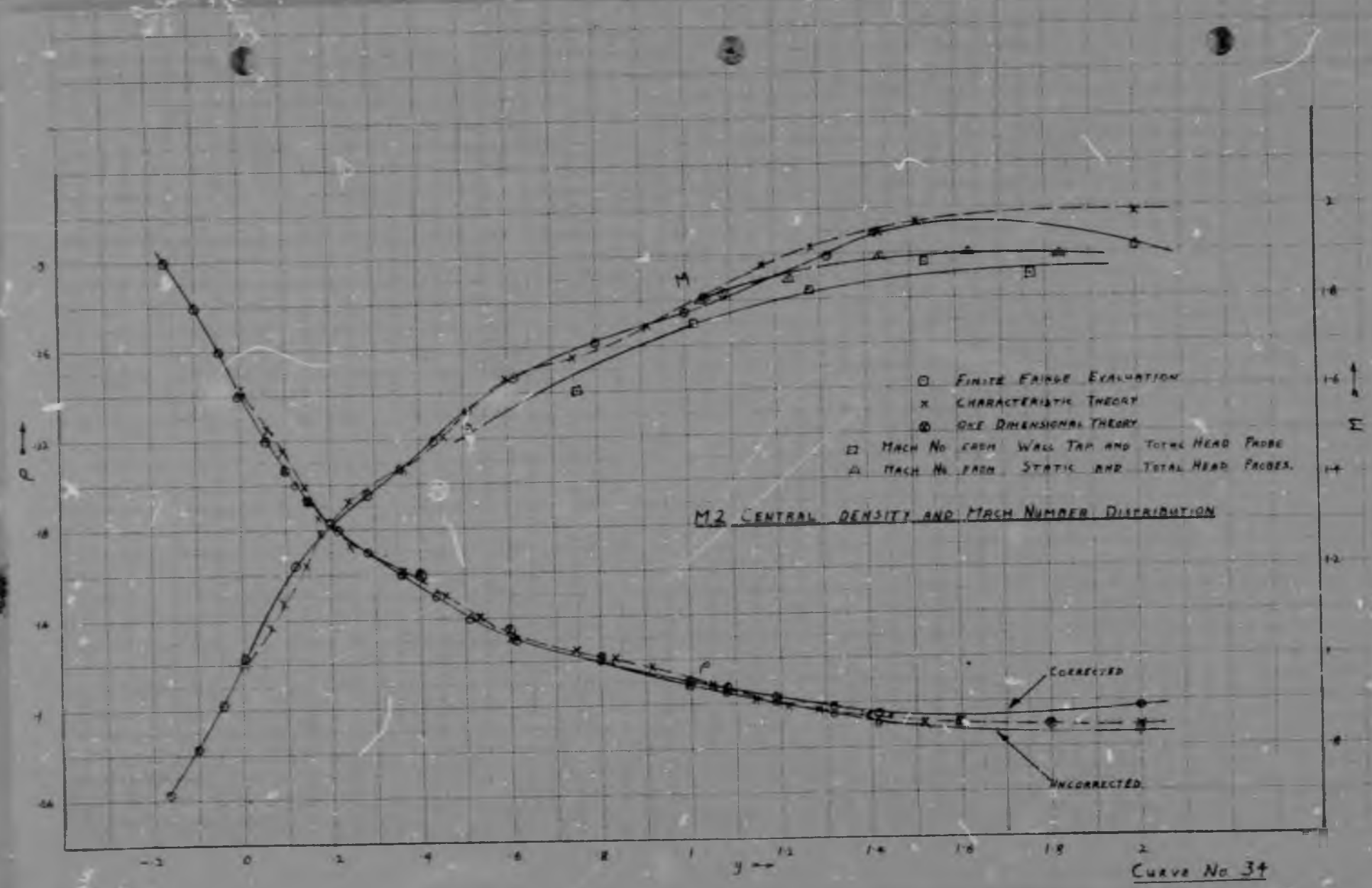
□ FINITE FAIRLE EVALUATION
× CHARACTERISTIC THEORY
⊗ ONE DIMENSIONAL THEORY
⊡ MACH No FROM WALL TAP AND TOTAL HEAD PROBE
△ MACH No FROM STATIC AND TOTAL HEAD PROBES.
M2 CENTRAL DENSITY AND MACH NUMBER DISTRIBUTION
CORRECTED
UNCORRECTED
ρ
Σ
y
-2
0
2
4
6
8
1
1·2
1·4
1·6
1·8
2
1·6
1·4
1·2
1
·8

Curve No 34

M2 CENTRAL DENSITY DISTRIBUTION

- X ONE DIMENSIONAL THEORY
- ● COMPOSITE FRINGES
- △ INFINITE FRINGES BASED ON PRESSURE TAPS
- ○ INFINITE FRINGES.
- □ WALL TAP MEASUREMENTS
- ⊗ STATIC PROBE MEASUREMENTS.

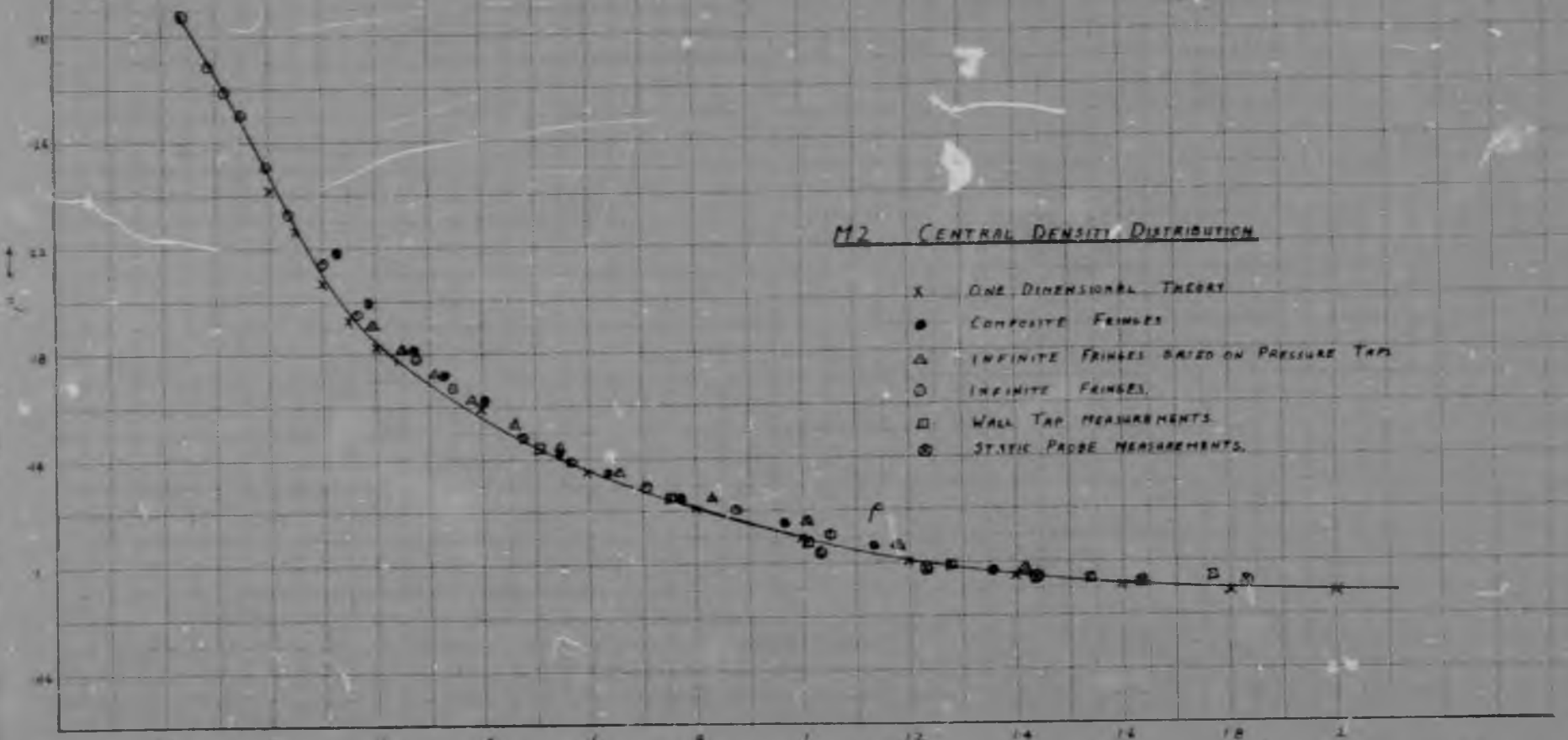

CURVE No 35

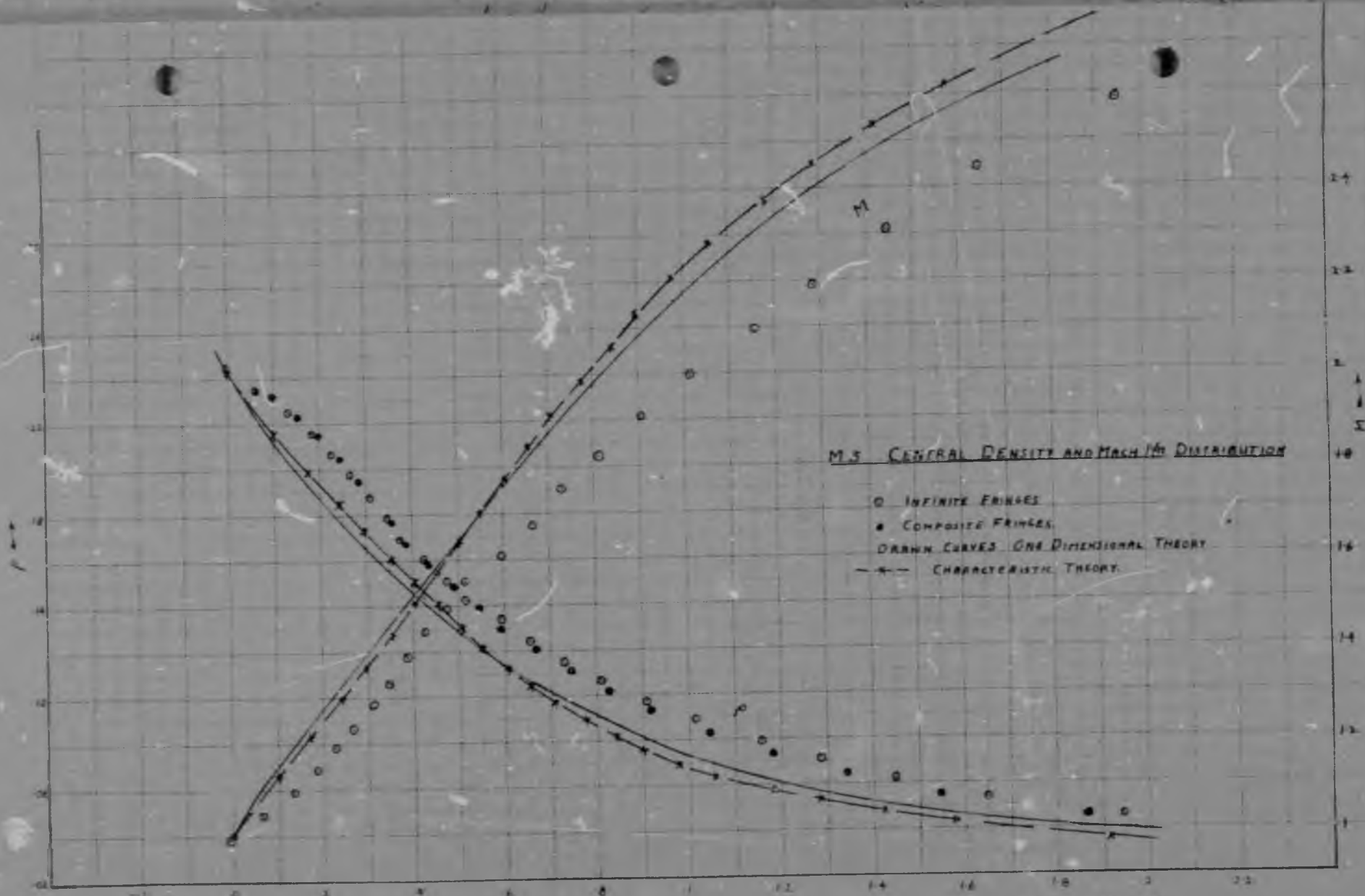
M
M.5 CENTRAL DENSITY AND MACH No DISTRIBUTION
INFINITE FRINGES
COMPOSITE FRINGES
DRAWN CURVES ONE DIMENSIONAL THEORY
CHARACTERISTIC THEORY

CURVE No 36

N = 10 y = 1·2"

○ Boundary Layer on Wall Fig. 35

△ Boundary Layer on Glass Fig. 37

N = 5 y = 2·15"

Table No 12
Figs 35 & 36

N = 15 y = 1·7"

N = 20 y = 1·5"

N = 25 y = 1·3"

N = 0 y = 0·2"

N = 5 y = 0·475"

N = 10 y = 0·525"

N = 15 y = 0·4"

N = 20 y = 0·3"

N = 25 y = 0·175"

N = 30 y = 0·06"

M2 Boundary Layer Curves

Curve No 37

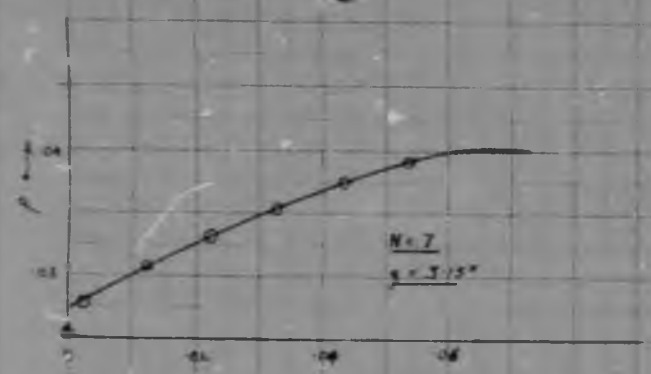

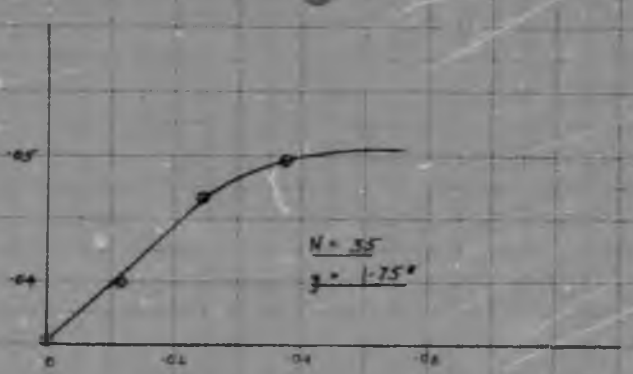

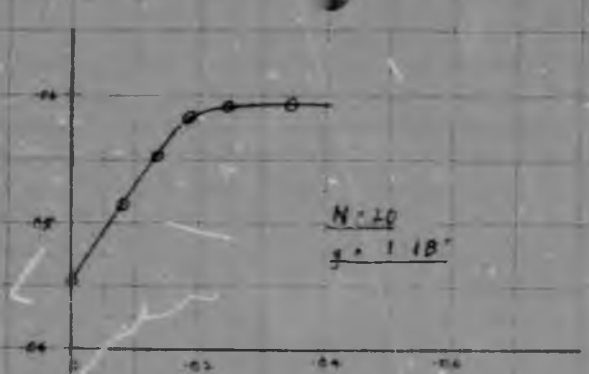

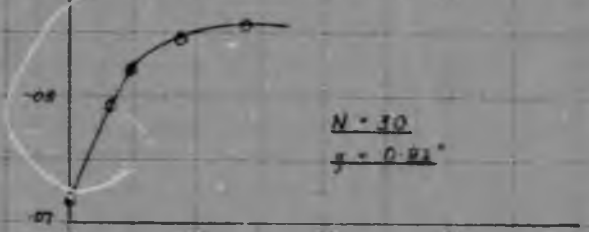

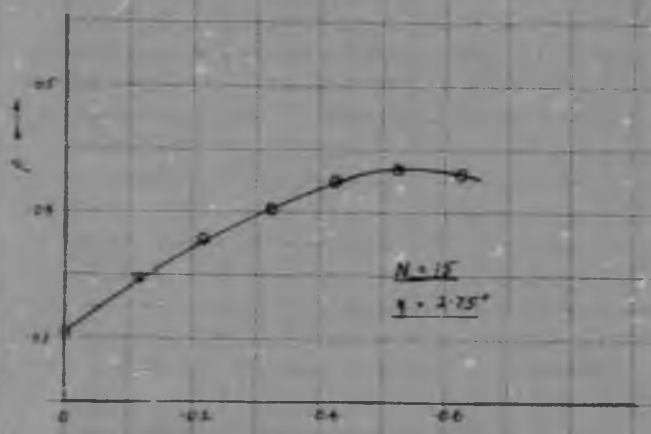

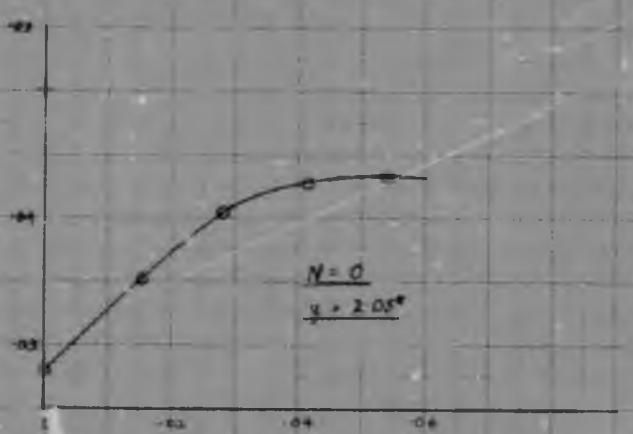

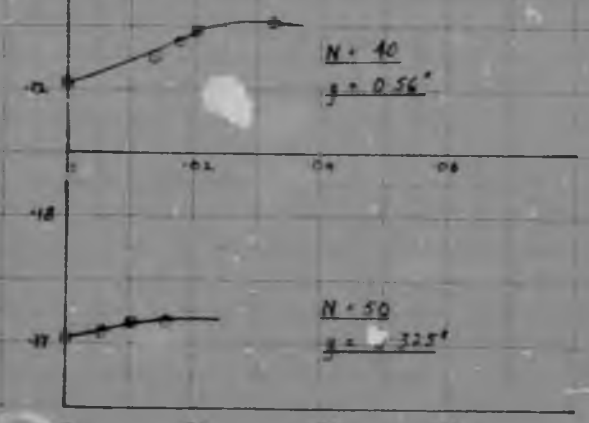

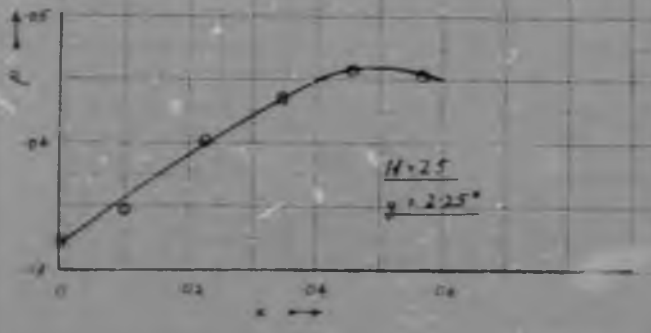

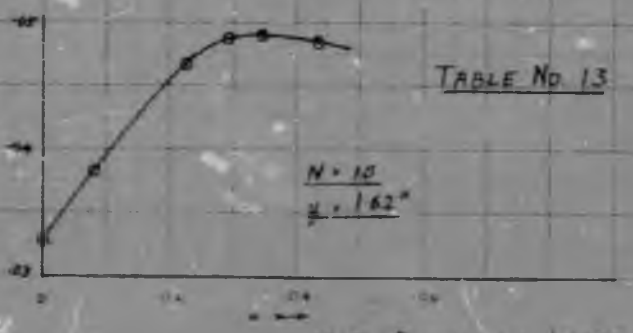

TABLE No 13

M 3 BOUNDARY LAYER CURVES

CURVE No 38

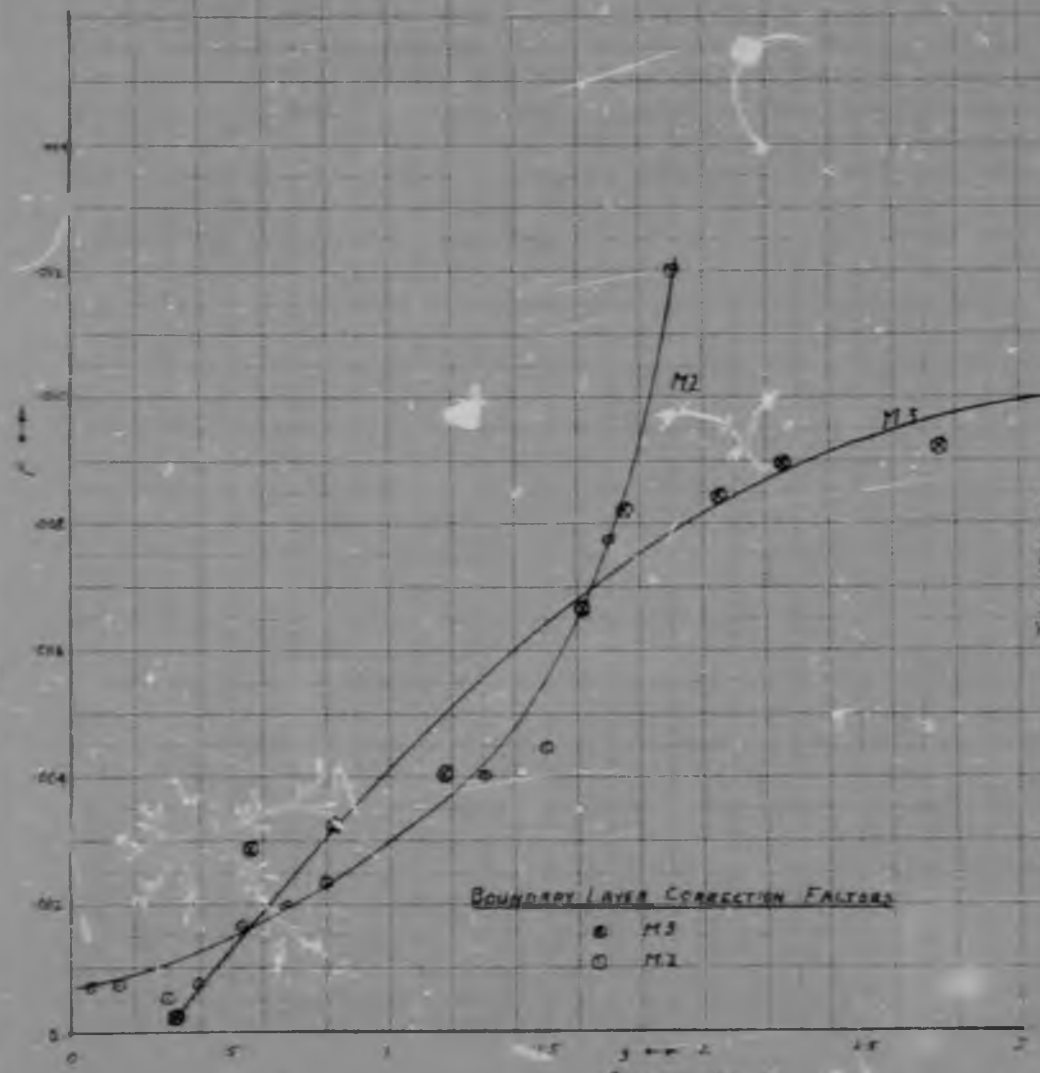

CURVE No 39

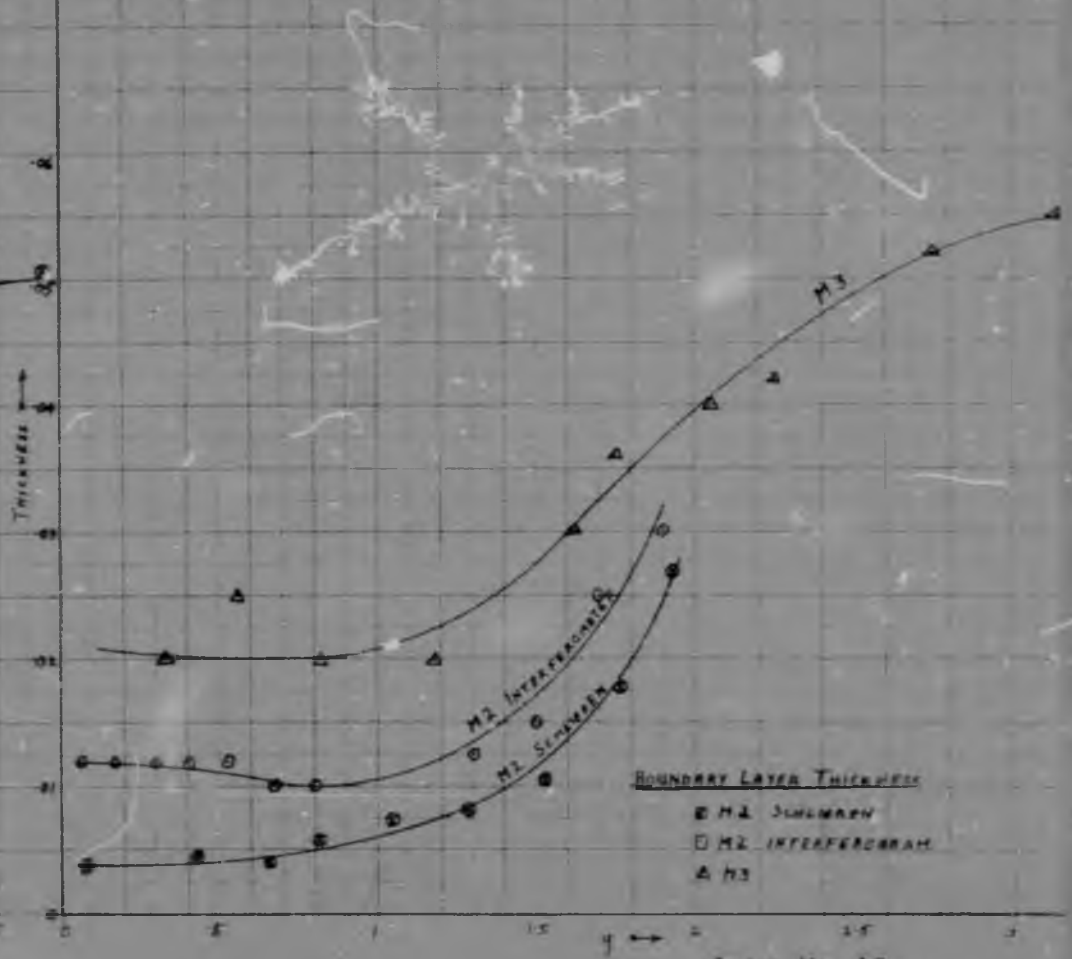

CURVE No. 40

*1 M2 WALL PRESSURES

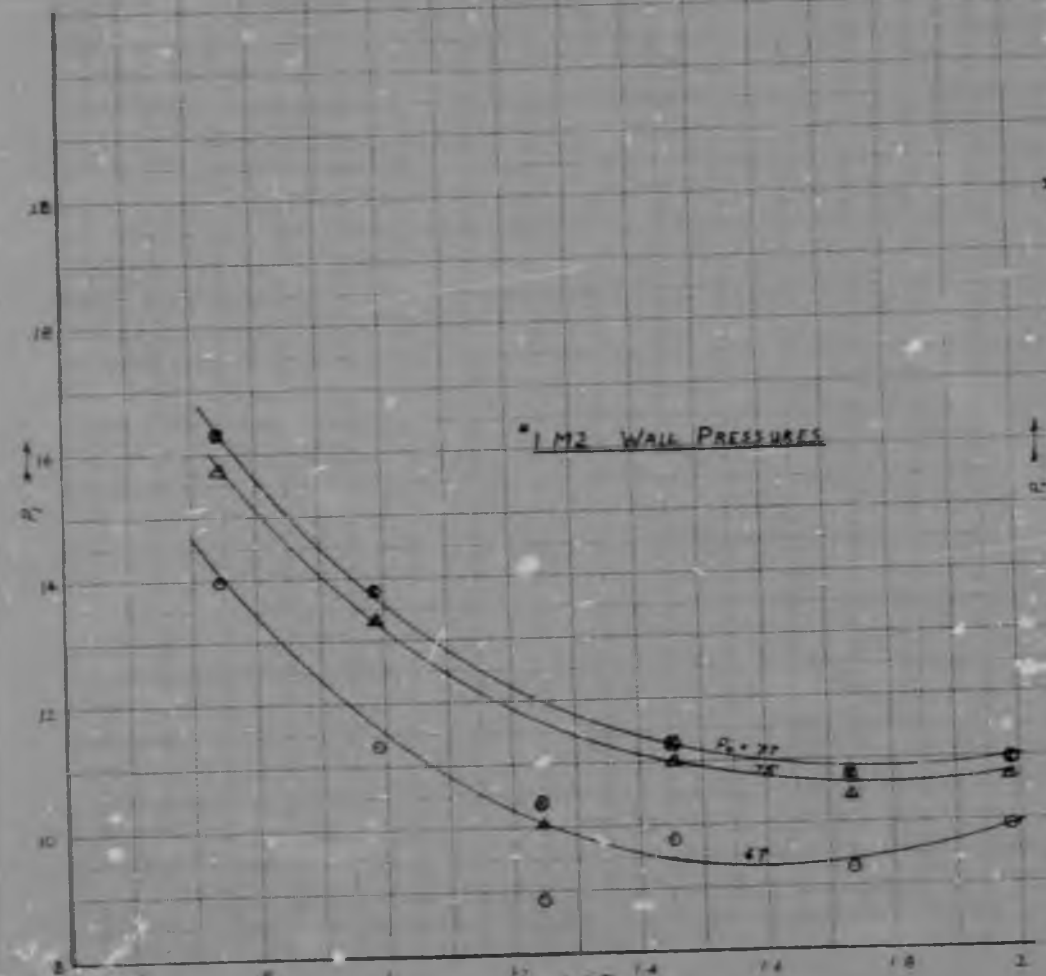

*2 M2 WALL PRESSURES

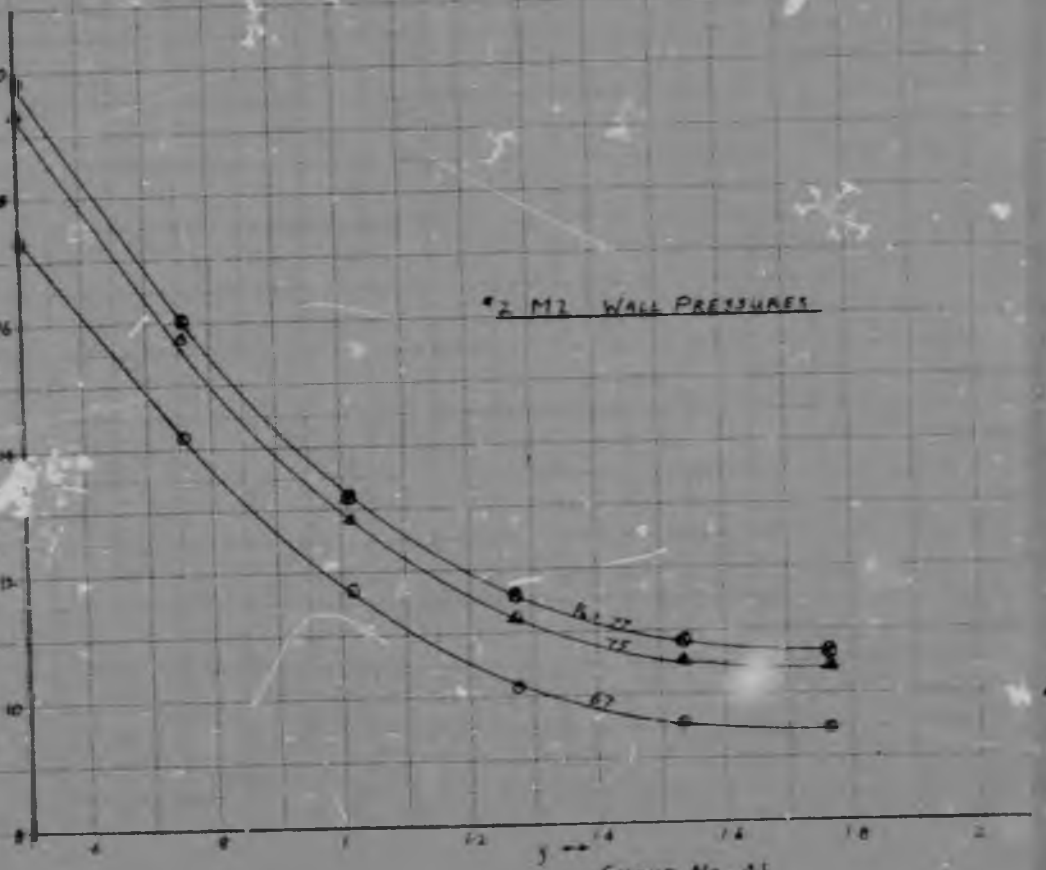

CURVE No 41

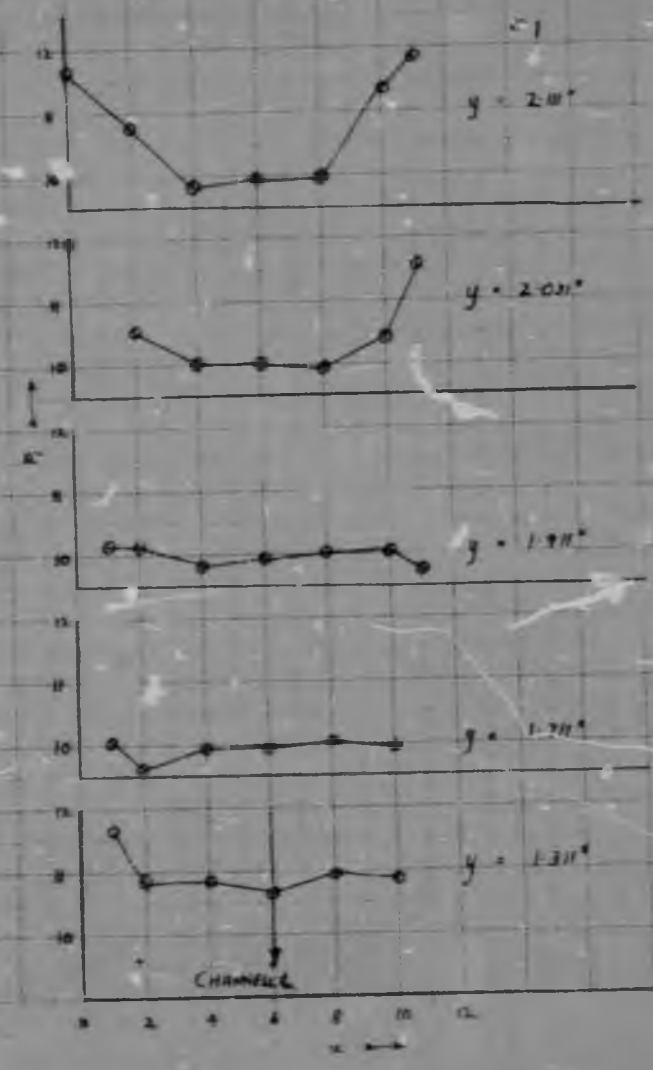

M2 STATIC PROBE PRESSURES

SCALE: 1 cm = 2 inches
1 inch = 0.04"
1 cm = 1 psi.

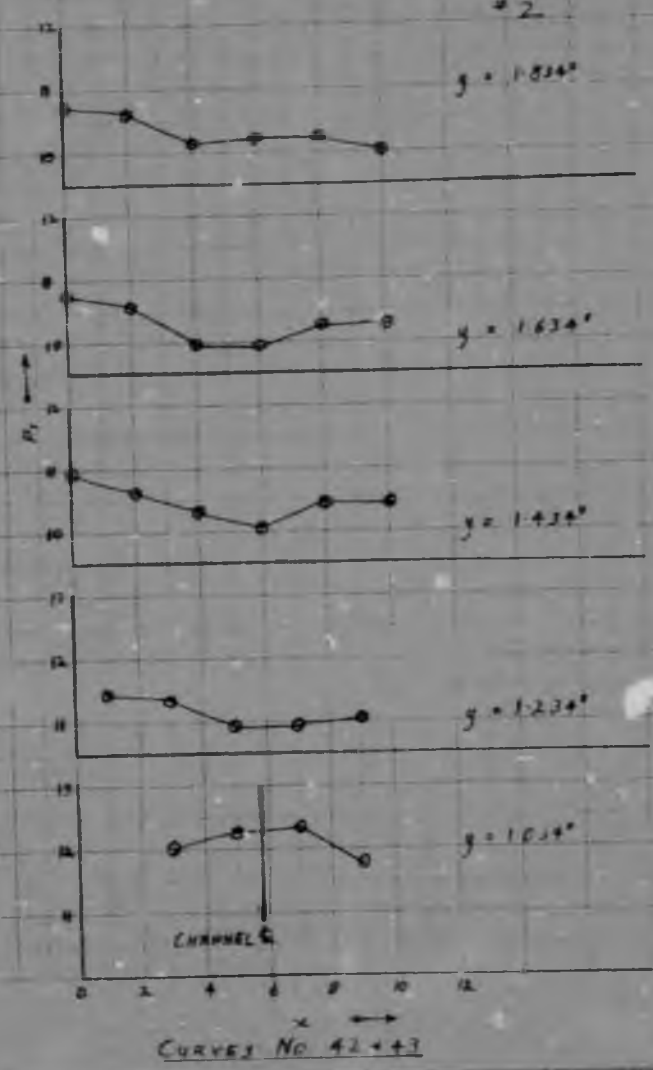

CURVES NO 42 + 43

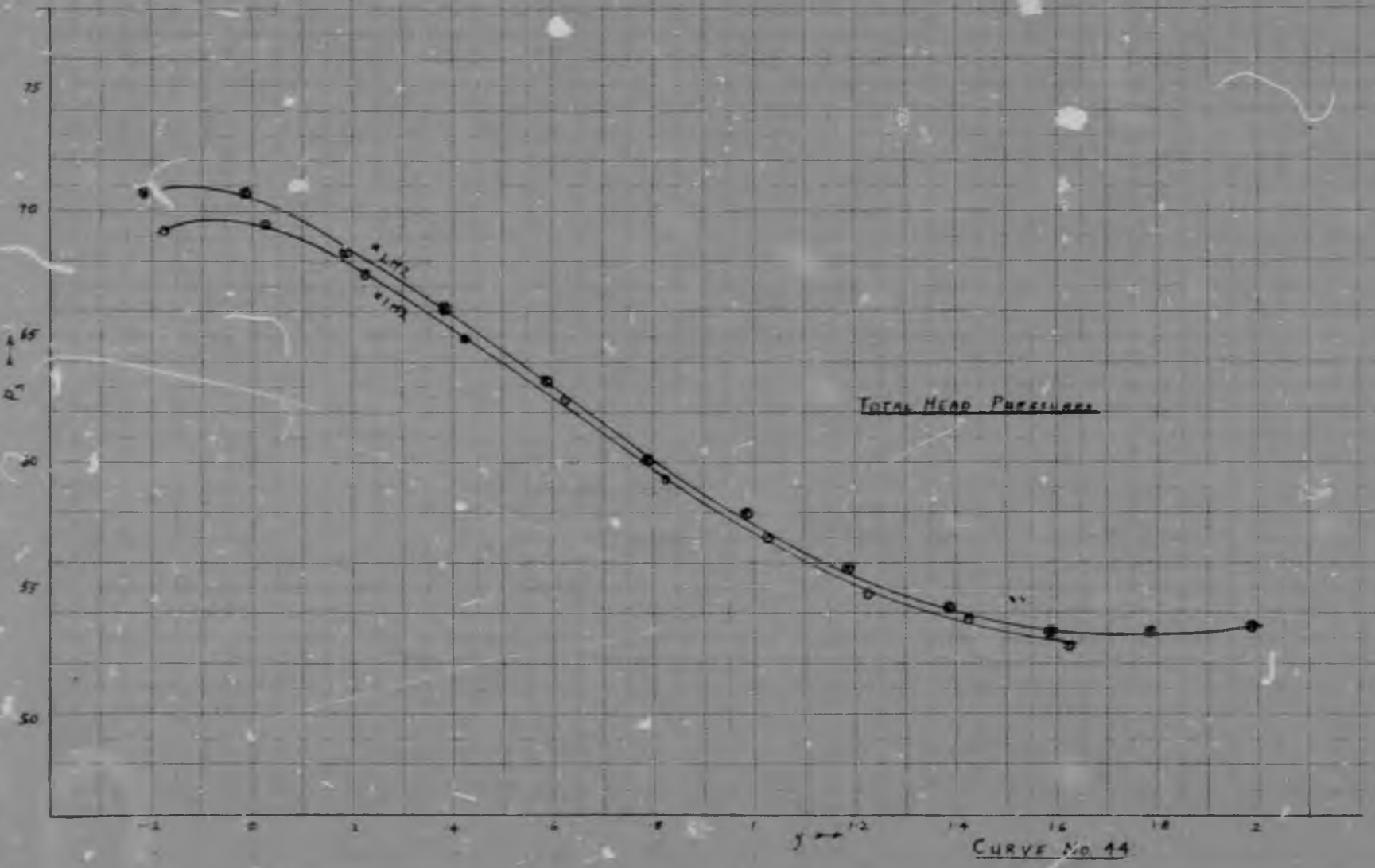

TOTAL HEAD PRESSURES

CURVE NO 44

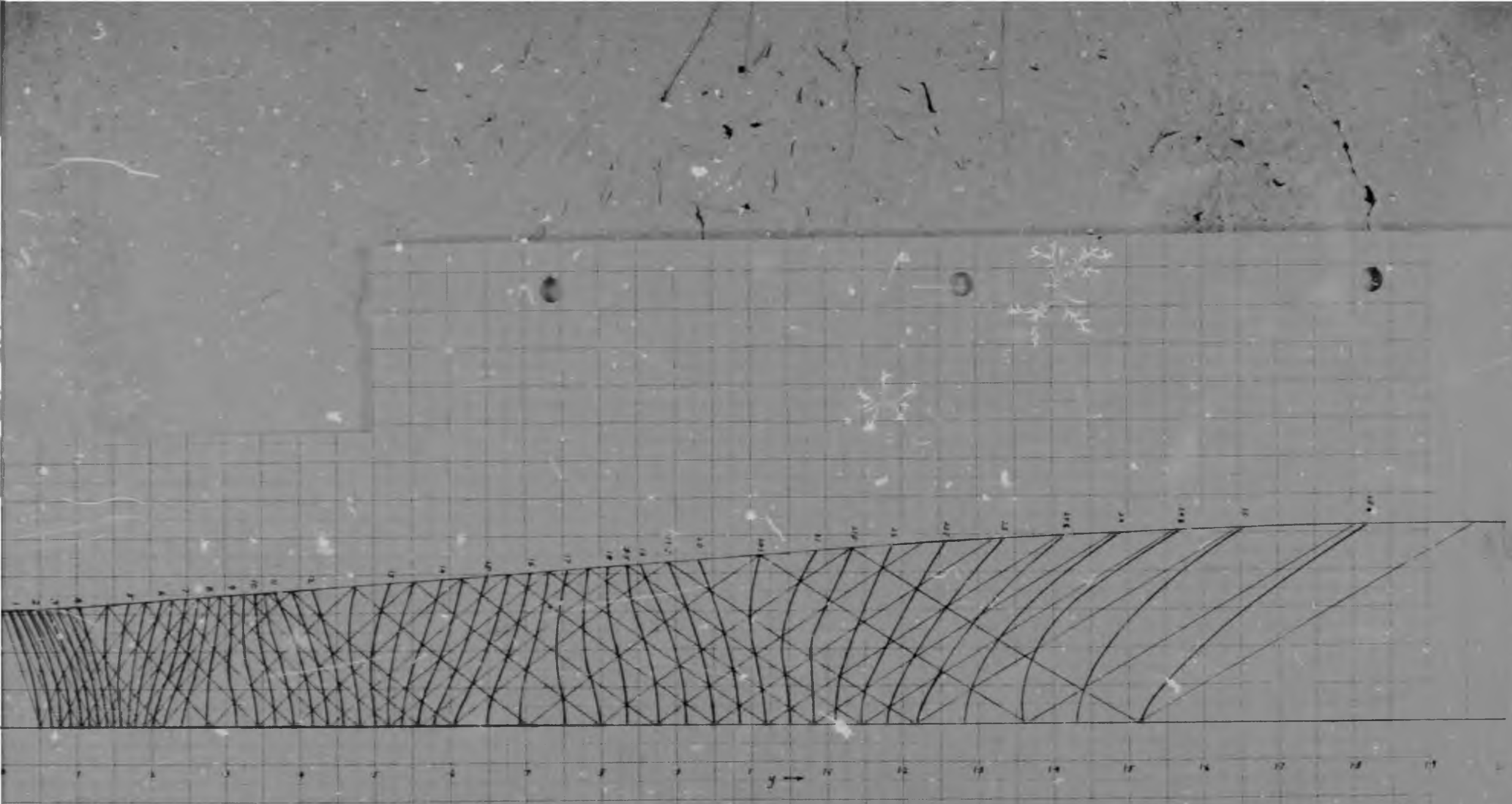

SCALE: 1 cm = 0.05 inch
DENSITIES MEASURED IN TERMS OF ρ₀

DENSITY CONTOURS BY THE METHOD OF CHARACTERISTICS

CURVE No 45

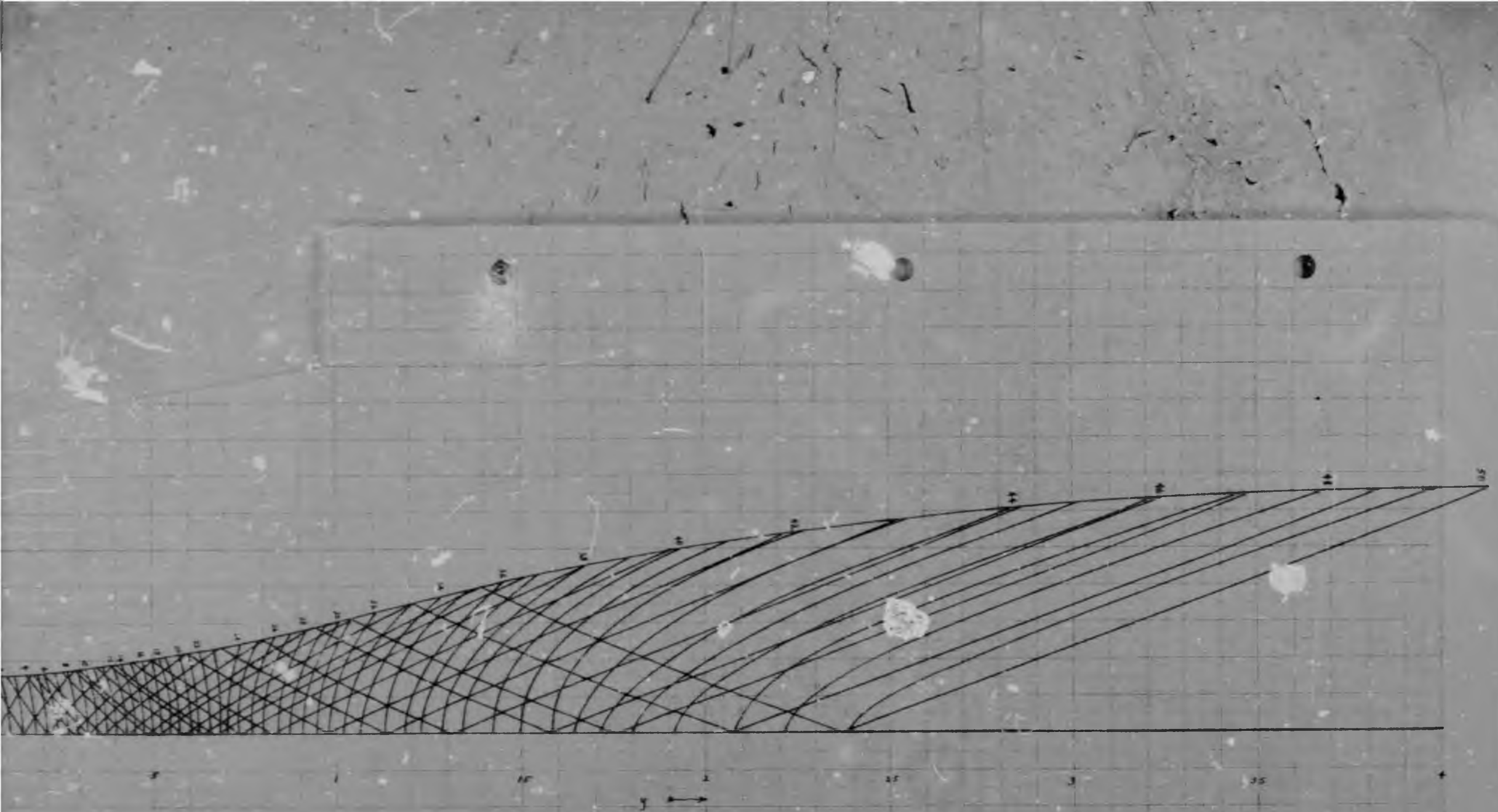

SCALE 1cm = 0·1 inch

DENSITIES MARKED IN TERMS OF M_∞

M3 DENSITY CONTOURS BY THE METHOD OF CHARACTERISTICS

CURVE No 46

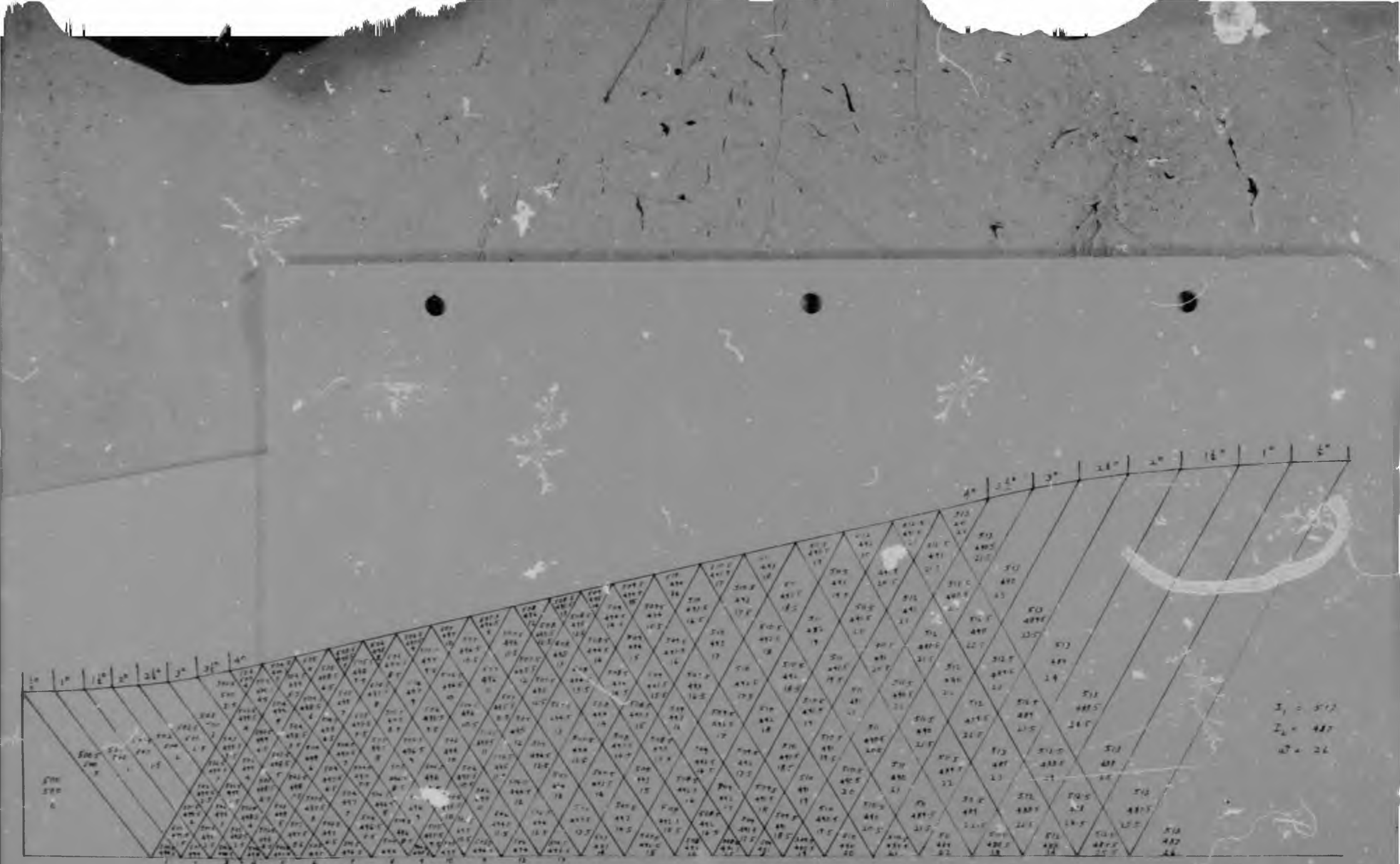

MACH NET FOR MACH 2 CHANNEL

CURVE No. 47

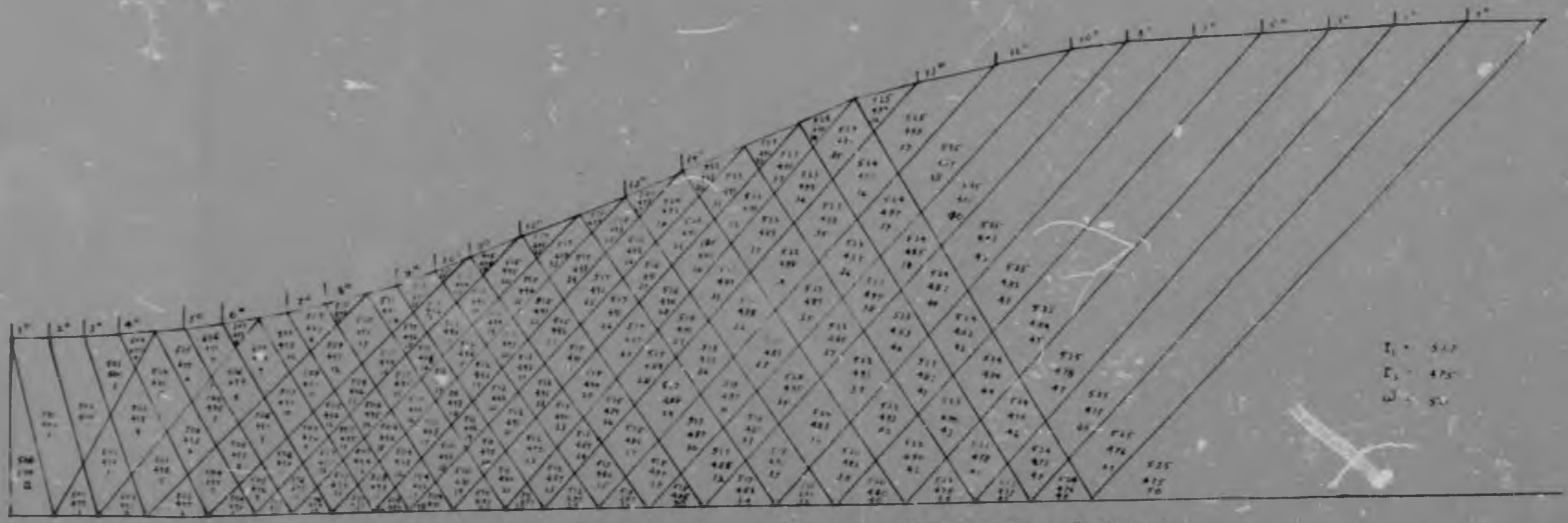

MACH NET FOR MACH 3 CHANNEL

CURVE NO. 48

Author Herrmann W
Name of thesis Application of interferometery to supersonic channel flow 1954

PUBLISHER:
University of the Witwatersrand, Johannesburg
©2013

LEGAL NOTICES:

Copyright Notice: All materials on the University of the Witwatersrand, Johannesburg Library website are protected by South African copyright law and may not be distributed, transmitted, displayed, or otherwise published in any format, without the prior written permission of the copyright owner.

Disclaimer and Terms of Use: Provided that you maintain all copyright and other notices contained therein, you may download material (one machine readable copy and one print copy per page) for your personal and/or educational non-commercial use only.

The University of the Witwatersrand, Johannesburg, is not responsible for any errors or omissions and excludes any and all liability for any errors in or omissions from the information on the Library website.